



Constraining scalar doublet and triplet leptoquarks with vacuum stability and perturbativity

Priyotosh Bandyopadhyay^{1,a}, Shilpa Jangid^{1,b}, Anirban Karan^{1,2,c}

¹ Indian Institute of Technology Hyderabad, Kandi, Sangareddy, Telangana 502284, India

² Instituto de Física Corpuscular (CSIC-Universitat de València), Apt. Correus 22085, 46071 Valencia, Spain

Received: 7 February 2022 / Accepted: 10 May 2022 / Published online: 8 June 2022

© The Author(s) 2022

Abstract We investigate the constraints on the leptoquark Yukawa couplings and the Higgs-leptoquark quartic couplings for scalar doublet leptoquark \tilde{R}_2 , scalar triplet leptoquark S_3 and their combination with both three generations and one generation with respect to perturbative unitarity and vacuum stability. The perturbative unitarity of all the dimensionless couplings is studied via one- and two-loop beta functions. New $SU(2)_L$ multiplets in terms of these leptoquarks are introduced to fabricate Landau poles at the two-loop level in the gauge coupling g_2 at $10^{19.7}$ GeV and $10^{14.4}$ GeV, respectively, for the S_3 and $\tilde{R}_2 + S_3$ models with three generations. However, such Landau poles cease to exist for \tilde{R}_2 and any of these extensions with both one and two generations up to Planck scale. The Higgs-leptoquark quartic couplings acquire severe constraints to protect Planck scale perturbativity, whereas leptoquark Yukawa couplings acquire some upper bound in order to respect Planck scale stability of Higgs vacuum. The Higgs quartic coupling at the two-loop level constrains the leptoquark Yukawa couplings for \tilde{R}_2 , S_3 , $\tilde{R}_2 + S_3$ with values $\lesssim 1.30, 3.90, 1.00$ with three generations. In the effective potential approach, the presence of any of these leptoquarks with any number of generations pushes the metastable vacuum of the Standard Model to the stable region.

Contents

1 Introduction	1
2 Leptoquark models	3
3 Perturbativity	5
3.1 Gauge couplings	5
3.1.1 Beta function of...	5
3.1.2 Scale variation of...	7

3.1.3 Beta function of...	7
3.1.4 Scale variation of...	9
3.1.5 Beta function of...	9
3.1.6 Scale variation of...	10
3.2 Higgs-leptoquark quartic couplings	11
3.2.1 Perturbativity of...	11
3.2.2 Perturbativity of...	13
3.2.3 Perturbativity of...	14
3.2.4 Perturbativity of...	15
3.2.5 Effects of self-quartic couplings of leptoquarks	17
4 Vacuum stability	18
4.1 Vacuum stability of...	18
4.2 Vacuum stability of...	20
4.3 Vacuum stability of...	21
4.4 Vacuum stability of...	21
4.5 Bounds from effective potential stability constraints	21
5 Phenomenology	24
6 Conclusion	28
Appendix A: Two-loop beta functions of g_3	29
Appendix B: Two-loop beta functions of g_1	30
Appendix C: Running of top Yukawa coupling	30
Appendix D: Running of leptoquark Yukawa couplings	32
Appendix E: Two-loop beta functions of Higgs-leptoquark quartic couplings for \tilde{R}_2	35
Appendix F: Two-loop beta functions of Higgs-leptoquark quartic couplings for S_3	36
Appendix G: Two-loop beta functions of Higgs-leptoquark quartic couplings for $\tilde{R}_2 + S_3$	38
References	39

1 Introduction

Over the past few decades, the Standard Model (SM) has been extremely successful in establishing itself as a well-accepted model providing beautiful theoretical descriptions of elemen-

^a e-mail: bpriyo@phy.iith.ac.in

^b e-mail: ph19resch02006@iith.ac.in (corresponding author)

^c e-mail: kanirban@iith.ac.in

tary particles. After the discovery of the Higgs boson [1,2], the last undetected particle of the SM, followed by precise measurement of its properties at the Large Hadron Collider (LHC), the particle spectrum of the SM was complete. However, because of the inability to explain various experimental facts such as matter–antimatter asymmetry, dark matter relic density, neutrino masses, Higgs mass hierarchy and several flavour anomalies, SM is considered an incomplete theory. This motivates one to extend the SM with some beyond-Standard Model (BSM) particles or new gauge groups or additional discrete symmetries. Various new physics (NP) models augmented with heavy fermions and bosons have been very well studied in the literature. Leptoquarks [3] lie under the category of bosonic extension of the SM, but with lepton and baryon number.

Though the notion of leptoquark [4,5] has existed in the literature for nearly 50 years, it has received much greater attention in recent years due to its prospects for addressing various flavour anomalies [6–31], unexplained with SM. Simply speaking, leptoquarks are hypothetical particles having both lepton number and baryon number. They are electromagnetically charged and colour triplet (fundamental or anti-fundamental) under the $SU(3)_C$ gauge group. Under the $SU(2)_L$ gauge group, they can be singlet, doublet and triplet as well. According to Lorentz representation, they might be scalar as well as vector. These leptoquarks emerge naturally in several higher gauge theories unifying matter [4,5,32–42]. In the literature, numerous efforts have been devoted to studying the phenomenology of these leptoquarks at colliders [43–73], in particular at the LHC. Mainly focusing on the angular distributions, distinguishing features of scalar and vector leptoquarks carrying different SM gauge quantum numbers have also been explored at electron–proton [74], electron–photon [75] and proton–proton [76,77] colliders. On the other hand, many experimental searches for these leptoquarks have been performed at electron–positron [78–81], electron–proton [82,83], proton–antiproton [84–86] and proton–proton [87–91] colliders, but no sign of them has yet been confirmed. Kaon and lepton physics have implemented strong constraints on the coupling of leptoquarks to the first generation of quarks and leptons [3,92,93]. ATLAS and CMS (Compact Muon Solenoid) have performed thorough generation-wise analyses on the allowed mass range of scalar and vector leptoquarks. These studies [87,90,91] suggest that if any leptoquark exists, it must have mass above 1.5 TeV with the coupling to quarks and leptons below the electromagnetic coupling constant.¹

¹ However, bounds on third-generation scalar leptoquarks are a bit relaxed [88,89], and by manipulating the branching fractions of the leptoquark to different generations of quarks and leptons, one can lower the bound of 1.5 TeV mass.

Now, the 125.5 GeV mass of the observed Higgs boson indicates that its vacuum cannot be completely stable all the way up to Planck scale or even Grand Unified Theory (GUT) scale [94]. In order for the Higgs potential to be bounded from below, the self-quartic-coupling (λ_h) of the Higgs boson must be positive. However, it is found that the negative quantum correction from the top quark pushes λ_h to negative values above the energy scale of 10^{10} GeV, thus hampering the stability of the SM. Technically speaking, it is generally considered that the SM is in a metastable state. In these circumstances, the presence of some BSM scalar extensions, i.e. simplest extension via singlet [95–104], $SU(2)_L$ doublet [105–112] or triplet representation of $SU(2)_L$ [113,114], is required to restore the stability of vacuum by neutralizing the destabilizing effect of the top quark. On the other hand, the inclusion of additional fermionic particles worsens the case by further lowering the energy scale within which λ_h remains positive. To avoid the stability issue, these models are also often extended with additional scalar particles [115–119]. However, it is important to note that fermions with $SU(2)_L$ gauge charge push for non-perturbativity, thus constraining the number of generations for the Planck scale perturbativity. [120]. This motivates us to investigate the stability of the vacuum in the presence of scalar leptoquarks, which has not been well explored so far.

Furthermore, it is expected that every dimensionless parameter of a fundamental model should be bounded from above in order to ensure the perturbative expansion of the correlation functions. Now, the presence of the leptoquark will hamper the perturbativity of the theory by imposing extra contributions on the renormalization group (RG) evolution of different SM couplings. Therefore, it is of paramount importance to examine the perturbativity of a model when studying the stability of its vacuum.

Along with perturbativity, the effects of the scalar singlet leptoquark S_1 in addressing the issue of vacuum stability has already been discussed in Ref. [121]. In this paper, we study the stability and perturbativity of the models with scalar triplet leptoquark S_3 and scalar doublet leptoquark \tilde{R}_2 . Since leptoquarks possess colour charge as well as hypercharge, their presence affects the RG evolution of all the couplings quite differently from that of conventional scalars. Moreover, doublet and triplet leptoquarks originate more positive effects, required for stability, than the singlet type, as they contain two and three different components, respectively. On similar grounds, such models are often more constrained by perturbativity. In addition, we study the BSM scenario having both leptoquarks \tilde{R}_2 and S_3 simultaneously. This model has attracted increasing interest given its prospects for generating the Majorana mass term for neutrinos at one- and two-loop levels, along with other beautiful features [3,122–128].

The paper is organized as follows. In the next section (Sect. 2), a brief illustration of all the leptoquark models considered

for this paper is presented. Section 3 deals with perturbativity of these models in terms of different gauge couplings, top and leptoquark Yukawa couplings and Higgs-leptoquark quartic couplings. In the following section (Sect. 4), we scrutinize the stability of the Higgs vacuum for all of these leptoquark models by studying the evolution of λ_h with the energy scale. Furthermore, we investigate the stability issue following the Coleman–Weinberg effective potential approach. In Sect. 5 we describe the phenomenology of leptoquarks in light of direct and indirect bounds on their parameter space. Finally, we conclude in Sect. 6.

2 Leptoquark models

This section provides a theoretical description of the leptoquarks \tilde{R}_2 and S_3 . First, we consider the model with scalar doublet leptoquark \tilde{R}_2 ($\mathbf{3}, \mathbf{2}, 1/6$), where the numbers in brackets denote its $SU(3)_c \otimes SU(2)_L \otimes U(1)_Y$ nature. Since this leptoquark is a doublet under $SU(2)_L$, it has two components with the electromagnetic charges $2/3$ and $-1/3$, and we designate them as $\tilde{R}_2^{2/3}$ and $\tilde{R}_2^{-1/3}$. The corresponding Lagrangian is given by:

$$\mathcal{L}_2 \supset (D^\mu \tilde{R}_2)^\dagger (D_\mu \tilde{R}_2) - (m_2^2 + \lambda_2 H^\dagger H) (\tilde{R}_2^\dagger \tilde{R}_2) - \tilde{\lambda}_2 H^\dagger \tilde{R}_2 \tilde{R}_2^\dagger H - [Y_2 \overline{d}_R (\tilde{R}_2^\dagger i\sigma_2) L_L + h.c.], \tag{1}$$

where D^μ signifies the covariant derivative related to the kinetic term of fields, m_2 is the mass of the leptoquark \tilde{R}_2 before electroweak symmetry breaking (EWSB), λ_2 and $\tilde{\lambda}_2$ are the couplings for quartic interaction terms of \tilde{R}_2 with scalar doublet field H , and the 3×3 matrix Y_2 indicates the coupling of \tilde{R}_2 with quarks and leptons where L_L represents the $SU(2)$ lepton doublet. For simplicity, we hide the generation index. After EWSB, the scalar field H gives rise to Higgs boson h , and the two components of \tilde{R}_2 obtain additional contributions in their masses from the quartic coupling terms. It is important to mention that the generation indices have been suppressed here. However, to realize the full mathematical description of this model, one has to add the SM Lagrangian as well. In our notation, we denote the SM Yukawa couplings for the charged leptons, up-type quarks and down-type quarks as Y_l , Y_u and Y_d , respectively. The SM Higgs potential is given by:

$$V_0 = -\mu_h |H|^2 + \lambda_h |H|^4 \quad \text{with} \quad H = \frac{1}{\sqrt{2}} \begin{pmatrix} 0 \\ v+h \end{pmatrix}, \tag{2}$$

under unitary gauge, where the tree-level mass of the Higgs boson becomes $M_h = \sqrt{2\mu_h}$, and the vacuum expectation value (VEV) of the scalar field can be expressed as $v = \sqrt{\mu_h/\lambda_h}$. After EWSB, the squared masses for the leptoquarks

$\tilde{R}_2^{2/3}$ and $\tilde{R}_2^{-1/3}$ respectively become:

$$m_{2,2/3}^2 = m_2^2 + \frac{1}{2} \lambda_2 v^2, \\ m_{2,1/3}^2 = m_2^2 + \frac{1}{2} (\lambda_2 + \tilde{\lambda}_2) v^2, \tag{3}$$

and thus the two components of the doublet no longer remain degenerate and acquire a mass gap of $\frac{1}{2} \tilde{\lambda}_2 v^2$.

In principle, there could be some other gauge-invariant dimension-four terms for \tilde{R}_2 , for example, $\epsilon_{\alpha\beta\gamma} (H^T i\sigma_2 \tilde{R}_{2,\alpha}) (\tilde{R}_{2,\beta}^\dagger i\sigma_2 \tilde{R}_{2,\gamma})$ or $(\tilde{R}_2^\dagger \tilde{R}_2) (\tilde{R}_2^\dagger \tilde{R}_2)$. The first term does not conserve the baryon and lepton number separately; additionally, it initiates proton decay via the mode $p \rightarrow \pi^+ \pi^+ e^- \nu \nu$ [3, 129, 130], which in turn forces the leptoquark mass to be very high to reach the experimental value of proton lifetime. Thus, one should either neglect the term or assume that it is forbidden by some other symmetry. For example, if we impose a Z_2^l discrete symmetry under which all the SM leptons and the leptoquarks are both odd, but other particles like quarks and the scalar doublet H are even, this particular term will be prohibited. The same effect can be achieved by imposing Z_2^q discrete symmetry for which the quarks and leptoquarks are odd and all the other particles are even. On the other hand, the second term does not affect any other SM couplings up to the two-loop level. So, for simplicity, we ignore it as well.

In the second scenario, we study the extension of SM with the scalar triplet leptoquark S_3 ($\mathbf{3}, \mathbf{3}, 1/3$). The three excitations of this multiplet possess the electromagnetic charges $4/3, 1/3$ and $-2/3$, and therefore we designate them as $S_3^{4/3}, S_3^{1/3}$ and $S_3^{-2/3}$, respectively. The Lagrangian for this leptoquark is given by:

$$\mathcal{L}_3 \supset \text{Tr}[(D^\mu S_3^{ad})^\dagger (D_\mu S_3^{ad})] - \tilde{\lambda}_3 H^\dagger S_3^{ad} (S_3^{ad})^\dagger H - (m_3^2 + \lambda_3 H^\dagger H) \text{Tr}[(S_3^{ad})^\dagger S_3^{ad}] + [Y_3 \overline{Q}_L^c (i\sigma_2 S_3^{ad}) L_L + h.c.], \tag{4}$$

where S_3^{ad} signifies S_3 in adjoint representation, m_3 is the mass of S_3 before EWSB, λ_3 and $\tilde{\lambda}_3$ are the couplings for quartic interaction terms of this leptoquark with Higgs boson, and Y_3 indicates its coupling with different quarks and leptons where Q_L represents the $SU(2)$ quark doublet. It is interesting to note that the term $H^\dagger (S_3^{ad})^\dagger S_3^{ad} H$ is absent in the Lagrangian, given by Eq. (4), since it is not an independent term. It can be easily checked that $H^\dagger [S_3^{ad} (S_3^{ad})^\dagger + (S_3^{ad})^\dagger S_3^{ad}] H = (H^\dagger H) \text{Tr}[(S_3^{ad})^\dagger S_3^{ad}]$ under unitary gauge. After EWSB, the squared masses for leptoquarks $S_3^{4/3}, S_3^{1/3}$ and $S_3^{-2/3}$ become:

$$m_{3,4/3}^2 = m_3^2 + \frac{1}{2} \lambda_3 v^2,$$

$$\begin{aligned}
 m_{3,2/3}^2 &= m_3^2 + \frac{1}{2}(\lambda_3 + \tilde{\lambda}_3)v^2, \\
 m_{3,1/3}^2 &= m_3^2 + \frac{1}{2}\left(\lambda_3 + \frac{1}{2}\tilde{\lambda}_3\right)v^2,
 \end{aligned}
 \tag{5}$$

which lifts the degeneracy among these three states like the previous scenario. In this case, apart from the leptoquark self-quartic interactions, i.e. $\text{Tr}[(S_3^{ad})^\dagger S_3^{ad} (S_3^{ad})^\dagger S_3^{ad}]$ and $\text{Tr}[(S_3^{ad})^\dagger S_3^{ad}]^2$, which we neglect for simplicity as in the doublet leptoquark scenario, there could exist a diquark term like $\overline{Q}_L^c (i\sigma_2) (S_3^{ad})^\dagger Q_L$ allowed by gauge symmetry. However, this term neither respects baryon and lepton number separately nor protects protons from decay through $p \rightarrow e^+\pi^0$ or $p \rightarrow \pi^+\bar{\nu}_e$ [3, 131–133]. In the same fashion as in the \tilde{R}_2 case, here also one can impose Z_2^l or Z_2^q symmetry to forbid this term. For our analysis, we neglect it as well.

Lastly, we consider the scenario having both the leptoquarks \tilde{R}_2 and S_3 . The relevant part of the Lagrangian for this model is given by:

$$\mathcal{L}_{23} = \mathcal{L}_2 + \mathcal{L}_3 - [\kappa_h H^\dagger S_3^{ad} \tilde{R}_2 + h.c.].
 \tag{6}$$

The interesting feature of this model is that, besides the individual interaction terms for doublet and triplet leptoquarks, it contains one additional dimension-three term which couples the doublet leptoquark to the triplet one through the Higgs boson. As in earlier cases, we have not considered the leptoquark self-quartic couplings.

In this scenario, it is important to note that although $S_3^{4/3}$ remains as mass eigenstate, the other components of \tilde{R}_2 and S_3 do not. For instance, the squared mass matrix for $\tilde{R}_2^{1/3}$ and $S_3^{1/3}$ becomes:

$$M_{1/3}^2 = \begin{pmatrix} m_{2,1/3}^2 & \frac{1}{2}\kappa_h v \\ \frac{1}{2}\kappa_h^* v & m_{3,1/3}^2 \end{pmatrix},
 \tag{7}$$

where κ_h^* indicates the complex conjugate of κ_h . Therefore, these two flavour states mix together to produce the energy eigenstates as:

$$\begin{pmatrix} \Omega_1 \\ \Omega_2 \end{pmatrix} = \begin{pmatrix} \cos \theta_1 & \sin \theta_1 e^{i\phi_1} \\ -\sin \theta_1 e^{-i\phi_1} & \cos \theta_1 \end{pmatrix} \begin{pmatrix} \tilde{R}_2^{1/3} \\ S_3^{1/3} \end{pmatrix},
 \tag{8}$$

where the mixing angle θ_1 and the CP-violating phase ϕ_1 are given by:

$$\tan 2\theta_1 = -\left(\frac{v |\kappa_h|}{m_{3,1/3}^2 - m_{2,1/3}^2}\right) \text{ and } e^{i\phi_1} = \frac{\kappa_h^*}{|\kappa_h|}.
 \tag{9}$$

The squared masses for the energy eigenstates $\Omega_{1,2}$ are given by:

$$m^2(\Omega_{1,2}) = \frac{1}{2}\left[m_{3,1/3}^2 + m_{2,1/3}^2\right]$$

$$\mp \sqrt{(m_{3,1/3}^2 - m_{2,1/3}^2)^2 + v^2 |\kappa_h|^2}.
 \tag{10}$$

Similarly, the squared mass matrix for $\tilde{R}_2^{2/3}$ and $S_3^{2/3}$ becomes:

$$M_{2/3}^2 = \begin{pmatrix} m_{2,2/3}^2 & -\frac{1}{\sqrt{2}}\kappa_h v \\ -\frac{1}{\sqrt{2}}\kappa_h^* v & m_{3,2/3}^2 \end{pmatrix},
 \tag{11}$$

and these two flavour states also mix together to produce the energy eigenstates as:

$$\begin{pmatrix} \chi_1 \\ \chi_2 \end{pmatrix} = \begin{pmatrix} \cos \theta_2 & \sin \theta_2 e^{i\phi_2} \\ -\sin \theta_2 e^{-i\phi_2} & \cos \theta_2 \end{pmatrix} \begin{pmatrix} \tilde{R}_2^{2/3} \\ S_3^{2/3} \end{pmatrix},
 \tag{12}$$

where the mixing angle θ_2 and the CP-violating phase ϕ_2 are given by:

$$\tan 2\theta_2 = \left(\frac{\sqrt{2} v |\kappa_h|}{m_{3,2/3}^2 - m_{2,2/3}^2}\right) \text{ and } e^{i\phi_2} = \frac{\kappa_h^*}{|\kappa_h|}.
 \tag{13}$$

The squared masses for the energy eigenstates $\Omega_{1,2}$ are given by:

$$\begin{aligned}
 m^2(\chi_{1,2}) &= \frac{1}{2}\left[m_{3,2/3}^2 + m_{2,2/3}^2\right] \\
 &\mp \sqrt{(m_{3,2/3}^2 - m_{2,2/3}^2)^2 + 2 v^2 |\kappa_h|^2}.
 \end{aligned}
 \tag{14}$$

As a special case, if κ_h becomes zero, i.e. no mixing between doublet and triplet, then the mass and flavour states remain the same, i.e. the mixing angle becomes zero. On the other hand, if the masses of the doublet and triplet flavour eigenstates become the same, the mixing angles turn to $\pi/4$ and mass differences of $v|\kappa_h|$ and $\sqrt{2}v|\kappa_h|$ are generated between the mass-eigenstates with charge 1/3 and 2/3, respectively.

Now, regarding the generation of leptoquarks, we follow two different conventions: (a) there is one generation of leptoquark that couples to one generation of quark and lepton only; (b) there exist three generations of leptoquarks, each of which couples to one generation of quark and lepton only. Both conventions have different pros and cons when considering several low-energy and collider bounds on leptoquarks. However, for our analysis we study both of them. For the first scenario, we consider only diagonal coupling of the leptoquarks given by $Y_\gamma^{rs} = Y_\phi \text{diag}(1, 0, 0)$, with r, s being the generation indices for quarks and leptons and $\gamma \in \{2, 3\}$. Obviously, one can choose $\text{diag}(0, 1, 0)$ or $\text{diag}(0, 0, 1)$ as well. In the second case, we assume $Y_{\gamma,i}^{rs} = Y_\phi \delta^{ir} \delta^{is}$, with i being the generation of the leptoquark. In this scenario, the terms λ_γ and $\tilde{\lambda}_\gamma$ also become 3×3 matrices, but we also consider them diagonal, restricting the generation mixing of the leptoquarks.

3 Perturbativity

In this section we study the perturbativity of the theory with respect to different dimensionless couplings. It is well known that expansion of amplitude or cross section in perturbative series is plausible only when the expansion parameter is less than unity. Therefore, the constraints that must be satisfied by different couplings in order to respect the perturbativity of the theory are as follows: [118, 120, 121]:

$$|\lambda_\alpha| \leq 4\pi, \quad |\tilde{\lambda}_\gamma| \leq 4\pi, \quad |g_k| \leq 4\pi \quad |Y_l^{rs}| \leq \sqrt{4\pi}, \quad (15)$$

where λ_α and $\tilde{\lambda}_\gamma$, with $\alpha \in \{h, 2, 3\}$ and $\gamma \in \{2, 3\}$, indicate the quartic couplings of the Higgs boson with leptoquarks as well as the self-quartic coupling of the Higgs boson, g_k with $k \in \{1, 2, 3\}$ signifies the gauge couplings corresponding to $U(1)_Y, SU(2)_L$ and $SU(3)_C$ gauge symmetry, respectively, and Y_l^{rs} with $l \in \{2, 3, \ell, u, d\}$ represents the (r, s) element of the Yukawa (or Yukawa-like) coupling matrices for quarks and leptons. We generate two-loop beta functions for different couplings through SARAH [134, 135] in the $\overline{\text{MS}}$ scheme and analyse them. We use the usual definition of beta function

$$\beta(x) = \frac{\partial x}{\partial(\log \mu)}, \quad (16)$$

when considering the running of any coupling parameter x with the energy scale μ . The running of different parameters in generalized field theory with dimensional regularization [136] in the $\overline{\text{MS}}$ scheme has already been addressed in Refs. [137–140]. The RG evolution of various parameters under the SM has been discussed in [141–144].

3.1 Gauge couplings

We first discuss the renormalization group (RG) evolution of the gauge couplings. Since the doublet and triplet leptoquarks possess all three gauge charges, namely weak hypercharge, isospin and colour, the running of all gauge couplings will differ from the SM. However, in some scenarios the weak coupling constant g_2 gradually increases to hit the Landau pole at some energy scale, which eventually leads to sudden divergences in the other two gauge couplings. Therefore, we present the running of g_2 at the beginning.

3.1.1 Beta function of g_2 : a brief review

It is well established that for any non-Abelian gauge group $G = SU(N)$, the one-loop beta function of the gauge coupling g is given by:

$$\beta(g)^{1\text{-loop}} = \frac{g^3}{16\pi^2} \left[\frac{4}{3}n_f T(R_f) + \frac{1}{3}n_s T(R_s) - \frac{11}{3}C_2(G) \right] \quad (17)$$

where n_f is the number of Dirac fermionic multiplets in representation R_f , n_s is the number of complex scalar multiplets in representation R_s , $C_2(G)$ is the quadratic Casimir of the gauge group G and is equal to N since the gauge fields lie in the adjoint representation of G , and finally, $T(R_{f/s})$ are other Casimir invariants defined by $\text{Tr}(\mathcal{T}_{R_{f/s}}^a \mathcal{T}_{R_{f/s}}^b) = T(R_{f/s})\delta^{ab}$, with $\mathcal{T}_{R_{f/s}}^{a,b}$ being the generator of the Lie algebra in the representation $R_{f/s}$. At this point, it is worth mentioning that one should replace the factor $4/3$ with $2/3$ in Eq. (17) when dealing with Weyl or Majorana fermions, and similarly, the factor $1/3$ must be replaced with $1/6$ for real scalar multiplets.

If we consider the one-loop beta function of weak coupling constant g_2 in the SM, the corresponding gauge group will be $SU(2)_L$. Hence, the fermionic contribution would come from 12 Weyl fermionic doublets: (a) three generations of leptonic doublets and (b) nine quark doublets (three generations and three colours). However, since they are all Weyl fermions due to the left chiral nature of the weak interaction, one must take the $2/3$ factor instead of $4/3$ as the coefficient of the term $n_f T(R_f)$ in Eq. (17). On the other hand, there is only one charged scalar doublet interacting weakly in the SM. Moreover, $T(R_{f/s}) = 1/2$ for all the fermions and scalar under $SU(2)_L$ gauge group, as they are all in fundamental representation. Thus one-loop beta function of g_2 in the SM becomes:

$$\beta(g_2)_{\text{SM}}^{1\text{-loop}} = \frac{g_2^3}{16\pi^2} \left[\left(\frac{2}{3} \times 12 \times \frac{1}{2} \right) + \left(\frac{1}{3} \times 1 \times \frac{1}{2} \right) - \left(\frac{11}{3} \times 2 \right) \right] = -\frac{19}{6} \left(\frac{g_2^3}{16\pi^2} \right). \quad (18)$$

Now, if we add one generation of scalar doublet leptoquark \tilde{R}_2 to the SM, we can express the one-loop beta function of g_2 as:

$$\beta(g_2)_{\tilde{R}_2, 1\text{-gen}}^{1\text{-loop}} = \beta(g_2)_{\text{SM}}^{1\text{-loop}} + \Delta\beta(g_2)_{\tilde{R}_2}^{1\text{-loop}}, \quad (19)$$

where the term $\Delta\beta(g_2)_{\tilde{R}_2}^{1\text{-loop}}$ signifies the sole contribution from the single generation of the leptoquark \tilde{R}_2 . Since \tilde{R}_2 is a complex scalar in fundamental representation of $SU(2)_L$ having three colour choices, we find:

$$\begin{aligned} \Delta\beta(g_2)_{\tilde{R}_2}^{1\text{-loop}} &= \frac{g_2^3}{16\pi^2} \left(\frac{1}{3} \times 3 \times \frac{1}{2} \right) = \frac{1}{2} \left(\frac{g_2^3}{16\pi^2} \right), \\ \implies \beta(g_2)_{\tilde{R}_2, 1\text{-gen}}^{1\text{-loop}} &= -\frac{8}{3} \left(\frac{g_2^3}{16\pi^2} \right). \end{aligned} \quad (20)$$

Consequently, for the extension of SM with three generations of \tilde{R}_2 , the one-loop beta function of g_2 becomes:

$$\beta(g_2)_{\tilde{R}_2, 3\text{-gen}}^{1\text{-loop}} = \beta(g_2)_{\text{SM}}^{1\text{-loop}} + 3 \Delta\beta(g_2)_{\tilde{R}_2}^{1\text{-loop}}$$

$$= -\frac{5}{3} \left(\frac{g_2^3}{16\pi^2} \right). \tag{21}$$

Similarly, the one-loop beta function for g_2 in the SM plus one generation of scalar triplet leptoquark S_3 can also be expressed as:

$$\beta(g_2)_{S_3,1\text{-gen}}^{1\text{-loop}} = \beta(g_2)_{SM}^{1\text{-loop}} + \Delta\beta(g_2)_{S_3}^{1\text{-loop}}, \tag{22}$$

where $\Delta\beta(g_2)_{S_3}^{1\text{-loop}}$ contains the sole contribution of S_3 with one generation. However, since S_3 is a complex scalar triplet under $SU(2)_L$, it will be in adjoint representation; hence, $T(R_{S_3}) = 2$.²

Furthermore, there will be three copies of S_3 depending on the colour charges. Thus, one finds the contribution of S_3 in the one-loop beta function of g_2 as:

$$\begin{aligned} \Delta\beta(g_2)_{S_3}^{1\text{-loop}} &= \frac{g_2^3}{16\pi^2} \left(\frac{1}{3} \times 3 \times 2 \right) = 2 \left(\frac{g_2^3}{16\pi^2} \right), \\ \implies \beta(g_2)_{S_3,1\text{-gen}}^{1\text{-loop}} &= -\frac{7}{6} \left(\frac{g_2^3}{16\pi^2} \right), \end{aligned} \tag{23}$$

and the one-loop beta function of g_2 with SM plus three generations of S_3 necessarily becomes:

$$\begin{aligned} \beta(g_2)_{S_3,3\text{-gen}}^{1\text{-loop}} &= \beta(g_2)_{SM}^{1\text{-loop}} + 3 \Delta\beta(g_2)_{S_3}^{1\text{-loop}} \\ &= \frac{17}{6} \left(\frac{g_2^3}{16\pi^2} \right). \end{aligned} \tag{24}$$

If the SM is extended with both \tilde{R}_2 and S_3 , the one-loop beta function of g_2 can be calculated as:

$$\begin{aligned} \beta(g_2)_{\tilde{R}_2+S_3,1\text{-gen}}^{1\text{-loop}} &= \beta(g_2)_{SM}^{1\text{-loop}} + \Delta\beta(g_2)_{\tilde{R}_2}^{1\text{-loop}} \\ &+ \Delta\beta(g_2)_{S_3}^{1\text{-loop}} = -\frac{2}{3} \left(\frac{g_2^3}{16\pi^2} \right), \end{aligned} \tag{25}$$

$$\begin{aligned} \beta(g_2)_{\tilde{R}_2+S_3,3\text{-gen}}^{1\text{-loop}} &= \beta(g_2)_{SM}^{1\text{-loop}} + 3 \Delta\beta(g_2)_{\tilde{R}_2}^{1\text{-loop}} \\ &+ 3 \Delta\beta(g_2)_{S_3}^{1\text{-loop}} = \frac{13}{3} \left(\frac{g_2^3}{16\pi^2} \right). \end{aligned} \tag{26}$$

Now, we use SARAH to generate the two-loop contributions. For convenience, we define:

$$\mathcal{X}_a = Y_a Y_a^\dagger \quad \text{and} \quad \tilde{\mathcal{X}}_a = Y_a^\dagger Y_a, \tag{27}$$

where $a \in \{2, 3, \ell, u, d\}$. Thus the beta function of g_2 up to two-loop order for the different models we are working with becomes:

$$\beta(g_2)_{SM}^{2\text{-loop}} = -\frac{19}{6} \left(\frac{g_2^3}{16\pi^2} \right) + \frac{g_2^3}{(16\pi^2)^2} \left[\frac{9}{10} g_1^2 + \frac{35}{6} g_2^2 \right]$$

² If the generators $T_R^{a,b}$ of $SU(N)$ Lie algebra are in adjoint representation, then $T(R) = N$.

Table 1 Initial values for different SM parameters required for RG evolution at electroweak (EW) scale

g_1	g_2	g_3	Y_u^{33}	λ_h
0.46256 ^a	0.64779	1.1666	0.93690	0.12604

^aIn this paper, we have used $SU(5)$ normalization for g_1 , since SARAH inherently uses this convention. However, to achieve results involving the usual g_1 coupling, one has to replace g_1 with $\sqrt{\frac{5}{3}} g_1$ throughout the paper. In that case, the initial value for g_1 would become 0.358297

$$+ 12 g_3^2 - \frac{3}{2} \text{Tr} \left(\frac{1}{3} \mathcal{X}_\ell + \mathcal{X}_u + \mathcal{X}_d \right), \tag{28}$$

$$\begin{aligned} \beta(g_2)_{\tilde{R}_2,1\text{-gen}}^{2\text{-loop}} &= -\frac{8}{3} \left(\frac{g_2^3}{16\pi^2} \right) + \frac{g_2^3}{(16\pi^2)^2} \left[g_1^2 + \frac{37}{3} g_2^2 \right. \\ &+ 20 g_3^2 - \frac{3}{2} \text{Tr} \left(\frac{1}{3} \mathcal{X}_\ell + \mathcal{X}_u + \mathcal{X}_d + \mathcal{X}_2 \right) \left. \right], \end{aligned} \tag{29}$$

$$\begin{aligned} \beta(g_2)_{\tilde{R}_2,3\text{-gen}}^{2\text{-loop}} &= -\frac{5}{3} \left(\frac{g_2^3}{16\pi^2} \right) + \frac{g_2^3}{(16\pi^2)^2} \left[\frac{6}{5} g_1^2 + \frac{76}{3} g_2^2 \right. \\ &+ 36 g_3^2 - \frac{3}{2} \text{Tr} \left(\frac{1}{3} \mathcal{X}_\ell + \mathcal{X}_u + \mathcal{X}_d + \sum_{i=1}^3 \mathcal{X}_{2,i} \right) \left. \right], \end{aligned} \tag{30}$$

$$\begin{aligned} \beta(g_2)_{S_3,1\text{-gen}}^{2\text{-loop}} &= -\frac{7}{6} \left(\frac{g_2^3}{16\pi^2} \right) + \frac{g_2^3}{(16\pi^2)^2} \left[\frac{5}{2} g_1^2 + \frac{371}{6} g_2^2 \right. \\ &+ 44 g_3^2 - \frac{3}{2} \text{Tr} \left(\frac{1}{3} \mathcal{X}_\ell + \mathcal{X}_u + \mathcal{X}_d + 3 \mathcal{X}_3 \right) \left. \right], \end{aligned} \tag{31}$$

$$\begin{aligned} \beta(g_2)_{S_3,3\text{-gen}}^{2\text{-loop}} &= \frac{17}{6} \left(\frac{g_2^3}{16\pi^2} \right) + \frac{g_2^3}{(16\pi^2)^2} \left[\frac{57}{10} g_1^2 + \frac{1043}{6} g_2^2 \right. \\ &+ 108 g_3^2 - \frac{3}{2} \text{Tr} \left(\frac{1}{3} \mathcal{X}_\ell + \mathcal{X}_u + \mathcal{X}_d + 3 \sum_{i=1}^3 \mathcal{X}_{3,i} \right) \left. \right], \end{aligned} \tag{32}$$

$$\begin{aligned} \beta(g_2)_{\tilde{R}_2+S_3,1\text{-gen}}^{2\text{-loop}} &= -\frac{2}{3} \left(\frac{g_2^3}{16\pi^2} \right) + \frac{g_2^3}{(16\pi^2)^2} \left[\frac{13}{5} g_1^2 \right. \\ &+ \frac{205}{3} g_2^2 + 52 g_3^2 \\ &- \frac{3}{2} \text{Tr} \left(\frac{1}{3} \mathcal{X}_\ell + \mathcal{X}_u + \mathcal{X}_d + \mathcal{X}_2 + 3 \mathcal{X}_3 \right) \left. \right], \end{aligned} \tag{33}$$

$$\begin{aligned} \beta(g_2)_{\tilde{R}_2+S_3,3\text{-gen}}^{2\text{-loop}} &= \frac{13}{3} \left(\frac{g_2^3}{16\pi^2} \right) + \frac{g_2^3}{(16\pi^2)^2} \left[6 g_1^2 + \frac{580}{3} g_2^2 \right. \\ &+ 132 g_3^2 \\ &- \frac{3}{2} \text{Tr} \left(\frac{1}{3} \mathcal{X}_\ell + \mathcal{X}_u + \mathcal{X}_d + \sum_{i=1}^3 \mathcal{X}_{2,i} + 3 \sum_{i=1}^3 \mathcal{X}_{3,i} \right) \left. \right]. \end{aligned} \tag{34}$$

In Eqs. (30), (32) and (34), the index i represents the generation of the leptoquark. Now, as we have defined $\Delta\beta(g_2)$ for one loop in Eqs. (19) and (22), one can define it for two

loops in similar fashion. Then one can easily verify that the above-described two-loop beta functions obey the following relations:

$$\beta(g_2)_{\tilde{R}_{2,3\text{-gen}}}^{2\text{-loop}} = \beta(g_2)_{\text{SM}}^{2\text{-loop}} + \sum_{i=1}^3 \left[\Delta\beta(g_2)_{\tilde{R}_2}^{2\text{-loop}} \right]_i, \tag{35}$$

$$\beta(g_2)_{\tilde{S}_{3,3\text{-gen}}}^{2\text{-loop}} = \beta(g_2)_{\text{SM}}^{2\text{-loop}} + \sum_{i=1}^3 \left[\Delta\beta(g_2)_{\tilde{S}_3}^{2\text{-loop}} \right]_i, \tag{36}$$

$$\beta(g_2)_{\tilde{R}_2+\tilde{S}_3,1\text{-gen}}^{2\text{-loop}} = \beta(g_2)_{\text{SM}}^{2\text{-loop}} + \Delta\beta(g_2)_{\tilde{R}_2}^{2\text{-loop}} + \Delta\beta(g_2)_{\tilde{S}_3}^{2\text{-loop}}, \tag{37}$$

$$\beta(g_2)_{\tilde{R}_2+\tilde{S}_3,3\text{-gen}}^{2\text{-loop}} = \beta(g_2)_{\text{SM}}^{2\text{-loop}} + \sum_{i=1}^3 \left[\Delta\beta(g_2)_{\tilde{R}_2}^{2\text{-loop}} \right]_i + \sum_{i=1}^3 \left[\Delta\beta(g_2)_{\tilde{S}_3}^{2\text{-loop}} \right]_i. \tag{38}$$

where $[\beta]_i$ for any parameter indicates the beta function of that parameter with the replacement of $f(Y_\gamma, X_\gamma, \tilde{X}_\gamma, \lambda_\gamma, \tilde{\lambda}_\gamma)$ to $f(Y_{\gamma,i}, X_{\gamma,i}, \tilde{X}_{\gamma,i}, \lambda_{\gamma,i}^{ii}, \tilde{\lambda}_{\gamma,i}^{ii})$ with $\gamma \in \{2, 3\}$ and i representing the generation. Similar notation is applicable for $\Delta\beta$.

3.1.2 Scale variation of g_2

Using the above Eqs.³ (28)–(34), we plot the dependence of coupling g_2 for different models on the energy scale μ in Fig. 1. While Fig. 1a depicts the behaviour of g_2 at one loop, Fig. 1b illustrates the same for the two-loop level. The SM is represented by the green curve; the red and yellow lines depict the extension of the SM with one and three generations of \tilde{R}_2 , respectively; the blue and cyan lines indicate the addition of one and three generations of \tilde{S}_3 , respectively, to SM; finally, the brown and dashed black curves illustrate the SM extension with one and three generations of both doublet and triplet leptoquarks, respectively. The initial two-loop values at the electroweak (EW) scale for gauge couplings g_1, g_2, g_3 , Higgs quartic coupling λ_h and top-quark Yukawa coupling Y_u^{33} are given in Table 1, with the contributions from other Yukawa couplings neglected [143, 144]. Although the plots are made assuming Y_ϕ to be 0.1, they do not change significantly with the alteration of Y_ϕ , since the dominant contribution in the two-loop beta function of g_2 comes from different

gauge couplings, as can be realized from Eqs. (28)–(34). This statement holds for other gauge couplings as well.

In Fig. 1a, b, we present the variation in g_2 with respect to the scale μ at the one- and two-loop levels for the above-mentioned leptoquark scenarios. The ordering of different curves in Fig. 1 is mainly controlled by the one-loop beta functions for different models which are presented in Eqs. (18)–(26). The one-loop beta function of g_2 under SM is $-\frac{19}{6}(\frac{g_2^3}{16\pi^2})$, which is enhanced to $-\frac{8}{3}(\frac{g_2^3}{16\pi^2})$ and $-\frac{5}{3}(\frac{g_2^3}{16\pi^2})$ for one and three generations of \tilde{R}_2 , respectively. However, due to the greater number of components of leptoquarks in \tilde{S}_3 , the positive contributions will be greater. The one-loop beta functions of g_2 for \tilde{S}_3 with one and three generations become $-\frac{7}{6}(\frac{g_2^3}{16\pi^2})$ and $\frac{17}{6}(\frac{g_2^3}{16\pi^2})$. For the combined scenario of these two leptoquarks, the positive effects are even stronger. For one and three generations of the combined case, the beta functions become $-\frac{2}{3}(\frac{g_2^3}{16\pi^2})$ and $\frac{13}{3}(\frac{g_2^3}{16\pi^2})$, respectively. It is interesting to note that except for three generations of \tilde{S}_3 (cyan line) and $\tilde{R}_2 + \tilde{S}_3$ (black dotted curve), coupling, g_2 decreases monotonically for all scenarios due to the negative sign in the one-loop beta function, ensuring asymptotic freedom of weak interaction. However, when considering one-loop effects only, Planck scale perturbativity is achieved in all the scenarios, since the Landau pole in the two above-mentioned cases appears beyond the Planck scale, as can be seen from Fig. 1a. On the other hand, due to the positive value of the one-loop beta function, the gauge coupling g_2 in the three generations of the \tilde{S}_3 (cyan) and $\tilde{R}_2 + \tilde{S}_3$ (black dashed) models increases monotonically. Now, for the two-loop case, all the models acquire additional positive effects that push the RG evolution curves upwards. Therefore, the two-loop beta functions of the \tilde{S}_3 and $\tilde{R}_2 + \tilde{S}_3$ models hit the Landau pole at lower scales, i.e. $10^{19.7}$ GeV (just above the Planck scale) and $10^{14.4}$ GeV (below the GUT scale), respectively, as can be observed from Fig. 1(c).

3.1.3 Beta function of g_3 : a brief review

In the case of the SM, as the scalar and leptons are colour neutral, the one-loop beta function of strong coupling g_3 receives contributions only from six quarks which are essentially Dirac fermionic colour triplets under the $SU(3)$ gauge group. Thus, substituting $T(R_f) = 1/2$ and $C_2(G) = 3$ in Eq. (17), we get:

$$\begin{aligned} \beta(g_3)_{\text{SM}}^{1\text{-loop}} &= \frac{g_3^3}{16\pi^2} \left[\left(\frac{4}{3} \times 6 \times \frac{1}{2} \right) - \left(\frac{11}{3} \times 3 \right) \right] \\ &= -7 \left(\frac{g_3^3}{16\pi^2} \right). \end{aligned} \tag{39}$$

Now, all the leptoquarks are colour triplet complex scalars, i.e. they are in fundamental representation of $SU(3)$ enfor-

³ Actually, one needs to consider running all the couplings in a model simultaneously, since the above expressions for two-loop beta functions are coupled equations.

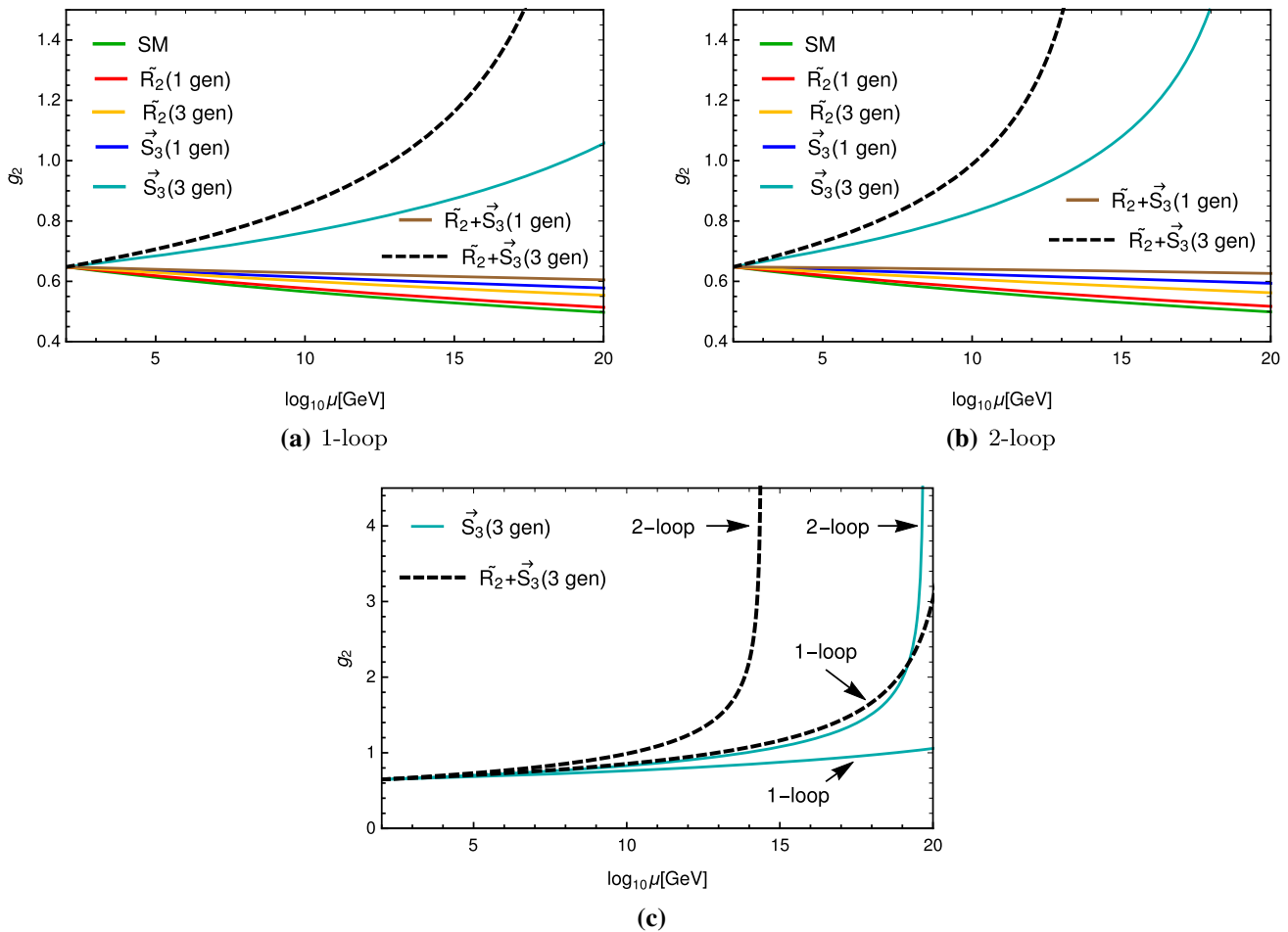


Fig. 1 Running of gauge coupling g_2 with the energy scale μ for SM and different leptoquark scenarios with one loop and two loops. The green curve represents the SM; the red and yellow curves signify the extension of the SM with one and three generations of \tilde{R}_2 , respectively; the addition of one and three generations of S_3 to SM are indicated by

the blue and cyan lines, respectively; the brown and dashed black curves illustrate the SM extension with one and three generations of both \tilde{R}_2 and S_3 , respectively. The initial values for the SM parameters are listed in Table 1 along with $Y_\phi = 0.1$

ing $T(R_s) = 1/2$. However, for the doublet leptoquark we have two such copies of triplets, namely $\tilde{R}_2^{2/3}$ and $\tilde{R}_2^{1/3}$, whereas there are three scalar triplets for S_3 , namely $S_3^{4/3}$, $S_3^{2/3}$ and $S_3^{1/3}$. Thus the sole contribution of one generation $\tilde{R}_2^{2/3}$ and S_3 in the beta function of g_3 , as described in the previous subsection for g_2 , can be written as:

$$\Delta\beta(g_3)_{\tilde{R}_2}^{1\text{-loop}} = \frac{g_3^3}{16\pi^2} \left(\frac{1}{3} \times 2 \times \frac{1}{2} \right) = \frac{1}{3} \left(\frac{g_3^3}{16\pi^2} \right), \quad (40)$$

$$\Delta\beta(g_3)_{S_3}^{1\text{-loop}} = \frac{g_3^3}{16\pi^2} \left(\frac{1}{3} \times 3 \times \frac{1}{2} \right) = \frac{1}{2} \left(\frac{g_3^3}{16\pi^2} \right). \quad (41)$$

Therefore, the one-loop beta functions of strong coupling g_3 for different SM extensions with \tilde{R}_2 and S_3 are as follows:

$$\begin{aligned} \beta(g_3)_{\tilde{R}_2, 1\text{-gen}}^{1\text{-loop}} &= \beta(g_3)_{SM}^{1\text{-loop}} + \Delta\beta(g_3)_{\tilde{R}_2}^{1\text{-loop}} \\ &= -\frac{20}{3} \left(\frac{g_3^3}{16\pi^2} \right), \end{aligned} \quad (42)$$

$$\begin{aligned} \beta(g_3)_{\tilde{R}_2, 3\text{-gen}}^{1\text{-loop}} &= \beta(g_3)_{SM}^{1\text{-loop}} + 3 \Delta\beta(g_3)_{\tilde{R}_2}^{1\text{-loop}} \\ &= -6 \left(\frac{g_3^3}{16\pi^2} \right), \end{aligned} \quad (43)$$

$$\begin{aligned} \beta(g_3)_{S_3, 1\text{-gen}}^{1\text{-loop}} &= \beta(g_3)_{SM}^{1\text{-loop}} + \Delta\beta(g_3)_{S_3}^{1\text{-loop}} \\ &= -\frac{13}{2} \left(\frac{g_3^3}{16\pi^2} \right), \end{aligned} \quad (44)$$

$$\begin{aligned} \beta(g_3)_{S_3, 3\text{-gen}}^{1\text{-loop}} &= \beta(g_3)_{SM}^{1\text{-loop}} + 3 \Delta\beta(g_3)_{S_3}^{1\text{-loop}} \\ &= -\frac{11}{2} \left(\frac{g_3^3}{16\pi^2} \right), \end{aligned} \quad (45)$$

$$\begin{aligned} \beta(g_3)_{\tilde{R}_2+S_3, 1\text{-gen}}^{1\text{-loop}} &= \beta(g_3)_{SM}^{1\text{-loop}} + \Delta\beta(g_3)_{\tilde{R}_2}^{1\text{-loop}} \\ &\quad + \Delta\beta(g_3)_{S_3}^{1\text{-loop}} = -\frac{37}{6} \left(\frac{g_3^3}{16\pi^2} \right), \end{aligned} \quad (46)$$

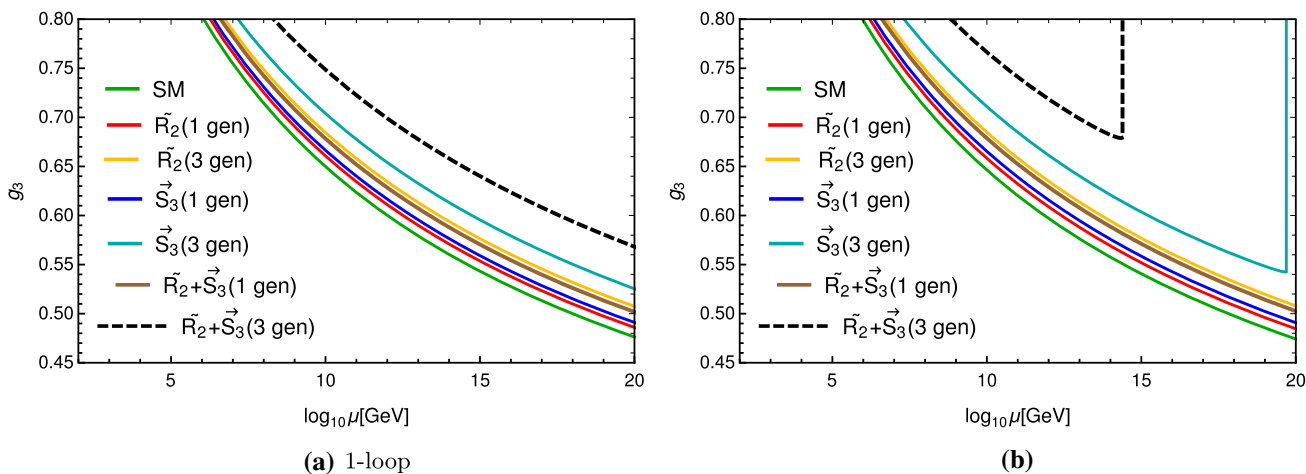


Fig. 2 Running of gauge coupling g_3 with the energy scale μ for different leptokuark models at one-loop and two-loop order. The green curve represents SM; the red and yellow ones signify the extension of SM with one and three generations of \tilde{R}_2 , respectively; the addition of one and three generations of \tilde{S}_3 to SM is indicated by the blue and

cyan lines, respectively; the brown and dashed black curves illustrate the SM extension with one and three generations of both \tilde{R}_2 and \tilde{S}_3 , respectively. The initial values for SM parameters are listed in Table 1 along with $Y_\phi = 0.1$

$$\beta(g_3)_{\tilde{R}_2+\tilde{S}_3,3\text{-gen}}^{1\text{-loop}} = \beta(g_3)_{\text{SM}}^{1\text{-loop}} + 3 \Delta\beta(g_3)_{\tilde{R}_2}^{1\text{-loop}} + 3 \Delta\beta(g_3)_{\tilde{S}_3}^{1\text{-loop}} = -\frac{9}{2} \left(\frac{g_3^3}{16\pi^2} \right). \tag{47}$$

The two-loop beta functions of g_3 for all these models are listed in Appendix A.

3.1.4 Scale variation of g_3

The variations in strong gauge coupling g_3 at the one-loop and two-loop levels with energy scale μ for different models are depicted in Fig. 2. The left panel shows the one-loop results, while the right panel indicates the full two-loop contributions. The same colour code as mentioned in previous section is also followed here. The relative positions of the different curves in this plot are mainly determined by coefficients of $(\frac{g_3^3}{16\pi^2})$ in the one-loop beta functions, given by Eqs. (39)–(47). This coefficient for SM (green) is -7 , which is enhanced to $-20/3$, $-13/2$ and $-37/6$ for the \tilde{R}_2 (red), \tilde{S}_3 (blue) and the combined scenario (brown) for one generation, respectively. For the case of three generations, this factor receives even more contributions to become -6 , $-11/2$ and $-9/2$, respectively, for the \tilde{R}_2 (yellow), \tilde{S}_3 (cyan) and the combined scenario (black dashed). As the one-loop beta function of g_3 for all the models remains negative, g_3 decreases gradually with the increase in energy, showing asymptotic freedom. As can be seen from Fig. 2a, all the models show Planck scale perturbativity at one-loop order. At two-loop order, all of these curves shift upwards due to the additional positive contributions as shown in Appendix A. All but two of the models exhibit no unusual behaviour.

However, as g_2 hits the Landau pole at $10^{19.7}$ GeV and $10^{14.4}$ GeV for three generations of the \tilde{S}_3 (cyan) and $\tilde{R}_2 + \tilde{S}_3$ (black dashed) models, respectively, g_3 shows sudden divergence for these two models at the above-mentioned energy scales (see Fig. 2b).

3.1.5 Beta function of g_1 : a brief review

The one-loop beta function for $U(1)_Y$ gauge coupling g_1 is given by:

$$\beta(g_1)^{1\text{-loop}} = \frac{3}{5} \left(\frac{g_1^3}{16\pi^2} \right) \left[\frac{2}{3} \sum_f \mathcal{Y}_f^2 + \frac{1}{3} \sum_s \mathcal{Y}_s^2 \right], \tag{48}$$

where $\mathcal{Y}_{f,s}$ signify the hypercharge of the Weyl fermions and the scalars, respectively.^{4,5} The 3/5 factor arises because of $SU(5)$ normalization of the coupling g_1 . On the other hand, since the $U(1)_Y$ gauge boson interacts with left- and right-handed fermions with different hypercharges, one has to sum over the contributions from all the Weyl fermions, and hence the 2/3 factor appears for the fermionic effects instead of 4/3. In the SM, there are 18 left-handed quarks (six flavours, three colours) with hypercharge 1/6, nine right-handed up-type quarks (three generations, three colours) with hypercharge

⁴ To relate electromagnetic charge Q with hypercharge \mathcal{Y} , we have followed the convention: $Q = \mathcal{I}_3 + \mathcal{Y}$.

⁵ One can easily compare the above formula with the one-loop beta function for the electromagnetic coupling e given by: $\beta(e)^{1\text{-loop}} = \frac{e^3}{16\pi^2} \left[\frac{4}{3} \sum_f Q_f^2 + \frac{1}{3} \sum_s Q_s^2 \right]$ where $Q_{f,s}$ are the electromagnetic charges of Dirac fermions and scalars.

2/3, nine right-handed down-type quarks (three generations, three colours) with hypercharge $-1/3$, six left-handed leptons with $\mathcal{Y}_f = 1/2$ and three right-handed charged leptons with $\mathcal{Y}_f = -1$. Additionally, there are two scalars (H^+ and H^0 , the components of scalar doublet H), each with $\mathcal{Y}_s = 1/2$. Thus the one-loop beta function for g_1 in the SM becomes:

$$\beta(g_1)_{\text{SM}}^{1\text{-loop}} = \frac{3}{5} \left(\frac{g_1^3}{16\pi^2} \right) \left[\frac{2}{3} \times \left(\frac{1}{2} + 4 + 1 + \frac{3}{2} + 3 \right) + \frac{1}{3} \times \frac{1}{2} \right] = \frac{41}{10} \left(\frac{g_1^3}{16\pi^2} \right). \quad (49)$$

Now, for SM plus one generation of \tilde{R}_2 , contribution from six scalars (two flavours, three colours) with hypercharge $1/6$ needs to be added to the SM contribution. Similarly, the effects of nine scalars (three flavours, three colours) with $\mathcal{Y}_s = 1/3$ must be considered when dealing with SM extension by one generation of S_3 . Thus the sole contribution from one generation of \tilde{R}_2 and S_3 to the one-loop beta function of g_1 can be calculated as:

$$\Delta\beta(g_1)_{\tilde{R}_2}^{1\text{-loop}} = \frac{3}{5} \left(\frac{g_1^3}{16\pi^2} \right) \left[\frac{1}{3} \times 6 \times \frac{1}{36} \right] = \frac{1}{30} \left(\frac{g_1^3}{16\pi^2} \right), \quad (50)$$

$$\Delta\beta(g_1)_{S_3}^{1\text{-loop}} = \frac{3}{5} \left(\frac{g_1^3}{16\pi^2} \right) \left[\frac{1}{3} \times 9 \times \frac{1}{9} \right] = \frac{1}{5} \left(\frac{g_1^3}{16\pi^2} \right), \quad (51)$$

and hence, the one-loop beta function of g_1 for different models we considered becomes:

$$\begin{aligned} \beta(g_1)_{\tilde{R}_2, 1\text{-gen}}^{1\text{-loop}} &= \beta(g_1)_{\text{SM}}^{1\text{-loop}} + \Delta\beta(g_1)_{\tilde{R}_2}^{1\text{-loop}} \\ &= \frac{62}{15} \left(\frac{g_1^3}{16\pi^2} \right), \end{aligned} \quad (52)$$

$$\begin{aligned} \beta(g_1)_{\tilde{R}_2, 3\text{-gen}}^{1\text{-loop}} &= \beta(g_1)_{\text{SM}}^{1\text{-loop}} + 3 \Delta\beta(g_1)_{\tilde{R}_2}^{1\text{-loop}} \\ &= \frac{21}{5} \left(\frac{g_1^3}{16\pi^2} \right), \end{aligned} \quad (53)$$

$$\begin{aligned} \beta(g_1)_{S_3, 1\text{-gen}}^{1\text{-loop}} &= \beta(g_1)_{\text{SM}}^{1\text{-loop}} + \Delta\beta(g_1)_{S_3}^{1\text{-loop}} \\ &= \frac{43}{10} \left(\frac{g_1^3}{16\pi^2} \right), \end{aligned} \quad (54)$$

$$\begin{aligned} \beta(g_1)_{S_3, 3\text{-gen}}^{1\text{-loop}} &= \beta(g_1)_{\text{SM}}^{1\text{-loop}} + 3 \Delta\beta(g_1)_{S_3}^{1\text{-loop}} \\ &= \frac{47}{10} \left(\frac{g_1^3}{16\pi^2} \right), \end{aligned} \quad (55)$$

$$\begin{aligned} \beta(g_1)_{\tilde{R}_2 + S_3, 1\text{-gen}}^{1\text{-loop}} &= \beta(g_1)_{\text{SM}}^{1\text{-loop}} + \Delta\beta(g_1)_{\tilde{R}_2}^{1\text{-loop}} \\ &\quad + \Delta\beta(g_1)_{S_3}^{1\text{-loop}} = \frac{13}{3} \left(\frac{g_1^3}{16\pi^2} \right), \end{aligned} \quad (56)$$

$$\begin{aligned} \beta(g_1)_{\tilde{R}_2 + S_3, 3\text{-gen}}^{1\text{-loop}} &= \beta(g_1)_{\text{SM}}^{1\text{-loop}} + 3 \Delta\beta(g_1)_{\tilde{R}_2}^{1\text{-loop}} \\ &\quad + 3 \Delta\beta(g_1)_{S_3}^{1\text{-loop}} = \frac{24}{5} \left(\frac{g_1^3}{16\pi^2} \right). \end{aligned} \quad (57)$$

The two-loop beta functions of g_1 for all these models are listed in Appendix B.

3.1.6 Scale variation of g_1

The variations in g_1 with the energy scale μ are displayed in the Fig. 3. The left panel illustrates the one-loop effects and the right panel demonstrates the two-loop effects. The colour codes are same as mentioned before. Likewise, the positions of different curves are mainly controlled by the one-loop beta functions, given by Eqs. (49)–(57). The coefficient of $(g_1^3/16\pi^2)$ in the SM scenario is $41/10$, which is enhanced to $62/15$ and $21/5$ for one (red) and three (yellow) generations of \tilde{R}_2 , respectively. For S_3 with one (blue) and three (cyan) generations, this factor increases to $43/10$ and $47/10$, respectively. For the combined scenario with one (brown) and three generations (black dashed), this prefactor of $(g_1^3/16\pi^2)$ in the one-loop beta function of g_1 becomes $13/3$ and $24/5$, respectively. Since the one-loop beta functions for all the models are positive, g_1 increases moderately with energy. There is also no divergence for one-loop running of g_1 in any of the models up to the Planck scale, which can be verified from Fig. 3a. Furthermore, the two-loop beta function of g_1 receives additional positive contributions, presented in Appendix B, which moves all the curves of Fig. 3a in a slightly upward direction, resulting in Fig. 3b. Although all the other scenarios behave smoothly when taking into account the two-loop corrections, g_1 for three generations of S_3 (cyan) and $\tilde{R}_2 + S_3$ (black dashed) models goes to infinity abruptly at $10^{19.7}$ GeV and $10^{14.4}$ GeV, respectively, due to the divergence of g_2 .

Thus, we find that the running of gauge couplings at two-loop order for different leptoquark models is predominantly regulated by the corresponding one-loop beta functions, which are entirely reliant on the properties of the gauge group and the number of different types of particles existing in the model. The two-loop corrections insert additional positive contributions to the running of the gauge couplings. The Yukawa couplings of the SM as well as of leptoquarks affect the RG evolution of gauge couplings only at two-loop order, and therefore with the changes in Yukawa couplings of leptoquarks, we do not observe any significant changes. However, it is interesting to note that Higgs-leptoquark quartic couplings do not appear explicitly in the two-loop beta functions of the gauge couplings at all. It is worth mentioning again that the demand of Planck scale perturbativity rules out the three generations of the $\tilde{R}_2 + S_3$ scenario due to the appearance of divergences at much lower scale in the two-loop running

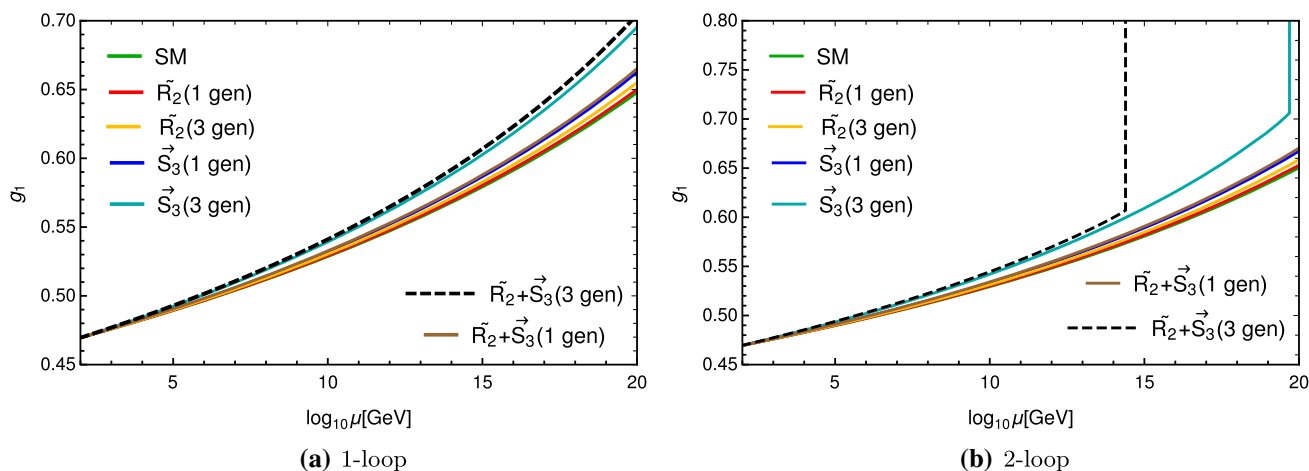


Fig. 3 Running of gauge coupling g_1 with the energy scale μ for different leptokuark models at one-loop and two-loop order. The green curve represents SM; the red and yellow ones signify extension of SM with one and three generations of \tilde{R}_2 , respectively; addition of one and three generations of \tilde{S}_3 to SM are indicated by the blue and cyan

lines, respectively; the brown and dashed black curves illustrate the SM extension with one and three generations of both \tilde{R}_2 and \tilde{S}_3 , respectively. The initial values for SM parameters are listed in Table 1 along with $Y_\phi = 0.1$

of the gauge coupling g_2 . On the other hand, the model with three generations of \tilde{S}_3 is marginally allowed from Planck scale stability since the gauge coupling g_2 hits the Landau pole at slightly higher energy scale. These divergences force the other gauge couplings as well as the Yukawa couplings of the top quark and leptokuarks (see Appendix C and Appendix D) for these models to diverge at the two-loop level.

3.2 Higgs-leptoquark quartic couplings

Now, we step forward to investigate the perturbative bounds on Higgs-leptoquark quartic couplings.

3.2.1 Perturbativity of \tilde{R}_2

In this section, we study the RG evolution of Higgs-lepton quark quartic couplings of leptokuark \tilde{R}_2 , i.e. λ_2 and $\tilde{\lambda}_2$. As already mentioned, these terms should always remain below 4π to maintain the perturbativity of the theory. The one-loop beta functions for these two parameters are given below:

$$\beta(\lambda_2)_{\tilde{R}_2, 1\text{-gen}}^{1\text{-loop}} = \frac{1}{16\pi^2} \left[4\lambda_2^2 + 2\tilde{\lambda}_2^2 + \frac{3}{10} \left(\frac{1}{10}g_1^4 - g_1^2g_2^2 + \frac{15}{2}g_2^4 \right) - \lambda_2 \left(g_1^2 + 9g_2^2 + 8g_3^2 \right) + 12\lambda_h \left(\lambda_2 + \frac{1}{3}\tilde{\lambda}_2 \right) + 6\lambda_2 \text{Tr} \left(X_u + X_d + \frac{1}{3}X_l + \frac{1}{3}X_2 \right) - 4\text{Tr} \left(X_2X_d + \tilde{X}_l\tilde{X}_2 \right) \right], \tag{58}$$

$$\beta(\tilde{\lambda}_2)_{\tilde{R}_2, 1\text{-gen}}^{1\text{-loop}} = \frac{1}{16\pi^2} \left[\frac{3}{5}g_1^2g_2^2 + 4\text{Tr} \left(\tilde{X}_2\tilde{X}_l \right) + \tilde{\lambda}_2 \left\{ 8\lambda_2 \right. \right.$$

$$\left. + 4\tilde{\lambda}_2 - g_1^2 - 9g_2^2 - 8g_3^2 + 4\lambda_h + 6\text{Tr} \left(X_u + X_d + \frac{1}{3}X_l + \frac{1}{3}X_2 \right) \right], \tag{59}$$

For the three-generation case, λ_2 and $\tilde{\lambda}_2$ become two 3×3 matrices whose ij -th element indicates the quartic coupling of the i -th and j -th generations of \tilde{R}_2 with two Higgs fields. However, as mentioned earlier, we restrict our parameter space with no mixing among the generations of leptokuarks at the initial scale; therefore, λ_2 and $\tilde{\lambda}_2$ become two diagonal matrices. The one-loop beta functions for these two parameters are simply given by:

$$\beta(\lambda_2^{ii})_{\tilde{R}_2, 3\text{-gen}}^{1\text{-loop}} = \left[\beta(\lambda_2)_{\tilde{R}_2, 1\text{-gen}}^{1\text{-loop}} \right]_i$$

$$\beta(\tilde{\lambda}_2^{ii})_{\tilde{R}_2, 3\text{-gen}}^{1\text{-loop}} = \left[\beta(\tilde{\lambda}_2)_{\tilde{R}_2, 1\text{-gen}}^{1\text{-loop}} \right]_i \tag{60}$$

The full two-loop beta functions for these two parameters with both one and three generations are presented in Appendix E.

Now, we study the variation in quartic coupling between the leptokuark and Higgs with perturbative scale, i.e. the scale at which any of the coupling diverges. The variations in the quartic couplings λ_2 and $\tilde{\lambda}_2$ for three generations of doublet leptokuark are explained in Fig.4. In the first two plots, Fig. 4a, b, λ_2 corresponds to the quartic coupling term for one particular generation of leptokuark while λ_2^{ij} denotes the remaining generations of λ_2 , and all the generations of the other quartic coupling term $\tilde{\lambda}_2$ are designated as $\tilde{\lambda}_2^{ii}$. Similarly, for $\tilde{\lambda}_2$ variation in Fig. 4c, d, $\tilde{\lambda}_2$ corresponds to any

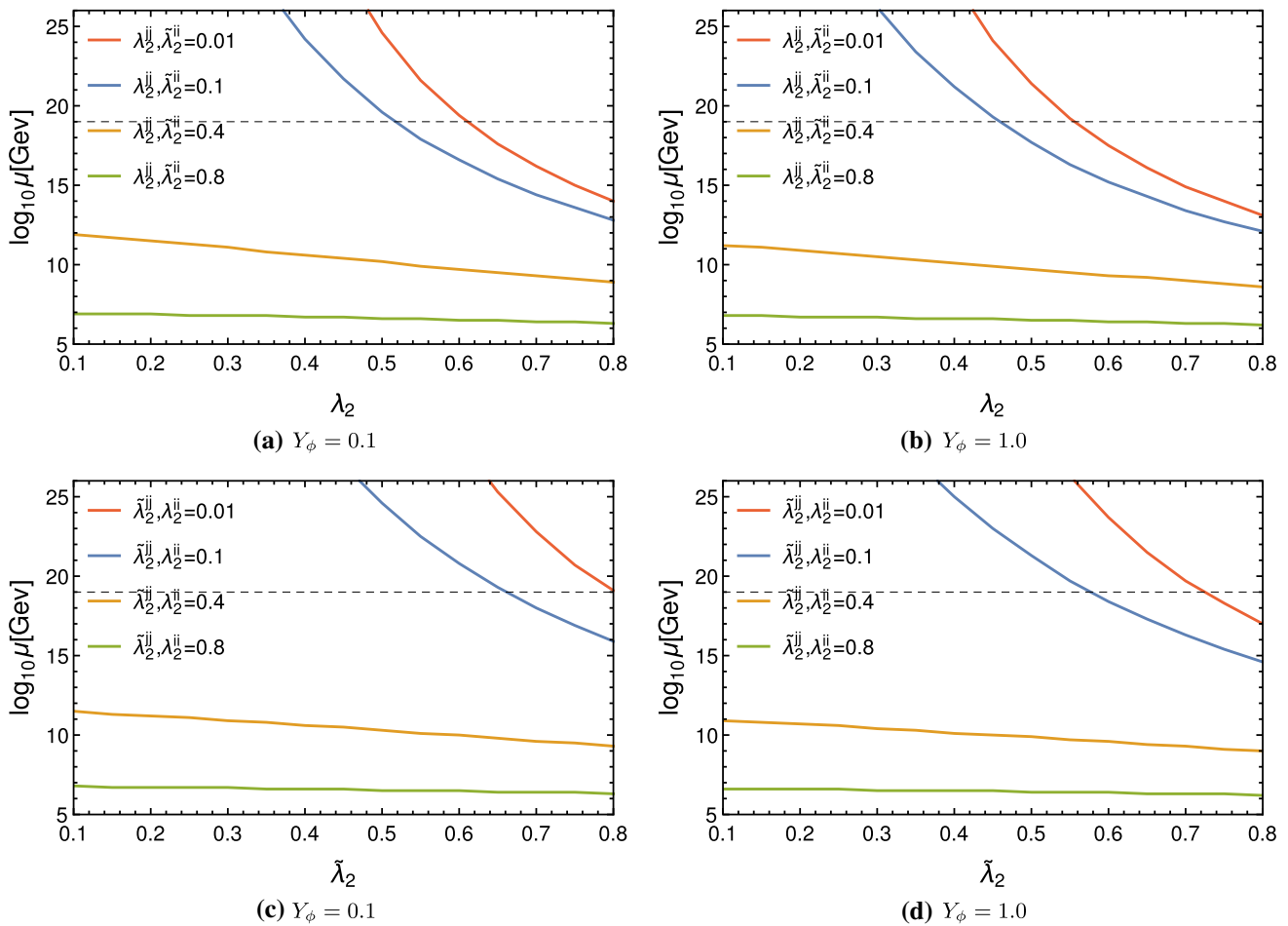


Fig. 4 Variation in leptoquark-Higgs quartic coupling λ_2 and $\tilde{\lambda}_2$ with perturbative scale for the doublet leptoquark \tilde{R}_2 with three generations. For plots in the first row, λ_2 variation is considered for any one generation of the leptoquark, and other generations are defined as λ_2^{jj} . The other quartic couplings are designated by $\tilde{\lambda}_2^{jj}$ for all three generations of leptoquark. The variations are taken for four different EW values of quartic couplings, i.e. 0.01, 0.1, 0.4 and 0.8, which are depicted by red,

blue, orange and green curves, respectively. Similarly, for the plots in the second row, $\tilde{\lambda}_2$ describes the variation in any particular generation, and the remaining generations are denoted by $\tilde{\lambda}^{jj}$. The other quartic coupling terms λ_2^{ii} are defined for all three generations of leptoquark. The variations are considered for lower and higher values of Y_ϕ , i.e. 0.1 (left) and 1.0 (right)

particular generation of leptoquark while the remaining generations are denoted by $\tilde{\lambda}_2^{jj}$, and the other quartic coupling terms λ_2^{ii} signify λ_2 for all three generations. The plots in the left panel indicate a relatively low value of Yukawa, i.e. $Y_\phi = 0.1$, whereas the same in the right panel illustrate the variation in the mentioned couplings for a higher value of Yukawa, i.e. $Y_\phi = 1.0$.

In the first two plots, the initial value of λ_2 is varied from 0.1 to 0.8 keeping the values for other quartic couplings at EW scale as 0.01, 0.1, 0.4 and 0.8, which are depicted by red, blue, orange and green curves, respectively. As can be observed from Eqs. (58) and (60), the one-loop beta function of λ_2 receives enhanced contributions from positive-valued $\tilde{\lambda}_2$, and hence λ_2 reaches non-perturbativity quickly for larger values of $\tilde{\lambda}_2$. It should be noted from Fig: 4a that for $(\lambda_2^{jj}, \tilde{\lambda}_2^{ii}) =$

0.01 and 0.1 at the EW scale, the theory remains perturbative up to Planck scale for $\lambda_2 \leq 0.62$ and 0.52 , respectively, with $Y_\phi = 0.1$. As we increase the EW values to 0.4 and 0.8, the positive contribution from quartic couplings makes the theory non-perturbative at $\sim 10^{12}$ GeV, 10^7 GeV for lower initial values of λ_2 . For higher EW values of λ_2 , this perturbative scale decreases slowly. The variation in λ_2 with perturbative scale for $Y_\phi = 1.0$, as displayed in Fig. 4b, looks quite similar to the previous case. However, as can be seen from Eqs. (58) and (60), the one-loop beta function of λ_2 obtains positive contributions from the $2\lambda_2 \text{Tr } \mathcal{X}_2$ term (since Y_d and Y_l are negligible), and therefore λ_2 becomes non-perturbative at a slightly lower energy scale than in the previous case. In this case, λ_2 is bounded above to 0.56 and 0.47 for EW values of other quartic couplings $\lambda_2^{jj}, \tilde{\lambda}_2^{ii}$ to be

0.01 and 0.1, respectively. Further increases in EW values to 0.4 and 0.8 make the theory non-perturbative around $10^{11.2}$ GeV and $10^{6.9}$ GeV, respectively, for lower initial values of λ_2 , and the scale diminishes gently with higher initial values of λ_2 . It is worth mentioning that the non-perturbativity of λ_2 and $\tilde{\lambda}_2$, attained with three generations of \tilde{R}_2 , is not a result of any Landau pole, which is also apparent from the different positioning of the non-perturbative scales compared to that of the gauge couplings.

In a similar fashion, $\tilde{\lambda}_2$ is altered gradually from 0.1 to 0.8 in the last two plots, fixing the values of other quartic couplings as 0.01, 0.1, 0.4 and 0.8, which are depicted by red, blue, orange and green curves, respectively. In this case, λ_2 provides a positive effect in the running of $\tilde{\lambda}_2$, see Eqs. (59) and (60); therefore, $\tilde{\lambda}_2$ moves to the non-perturbative region more rapidly for higher values of λ_2 . On the other hand, Y_2 also contributes positively through the term $2\tilde{\lambda}_2 \text{Tr}\mathcal{X}_2$, and hence λ_2 hits non-perturbativity at slightly lower energy scale for higher Yukawa coupling. From Fig. 4(c) we see that the demand of Planck scale perturbativity constrains $\tilde{\lambda}_2$ to be smaller than 0.8 and 0.66 if the EW values of other quartic couplings ($\tilde{\lambda}_2^{jj}, \lambda_2^{ii}$) are set as 0.01 and 0.1 respectively, with $Y_\phi = 0.1$. With higher values of $\tilde{\lambda}_2^{jj}, \lambda_2^{ii}$ at EW scale, i.e. 0.4 and 0.8, the model becomes non-perturbative at much lower energy than Planck scale. From Fig. 4d, in comparison with Fig. 4c, we observe that $\tilde{\lambda}_2$ is restricted to slightly lower values, i.e. 0.73 and 0.59, if we begin with 0.01 and 0.1, respectively, for the EW values of other quartic couplings along with $Y_\phi = 1.0$. The statement with higher initial values of the quartic couplings remains valid in this scenario as well.

3.2.2 Perturbativity of S_3

In this section, we scrutinize the RG evolution of Higgs-leptoquark quartic couplings for S_3 , namely λ_3 and $\tilde{\lambda}_3$. These two parameters also should be bounded above by 4π . The one-loop beta functions for these two parameters in the one-generation case are given below:

$$\begin{aligned} \beta(\lambda_3)_{S_3,1\text{-gen}}^{1\text{-loop}} &= \frac{1}{4\pi^2} \left[\lambda_3^2 + \frac{1}{4} \tilde{\lambda}_3^2 + \frac{3}{4} \left(\frac{1}{25} g_1^4 - \frac{2}{5} g_1^2 g_2^2 + 2g_2^4 \right) \right. \\ &\quad - \frac{1}{4} \lambda_3 \left(\frac{13}{10} g_1^2 + \frac{33}{2} g_2^2 + 8g_3^2 \right) + 3\lambda_h \left(\lambda_3 + \frac{1}{3} \tilde{\lambda}_3 \right) \\ &\quad \left. + \frac{3}{2} \lambda_3 \text{Tr} \left(\mathcal{X}_u + \mathcal{X}_d + \frac{1}{3} \mathcal{X}_l + \frac{1}{3} \mathcal{X}_3 \right) - \text{Tr} \left(\tilde{\mathcal{X}}_3 \tilde{\mathcal{X}}_l + \mathcal{X}_3 \tilde{\mathcal{X}}_d^T \right) \right], \end{aligned} \tag{61}$$

$$\begin{aligned} \beta(\tilde{\lambda}_3)_{S_3,1\text{-gen}}^{1\text{-loop}} &= \frac{1}{4\pi^2} \left[\tilde{\lambda}_3^2 + 2\lambda_3 \tilde{\lambda}_3 + \lambda_h \tilde{\lambda}_3 + \frac{3}{5} g_1^2 g_2^2 \right. \\ &\quad - \frac{1}{4} \tilde{\lambda}_3 \left(\frac{13}{10} g_1^2 + \frac{33}{2} g_2^2 + 8g_3^2 \right) + \frac{3}{2} \tilde{\lambda}_3 \text{Tr} \left(\mathcal{X}_u + \mathcal{X}_d \right. \\ &\quad \left. + \frac{1}{3} \mathcal{X}_l + \frac{1}{3} \mathcal{X}_3 \right) + \text{Tr} \left(\tilde{\mathcal{X}}_3 \tilde{\mathcal{X}}_l + \mathcal{X}_3 \tilde{\mathcal{X}}_d^T - \mathcal{X}_3 \tilde{\mathcal{X}}_u^T \right) \left. \right] \end{aligned} \tag{62}$$

Like the doublet leptoquark case, for the three-generation scenario, λ_3 and $\tilde{\lambda}_3$ become two 3×3 matrices whose ij -th element indicates the quartic coupling of i -th and j -th generations of S_3 with two Higgs fields. Nevertheless, as mentioned earlier, we have restricted our parameter space with no mixing among the generations of leptoquarks at the initial scale, making λ_3 and $\tilde{\lambda}_3$ two diagonal matrices. The one-loop beta functions for these two parameters are given simply by:

$$\begin{aligned} \beta(\lambda_3)_{S_3,3\text{-gen}}^{1\text{-loop}} &= \left[\beta(\lambda_3)_{S_3,1\text{-gen}}^{1\text{-loop}} \right]_i \\ \beta(\tilde{\lambda}_3)_{S_3,3\text{-gen}}^{1\text{-loop}} &= \left[\beta(\tilde{\lambda}_3)_{S_3,1\text{-gen}}^{1\text{-loop}} \right]_i \end{aligned} \tag{63}$$

The full two-loop beta functions for S_3 with both one and three generations are presented in Appendix E.

Now, we consider the variation in quartic coupling between the leptoquark S_3 and Higgs with perturbative scale, and it is illustrated in Fig. 5 for the case of three generations. In the first two plots, Fig. 5a, b, λ_3 corresponds to the quartic coupling term for one particular generation of leptoquark, while λ_3^{jj} denote the remaining generations of λ_3 , and all the generations of other quartic coupling terms $\tilde{\lambda}_3$ are designated as $\tilde{\lambda}_3^{ii}$. Similarly, for $\tilde{\lambda}_3$ variation in Fig. 5c, d, $\tilde{\lambda}_3$ corresponds to any particular generation of leptoquark, while the remaining generations are denoted by $\tilde{\lambda}_3^{jj}$, and the other quartic coupling terms λ_3^{ii} signify λ_3 for all three generations. The plots in the left panel indicate a relatively low value of Yukawa, i.e. $Y_\phi = 0.1$, whereas the same in the right panel illustrate the variation in the mentioned couplings for a higher value of Yukawa, i.e. $Y_\phi = 0.8$.

In the first two plots, Fig. 5a, b, we have gradually varied the initial values for λ_3 from 0.1 to 0.8, keeping the EW values for other quartic couplings as 0.01, 0.1, 0.4 and 0.8, respectively, which are presented by red, blue, orange and green lines. Similar conditions for $\tilde{\lambda}_3$ are presented in Fig. 5c, d. As we already showed in the earlier sections, all the other couplings for three generations of the triplet leptoquark diverge at $10^{19.7}$ GeV due to the gauge coupling g_2 . The couplings λ_3 and $\tilde{\lambda}_3$ are also not different from that behaviour. Therefore, unlike the \tilde{R}_2 case, here λ_3 and $\tilde{\lambda}_3$ diverge at $10^{19.7}$ GeV for any smaller initial values of λ_3 and $\tilde{\lambda}_3$ at EW scale with any value of Yukawa coupling Y_ϕ . Now, as can be observed from Eqs. (61) and (63), $\tilde{\lambda}_3$ contributes positively in the one-loop beta function of λ_3 , and hence λ_3 reaches non-perturbativity at an early stage with higher values of $\tilde{\lambda}_3$. On the other hand, due to the positive effect of \mathcal{X}_3 at one-loop order, all the lines shift slightly downward with higher values of Yukawa couplings, but the shifts are almost unnoticeable. Both of the above statements are also true for the running of $\tilde{\lambda}_3$. For λ_3 , Planck scale perturbativity is achieved until 0.51 and 0.37, with other quartic coupling at EW scale being 0.01 and 0.1,

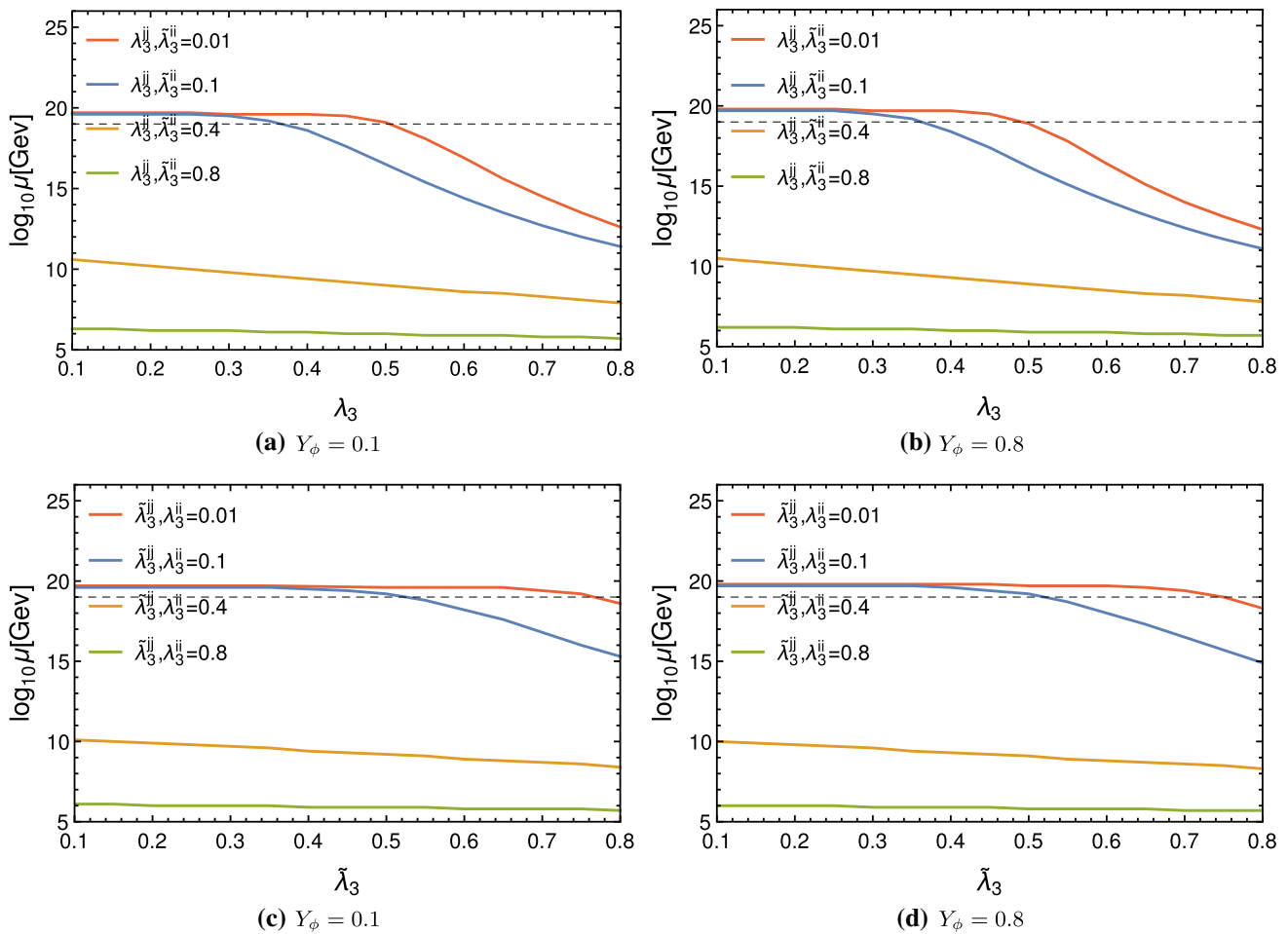


Fig. 5 Variation in leptoquark-Higgs quartic coupling λ_3 and $\tilde{\lambda}_3$ for triplet leptoquark S_3 with the perturbative scale. For the plots in the first row, λ_3 variation is considered for any particular generation of leptoquark, and the same for the remaining generations are denoted by λ_3^{jj} . The other leptoquark-Higgs quartic couplings $\tilde{\lambda}_3^{ii}$ include all three leptoquark generations. Similarly, for the plots in the second row, the variation in quartic coupling $\tilde{\lambda}_3$ for any particular leptoquark generation

is depicted while symbolizing the same for the remaining generations by $\tilde{\lambda}_3^{jj}$. The other quartic coupling λ_3^{ii} includes all three generations of leptoquark. The variations are considered for four different initial values, i.e. 0.01, 0.1, 0.4 and 0.8, at EW scale, which are described by red, blue, orange and green curves, respectively. Here, two different values for Y_ϕ are considered, which are 0.1 and 0.8

respectively, for both the Yukawa coupling. However, for higher values of other quartic couplings at EW scale, i.e. 0.4 and 0.8, λ_3 diverges at much lower scale, i.e. $10^{10.8}$ GeV and $10^{6.4}$ GeV, with its lower initial values, and this decreases with the increase in the beginning value of λ_3 . Likewise, the quartic coupling $\tilde{\lambda}_3$ is constrained to 0.76 and 0.52 for Planck scale perturbativity, with EW values of other quartic couplings at 0.01 and 0.1, respectively. For higher EW values of quartic couplings, the theory becomes non-perturbative at much lower scales as previously discussed.

3.2.3 Perturbativity of $\tilde{R}_2 + S_3$ with 3-gen

Now, we move to the combined scenario of \tilde{R}_2 and S_3 with three generations. The one-loop beta functions for all the

Higgs-leptoquark quartic couplings in this case can easily be written as:

$$\begin{aligned}
 \beta(\lambda_2^{ii})_{\tilde{R}_2+S_3,3\text{-gen}}^{1\text{-loop}} &= \beta(\lambda_2^{ii})_{\tilde{R}_2,3\text{-gen}}^{1\text{-loop}}, \\
 \beta(\tilde{\lambda}_2^{ii})_{\tilde{R}_2+S_3,3\text{-gen}}^{1\text{-loop}} &= \beta(\tilde{\lambda}_2^{ii})_{\tilde{R}_2,3\text{-gen}}^{1\text{-loop}}, \\
 \beta(\lambda_3^{ii})_{\tilde{R}_2+S_3,3\text{-gen}}^{1\text{-loop}} &= \beta(\lambda_3^{ii})_{S_3,3\text{-gen}}^{1\text{-loop}}, \\
 \beta(\tilde{\lambda}_3^{ii})_{\tilde{R}_2+S_3,3\text{-gen}}^{1\text{-loop}} &= \beta(\tilde{\lambda}_3^{ii})_{S_3,3\text{-gen}}^{1\text{-loop}}.
 \end{aligned}
 \tag{64}$$

The full two-loop beta functions of all the Higgs-leptoquark quartic couplings in this scenario are listed in Appendix G.

For three generations of $S_3 + \tilde{R}_2$, we have already seen that all the gauge couplings diverge below Planck scale, i.e.

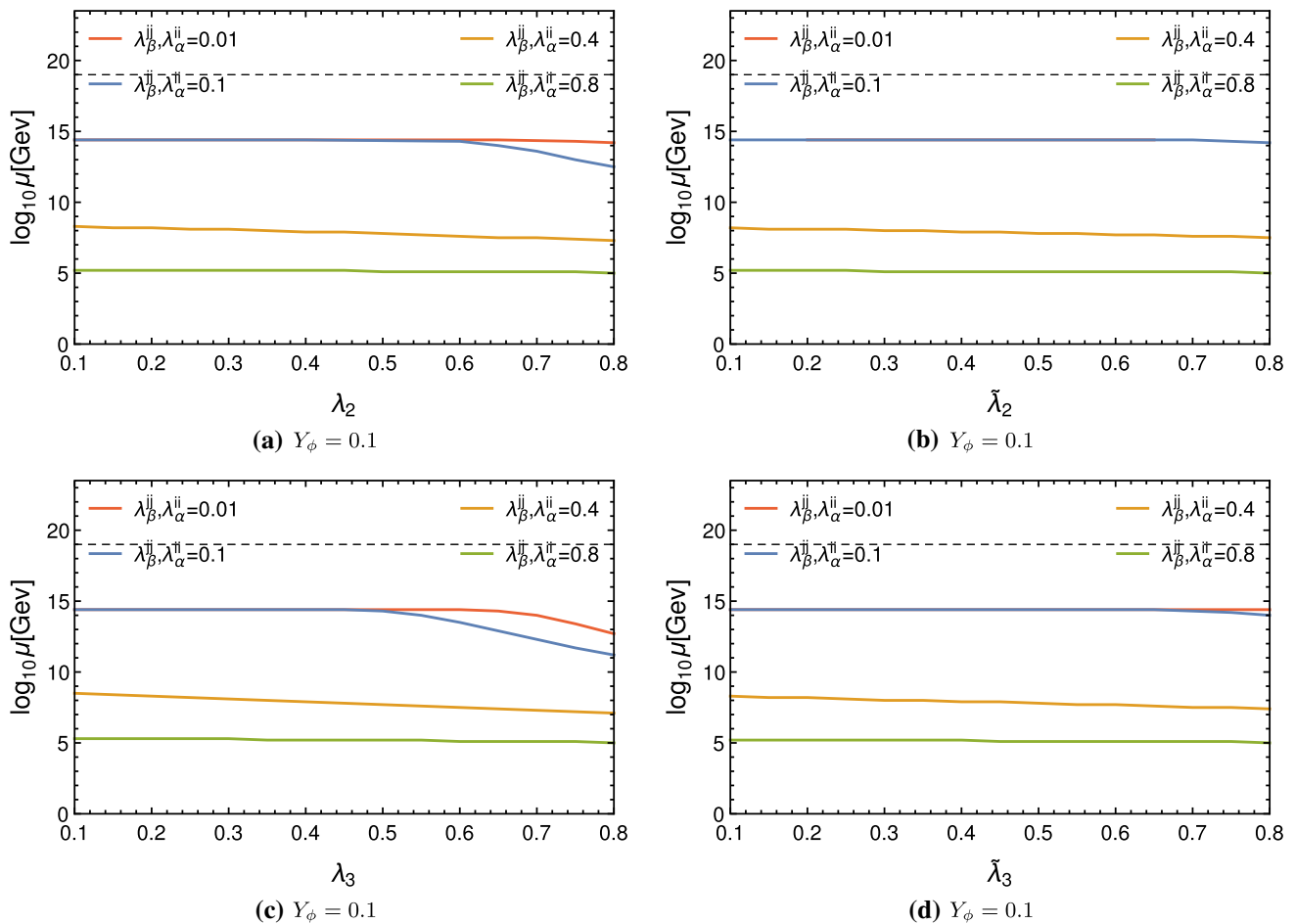


Fig. 6 Variation in quartic coupling $\lambda_2, \tilde{\lambda}_2, \lambda_3$ and $\tilde{\lambda}_3$ with perturbative scale for three generations of $\tilde{R}_2 + S_3$. Here, the variation in λ_2 is shown for any one generation of \tilde{R}_2 , and the remaining generations for the λ_2 term of R_2 are defined by λ_β^{jj} . The λ_α^{ii} term corresponds to three generations of \tilde{R}_2 for the $\tilde{\lambda}_2$ term and three generations of S_3 for the λ_3 and $\tilde{\lambda}_3$ term. Again, the $\tilde{\lambda}_2$ variation is depicted for any one generation of \tilde{R}_2 , and the remaining generations of \tilde{R}_2 are given by λ_β^{jj} for the $\tilde{\lambda}_2$

terms. In this case, the λ_α^{ii} term corresponds to three generations of \tilde{R}_2 for the λ_2 terms and three generations of S_3 for the λ_3 and $\tilde{\lambda}_3$ terms. Similar notation is followed for the variation in λ_3 and $\tilde{\lambda}_3$. The EW scale values for the quartic couplings other than the coupling whose variation is considered are set to four different values, i.e. 0.01, 0.1, 0.4 and 0.8, which are illustrated by red, blue, orange and green curves, respectively, taking $Y_\phi=0.1$. Here, Y_ϕ signifies both Y_2 and Y_3 with three generations

at $10^{14.4}$ GeV, mainly due to the typical behaviour of g_2 at two-loop order. This affects the running of quartic couplings as well. We study the variation in these couplings with perturbative scale in Fig. 6, assuming $Y_\phi = 0.1$. The adjustments in these plots with larger Y_ϕ are not very significant, and hence we do not present them. When examining the variation in λ_2 for any particular generation, the remaining generations of λ_2 are denoted as λ_β^{jj} , whereas the other quartic couplings including $\tilde{\lambda}_2, \lambda_3$ and $\tilde{\lambda}_3$ with all the generations are designated as λ_α^{ii} . The same notation is followed for all the other quartic couplings. The colour codes are as discussed previously. It can be observed from Fig. 6a–c that even for lower initial values of λ_α^{ii} and λ_β^{jj} , i.e. 0.01 and 0.1, the quartic couplings enter the non-perturbative region at $10^{14.4}$ GeV due to the appearance of the Landau pole in g_2 . For higher values

of the parameters at EW scale, non-perturbativity is reached even at much lower scale. Thus, the demand of Planck scale perturbativity rules out the three-generation scenario of the $S_3 + \tilde{R}_2$ model for any values of the leptoquark-Higgs quartic couplings. Therefore, we have to consider the one-generation scenario of the $S_3 + \tilde{R}_2$ model.

3.2.4 Perturbativity of $\tilde{R}_2 + S_3$ with 1-gen

In this section, we look into the perturbativity of Higgs-leptoquark quartic couplings for the combined scenario of \tilde{R}_2 and S_3 with one generation. The one-loop beta functions for all these parameters in this case can easily be written as:

$$\beta(\lambda_2)_{\tilde{R}_2+S_3, 1\text{-gen}}^{1\text{-loop}} = \beta(\lambda_2)_{\tilde{R}_2, 1\text{-gen}}^{1\text{-loop}},$$

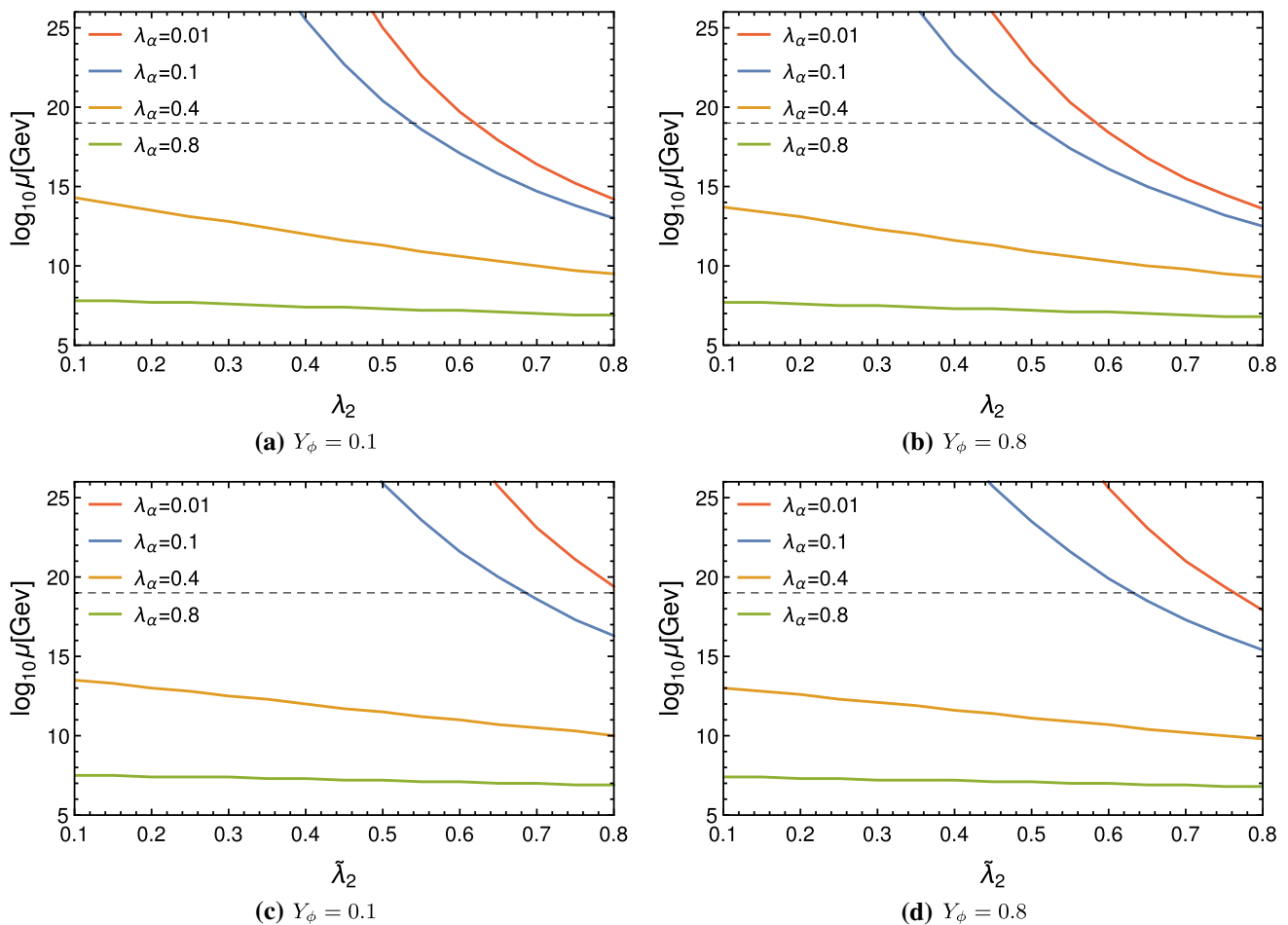


Fig. 7 Variation in quartic couplings λ_2 and $\tilde{\lambda}_2$ with the perturbative scale for one generation of $\tilde{R}_2 + \tilde{S}_3$. Here, for the λ_2 variation, λ_α corresponds to $\{\tilde{\lambda}_2, \lambda_3, \tilde{\lambda}_3\}$, and if we consider the behaviour of $\tilde{\lambda}_2$, then λ_α includes λ_2, λ_3 and λ_3 . All quartic couplings other than that for which the variation is considered are assigned four different values at the EW

scale, i.e. 0.01, 0.1, 0.4 and 0.8, and these are delineated by red, blue, orange and green curves, respectively. Two different values of Y_ϕ are i.e. 0.1 and 0.8, with Y_ϕ representing the Yukawa couplings for both the leptiquarks

$$\begin{aligned}
 \beta(\tilde{\lambda}_2)_{\tilde{R}_2+S_3, 1\text{-gen}}^{1\text{-loop}} &= \beta(\tilde{\lambda}_2)_{\tilde{R}_2, 1\text{-gen}}^{1\text{-loop}}, \\
 \beta(\lambda_3)_{\tilde{R}_2+S_3, 1\text{-gen}}^{1\text{-loop}} &= \beta(\lambda_3)_{S_3, 1\text{-gen}}^{1\text{-loop}}, \\
 \beta(\tilde{\lambda}_3)_{\tilde{R}_2+S_3, 1\text{-gen}}^{1\text{-loop}} &= \beta(\tilde{\lambda}_3)_{S_3, 1\text{-gen}}^{1\text{-loop}}.
 \end{aligned}
 \tag{65}$$

The full two-loop beta functions of all the Higgs-leptoquark quartic couplings in this scenario are listed in Appendix G.

Now, we study the variation in leptoquark-Higgs quartic couplings $\lambda_2, \tilde{\lambda}_2, \lambda_3$ and $\tilde{\lambda}_3$ with the perturbative scale for the one generation of $\tilde{R}_2 + \tilde{S}_3$ model. The results for the variation in λ_2 and $\tilde{\lambda}_2$ are presented in Fig. 7. When considering the variation in λ_2 , we denote all the other leptoquark-Higgs quartic couplings, namely $\tilde{\lambda}_2, \lambda_3$ and $\tilde{\lambda}_3$, as λ_α . By the same token, when examining the behaviour of $\tilde{\lambda}_2$, the other leptoquark-Higgs quartic couplings, i.e. λ_2, λ_3 and $\tilde{\lambda}_3$, are taken as λ_α . The colour codes are as described in earlier

sections. As can be seen from Fig. 7a, b, the initial value of λ_2 is restricted to 0.62 and 0.54 from Planck scale perturbativity for EW values of other quartic couplings of 0.01 and 0.1, respectively, with $Y_\phi = 0.1$, whereas with $Y_\phi = 0.8$, these upper bounds roll down to 0.59 and 0.51, respectively. For higher values of other quartic couplings at the EW scale, i.e. 0.4 and 0.8, the theory becomes non-perturbative around $10^{14.1}$ GeV and $10^{7.9}$ GeV with $Y_\phi = 0.1$, which differ slightly (about 0.2 GeV) in the $Y_\phi = 0.8$ case even if the initial value of λ_2 is taken to be very small. Similarly, for $\tilde{\lambda}_2$, Planck scale perturbativity with $Y_\phi = 0.1$ is achieved up to $\tilde{\lambda}_2 \leq 0.82$ and 0.68, which decrease to 0.76 and 0.63, respectively, with $Y_\phi = 0.8$, while taking the initial values for other quartic couplings as 0.01 and 0.1 at EW scale. Again, for higher EW values of λ_α , i.e. 0.4 and 0.8, the theory becomes non-perturbative at much lower scales, as shown in Fig. 7c,

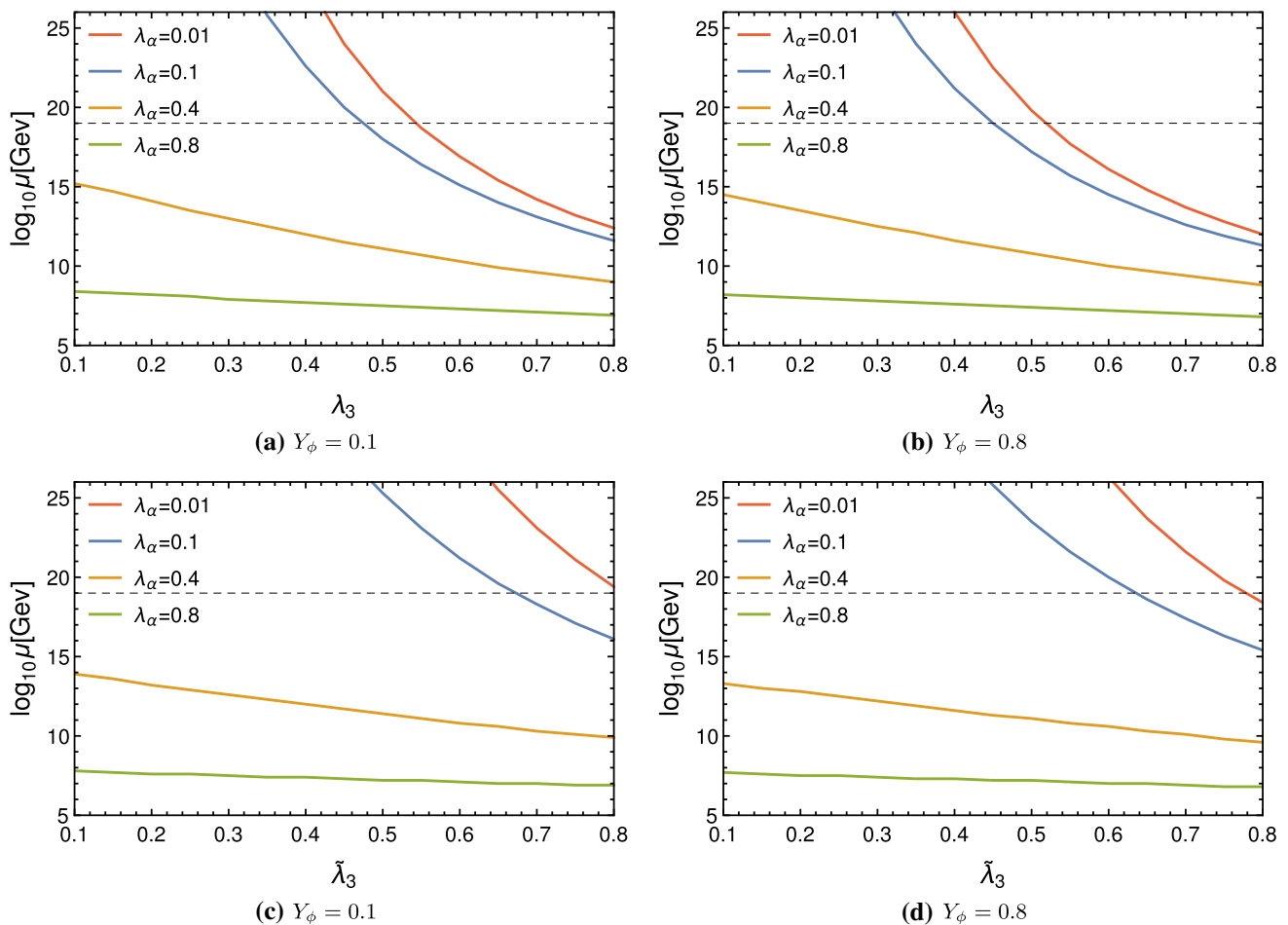


Fig. 8 Variation in triplet leptoquark-Higgs quartic coupling λ_3 and $\tilde{\lambda}_3$ for one generation of $\tilde{R}_2 + S_3$. Here, for the λ_3 variation, $\lambda_\alpha \in \{\lambda_2, \tilde{\lambda}_2, \tilde{\lambda}_3\}$, and for $\tilde{\lambda}_3$, $\lambda_\alpha \in \{\lambda_2, \tilde{\lambda}_2, \lambda_3\}$. We consider four differ-

ent values of λ_α at the EW scale, i.e. 0.01, 0.1, 0.4 and 0.8, which are denoted by red, blue, orange and green curves, respectively. The black dotted line parallel to the x-axis denotes the Planck scale

d. The reason for all these typical behaviours were already discussed in the previous Sect. 3.2.1.

Correspondingly, the changes in λ_3 and $\tilde{\lambda}_3$ with perturbative scale are displayed in Fig. 8. Here, for λ_3 variation, we designate $\{\lambda_2, \tilde{\lambda}_2, \tilde{\lambda}_3\}$ as λ_α , whereas for $\tilde{\lambda}_3$ variation, we assume $\lambda_\alpha \in \{\lambda_2, \tilde{\lambda}_2, \lambda_3\}$. The colour codes have already been discussed. Here, Planck scale perturbativity with $Y_\phi = 0.1$ restricts λ_3 to 0.55 and 0.47 (see Fig. 8a), which change to 0.53 and 0.45, respectively, with $Y_\phi = 0.8$ (Fig. 8b), for $\lambda_\alpha=0.01, 0.1$ at the EW scale. Similarly, from Fig. 8c, d, one can observe that for $Y_\phi = 0.1$, $\tilde{\lambda}_3$ should be bounded above to 0.83 and 0.67, which reduce to 0.78 and 0.62, respectively, for $Y_\phi = 0.8$, in order to respect Planck scale perturbativity with $\lambda_\alpha=0.01, 0.1$ at the EW scale. For higher initial values of λ_α , i.e. 0.4 and 0.8, the theory becomes non-perturbative at very low scale, i.e. $\sim 10^{14-15}$ GeV and 10^{8-9} GeV, even with very small EW value of λ_3 and $\tilde{\lambda}_3$ at both the Yukawa couplings, and the scale decreases gradually with the increase in initial values of these two parameters.

The reason for all these typical behaviours were already discussed in the previous Sect. 3.2.2. It is worth noting again that there is no Landau pole of any gauge coupling in this model, and the non-perturbativity discussed here appears because of the Higgs-leptoquark quartic couplings growing beyond 4 π during the RG evolution.

3.2.5 Effects of self-quartic couplings of leptoquarks

Up to this point, for the sake of simplicity, we have not considered self-quartic couplings of the leptoquark. In this subsection, we discuss the effects of such couplings on the perturbativity of the model. We find that the introduction of these couplings has little affect on the running of gauge couplings; however, it brings in a non-negligible positive contribution to the running of Higgs-leptoquark quartic couplings up to two-loop order. Therefore, Higgs-leptoquark quartic couplings attain the non-perturbative limit earlier than in the scenario wherein self-quartic couplings of leptoquarks

are neglected. For instance, one can add the self-interaction term of $\omega_2(\tilde{R}_2^\dagger \tilde{R}_2)(\tilde{R}_2^\dagger \tilde{R}_2)$ to the Lagrangian given by Eq. 1. With values of 0.47 and 0.64 at EW scale, λ_2 enters the non-perturbative region at Planck scale in this case for other quartic couplings $\lambda_2^{jj}, \tilde{\lambda}_2^{ii}$ and the newly introduced self-quartic coupling of \tilde{R}_2 (three generations, without any generation mixing) being 0.01 and 0.1, respectively, assuming $Y_\phi = 1.0$. Before the introduction of self-quartic coupling of \tilde{R}_2 , the values of λ_2 for which non-perturbativity was achieved at Planck scale under the same values of other quartic couplings were 0.47 and 0.31, respectively (see Fig. 4b). With the same value of Y_ϕ and other quartic couplings, $\tilde{\lambda}_2$ maintains Planck scale perturbativity until values at EW scale of 0.64 and 0.41, which were 0.73 and 0.58, respectively (see Fig. 4d), before the introduction of self-quartic coupling of \tilde{R}_2 (three generations, without any generation mixing). On the other hand, for S_3 with three generations, the positive effects of self-quartic couplings of leptoquarks are even stronger. As an example, we add a self-quartic term⁶ of $\text{Tr}[(S_3^{ad})^\dagger S_3^{ad}]^2$ to the Lagrangian given by Eq. 4. With $Y_\phi = 0.8$, the parameters λ_3 and $\tilde{\lambda}_3$ now cannot achieve Planck scale perturbativity for small values of other quartic couplings such as 0.01 at EW scale. Before the consideration of self-quartic coupling of the leptoquark, λ_3 and $\tilde{\lambda}_3$ achieved Planck scale perturbativity with other quartic couplings of 0.1 at EW scale (see Fig. 5b, d).

4 Vacuum stability

There exist two approaches in the literature regarding stability analysis. The first is the running of Higgs quartic coupling λ_h using beta functions, and the other method is the Coleman–Weinberg effective potential approach [145].

First, we scrutinize the running of self-quartic coupling for the Higgs boson, i.e. λ_h , which in turn would indicate the change in stability of the Higgs vacuum. This parameter is also expected to be below 4π in the entire energy scale to respect the perturbativity. However, for the purpose of this section, we focus on the stability of the vacuum, which suggests that λ_h should be a positive quantity throughout the energy scale. The one- and two-loop beta functions for λ_h under the SM are given by:

$$\beta(\lambda_h)_{\text{SM}}^{1\text{-loop}} = \frac{3}{8\pi^2} \left[\lambda_h^2 + \frac{3}{200} g_1^4 + \frac{3}{16} \left(\frac{g_1^2}{5} + g_2^2 - 4\lambda_h \right)^2 + 2\lambda_h \text{Tr} \left(X_u + X_d + \frac{1}{3} X_l \right) - \text{Tr} \left(X_u^2 + X_d^2 + \frac{1}{3} X_l^2 \right) \right], \tag{66}$$

⁶ There could be another term such as $\text{Tr}[(S_3^{ad})^\dagger S_3^{ad} (S_3^{ad})^\dagger S_3^{ad}]$.

$$\begin{aligned} \beta(\lambda_h)_{\text{SM}}^{2\text{-loop}} &= \beta(\lambda_h)_{\text{SM}}^{1\text{-loop}} + \frac{1}{(16\pi^2)^2} \left[\left(-\frac{3411}{2000} g_1^6 \right. \right. \\ &\quad - \frac{1677}{400} g_1^4 g_2^2 - \frac{289}{80} g_1^2 g_2^4 + \frac{305}{16} g_2^6 + \frac{1887}{200} g_1^4 \lambda_h \\ &\quad + \frac{117}{20} g_1^2 g_2^2 \lambda_h - \frac{73}{8} g_2^4 \lambda_h + \frac{108}{5} g_1^2 \lambda_h^2 + 108 g_2^2 \lambda_h^2 \\ &\quad - 312 \lambda_h^3 \left. \right) + \left\{ \frac{9}{20} \left(g_1^4 + 6g_1^2 g_2^2 - 5g_2^4 \right) + \frac{5}{2} \lambda_h \left(g_1^2 \right. \right. \\ &\quad + 9g_2^2 + 32g_3^2 \left. \right) - 144 \lambda_h^2 \left. \right\} \text{Tr} X_d - \left\{ \frac{3}{4} \left(3g_1^4 - \frac{22}{5} g_1^2 g_2^2 \right. \right. \\ &\quad + g_2^4 \left. \right) - \frac{15}{2} \lambda_h \left(g_1^2 + g_2^2 \right) + 48 \lambda_h^2 \left. \right\} \text{Tr} X_l - \left\{ \frac{9}{10} \right. \\ &\quad \left. \left(\frac{19}{10} g_1^4 - 7g_1^2 g_2^2 + \frac{5}{2} g_2^4 \right) - \lambda_h \left(\frac{17}{2} g_1^2 + \frac{45}{2} g_2^2 + 80g_3^2 \right) \right. \\ &\quad + 144 \lambda_h^2 \left. \right\} \text{Tr} X_u - \text{Tr} \left\{ \lambda_h \left(X_l^2 + 3X_u^2 + 3X_d^2 + 42\tilde{X}_u \tilde{X}_d \right) \right. \\ &\quad - \frac{4}{5} g_1^2 \left(X_d^2 - 2X_u^2 - 3X_l^2 \right) + 32 g_3^2 \left(X_u^2 + X_d^2 \right) \left. \right\} \\ &\quad + 10 \text{Tr} \left\{ X_l^3 + 3 \left(X_u^3 + X_d^3 \right) - \frac{3}{5} \tilde{X}_d \tilde{X}_u \left(\tilde{X}_u - \tilde{X}_d \right) \right\} \left. \right]. \tag{67} \end{aligned}$$

It is well known that in the case of the SM, λ_h enters the negative-valued region between the 10^9 GeV and 10^{10} GeV energy scale [144, 146] at two-loop order. At this point it is worth mentioning that in the case of λ_h , the two-loop contributions affect the running significantly. The addition of right-handed neutrinos pulls the stability scale further down with more negative contributions [115–119]. In contrast, the presence of scalar leptoquarks is expected to further push the stability scale by adding positive contributions to these beta functions.

4.1 Vacuum stability of \tilde{R}_2

First, we look into the effects of the doublet leptoquark \tilde{R}_2 . The one- and two-loop beta functions for λ_h in this case are given by:

$$\begin{aligned} \beta(\lambda_h)_{\tilde{R}_2, 1\text{-gen}}^{1\text{-loop}} &= \beta(\lambda_h)_{\text{SM}}^{1\text{-loop}} + \Delta\beta(\lambda_h)_{\tilde{R}_2}^{1\text{-loop}} \\ \beta(\lambda_h)_{\tilde{R}_2, 3\text{-gen}}^{1\text{-loop}} &= \beta(\lambda_h)_{\text{SM}}^{1\text{-loop}} + \sum_{i=1}^3 \left[\Delta\beta(\lambda_h)_{\tilde{R}_2}^{1\text{-loop}} \right]_i \\ \text{with } \Delta\beta(\lambda_h)_{\tilde{R}_2}^{1\text{-loop}} &= \frac{3}{8\pi^2} \left(\lambda_2^2 + \lambda_2 \tilde{\lambda}_2 + \frac{1}{2} \tilde{\lambda}_2^2 \right), \tag{68} \\ \beta(\lambda_h)_{\tilde{R}_2, 1\text{-gen}}^{2\text{-loop}} &= \beta(\lambda_h)_{\text{SM}}^{2\text{-loop}} + \Delta\beta(\lambda_h)_{\tilde{R}_2}^{2\text{-loop}} \\ \beta(\lambda_h)_{\tilde{R}_2, 3\text{-gen}}^{2\text{-loop}} &= \beta(\lambda_h)_{\text{SM}}^{2\text{-loop}} + \sum_{i=1}^3 \left[\Delta\beta(\lambda_h)_{\tilde{R}_2}^{2\text{-loop}} \right]_i \\ \text{with } \Delta\beta(\lambda_h)_{\tilde{R}_2, 1\text{-gen}}^{2\text{-loop}} &= \Delta\beta(\lambda_h)_{\tilde{R}_2}^{1\text{-loop}} + \frac{3}{(16\pi^2)^2} \end{aligned}$$

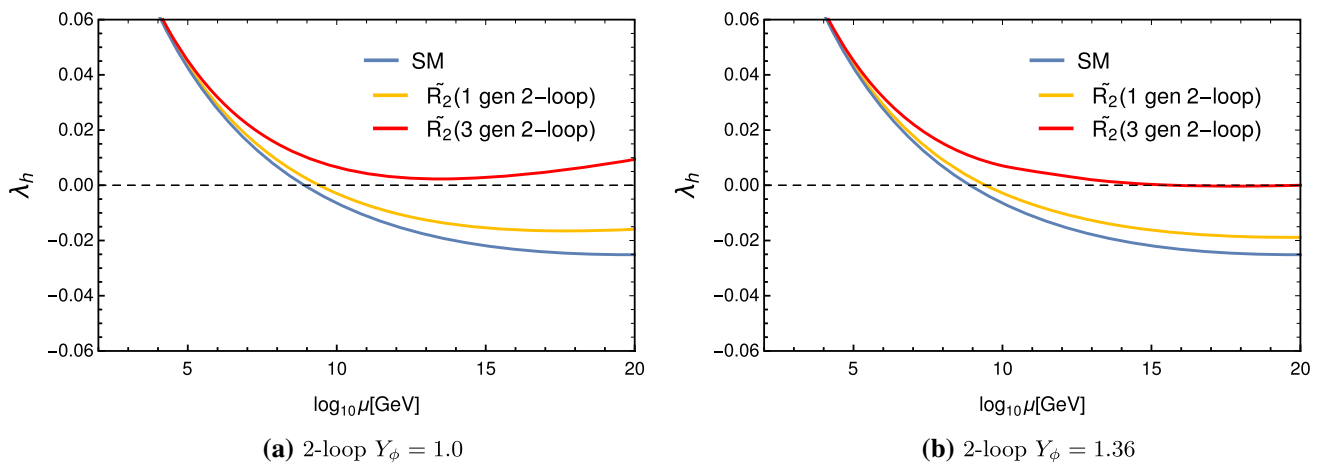


Fig. 9 Running of SM Higgs quartic coupling with scale for stability analysis. Stability scale is defined as the scale after which $\lambda_h < 0$. Here, blue, yellow and red curves describes the running of λ_h for SM, one generation and three generations of \tilde{R}_2 . With three generations of \tilde{R}_2 , the positive contribution from gauge couplings and other quartic couplings is large enough and is compensated by the negative contribution of Y_2 . The crucial value of Y_2 is 1.36; λ_h will go negative if higher values of Y_2 are considered and stability is lost. On the other hand, for one generation of \tilde{R}_2 , λ_h always goes to a negative value before Planck scale

plings is large enough and is compensated by the negative contribution of Y_2 . The crucial value of Y_2 is 1.36; λ_h will go negative if higher values of Y_2 are considered and stability is lost. On the other hand, for one generation of \tilde{R}_2 , λ_h always goes to a negative value before Planck scale

$$\begin{aligned}
 & \times \left[-\frac{7}{8} \left(\frac{1}{125} g_1^6 + \frac{1}{75} g_1^4 g_2^2 + \frac{1}{5} g_1^2 g_2^4 + g_2^6 \right) + \frac{15}{2} \left(\frac{1}{75} g_1^4 \right. \right. \\
 & \left. \left. + g_2^4 \right) \left(\lambda_2 + \frac{1}{2} \tilde{\lambda}_2 + \frac{11}{30} \lambda_h \right) + \frac{1}{2} g_1^2 g_2^2 \tilde{\lambda}_2 - 8 \tilde{\lambda}_2^2 \left(\lambda_2 \right. \right. \\
 & \left. \left. + \frac{1}{2} \tilde{\lambda}_2 + \frac{3}{8} g_2^2 + \frac{1}{4} \lambda_h \right) + 12 \left(\frac{1}{45} g_1^2 + g_2^2 + \frac{16}{9} g_3^2 \right. \right. \\
 & \left. \left. - \frac{5}{3} \lambda_h - \frac{2}{3} \lambda_2 - \frac{1}{3} \tilde{\lambda}_2 \right) \left(\lambda_2^2 + \lambda_2 \tilde{\lambda}_2 + \frac{1}{2} \tilde{\lambda}_2^2 \right) - 6 \lambda_h \right. \\
 & \left. \text{Tr} \left(\mathcal{X}_2 \mathcal{X}_d + \frac{1}{2} \tilde{\mathcal{X}}_2 \tilde{\mathcal{X}}_l \right) + 4 \text{Tr} \left(\mathcal{X}_2 \mathcal{X}_d^2 + Y_2 \mathcal{X}_l Y_2^\dagger \mathcal{X}_d \right. \right. \\
 & \left. \left. + \frac{1}{2} \tilde{\mathcal{X}}_2 \tilde{\mathcal{X}}_l^2 \right) \right]. \tag{69}
 \end{aligned}$$

In the last section, we observed that there is not much room for the Higgs-leptoquark quartic couplings to be varied randomly from the perspective of Planck scale perturbativity. However, the Yukawa couplings for leptoquarks do not attain such serious constraints. Therefore, we address the issue of vacuum stability from the effects of leptoquark Yukawa coupling. However, it should be noted from Eqs. (68) and (69) that the contributions of Y_2 appear at the two-loop level only. The effects of Y_2 in the running of λ_h for \tilde{R}_2 with both one-generation and three-generation cases are shown in Fig. 9. Here, the blue, yellow and red curves explain the running of λ_h for SM, one generation of \tilde{R}_2 and three generations of \tilde{R}_2 , respectively. For all the analyses, we assume every Higgs-leptoquark quartic coupling to be 0.01.

As already mentioned, the stability scale after which λ_h turns negative for the SM is just above 10^9 GeV at the two-loop level. However, when considering the RG evolution of λ_h in the \tilde{R}_2 case, the gauge couplings and other quartic couplings contribute positively whereas the Yukawa coupling of

the leptoquark inserts negative contributions at the two-loop level, as can be seen from Eqs. (68) and (69). Again, since the additional contribution in the beta function of λ_h for the case of three generations is the sum of all individual generations, and the gauge couplings at any particular scale for the three-generation case are higher than the same for the one-generation case, the three-generation scenario obtains more positive contributions than the one-generation case. It should also be noted that although there are two negative and three positive terms containing \mathcal{X}_2 in Eq. (69), the positive terms are quadratic in \mathcal{X}_d and \mathcal{X}_l , and therefore smaller than the negative terms which are linear in \mathcal{X}_d and \mathcal{X}_l . Thus the yellow curve representing leptoquark R_2 with one generation stays above the blue line depicting the SM, and the red curve signifying R_2 with three generations lies further above the region. However, due to the negative contributions of the Yukawa couplings of the leptoquark, the red and yellow line move downward with the enhancement in Y_ϕ . In Fig. 9a, b, we depict the variations in λ_h with the energy scale, taking the initial values for Y_ϕ as 1.0 and 1.36, respectively. As can be observed, for both cases the vacuum of the leptoquark model \tilde{R}_2 with one generation remains stable up to $\sim 10^{9.5}$ GeV, slightly higher than the SM estimates. However, it is interesting to observe in the left panel that the red curve remains in the positive region of λ_h for all energy values, indicating the stability of the vacuum all the way to Planck scale with three generations of \tilde{R}_2 and $Y_\phi = 1.0$. Once we start with an initial value of Y_ϕ of 1.36, we observe in the right panel that the red curve touches the $\lambda_h = 0$ line, and thus for higher values of Y_ϕ the Planck scale stability will be lost. One can also observe that for this particular value of Y_ϕ , the red curve touches the $\lambda_h = 0$ line at $\sim 10^{14.5}$ GeV and remains very flat up to the

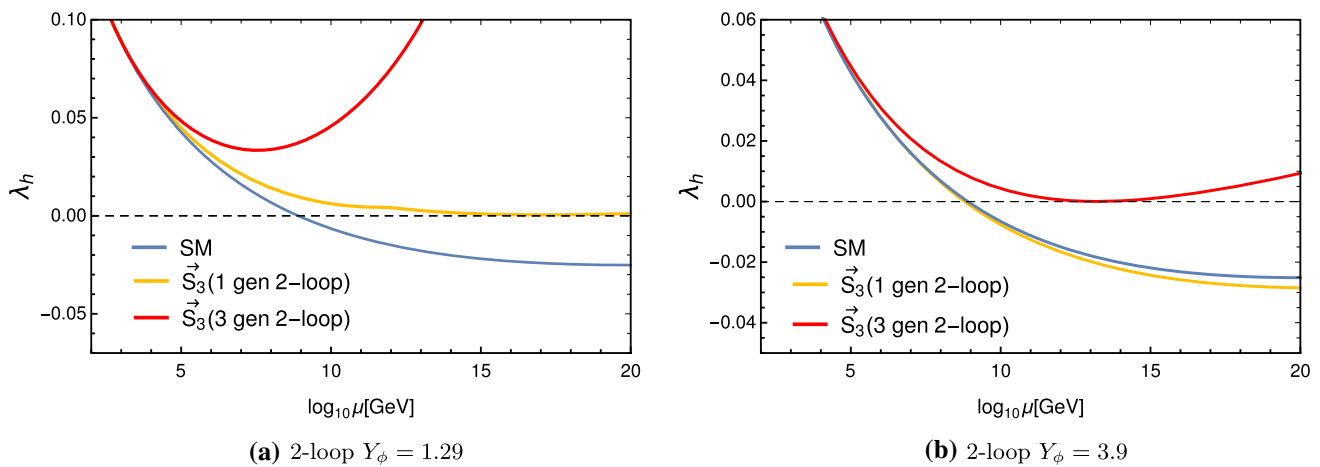


Fig. 10 Running of Higgs quartic coupling with scale for triplet leptoquark S_3 at two-loop level. Here, λ_h running for SM, one generation and three generations of S_3 is delineated by blue, yellow and red curves, respectively. If Y_ϕ is assumed to be greater than 1.29, the

one-generation model of S_3 loses stability at two-loop order, although the three-generation scenario remains stable. However, if we consider $Y_\phi > 3.9$, the three-generation scenario of the S_3 model also leaves the stable region at two-loop order

Planck scale. One can also find that this value of Y_ϕ of 1.36 is higher than the required Yukawa coupling Y_N in inert doublet+type III seesaw or inverse type III seesaw to maintain the Planck scale stability [120]. On the contrary, it should be noted that leptoquark \tilde{R}_2 with one generation does not show Planck scale stability even with very low Yukawa. Now, it is worth mentioning that with the change in Higgs-leptoquark couplings from 0.01 to 0.1, we do not find any significant changes in the behaviour of λ_h . Although very high values of λ_2 and $\tilde{\lambda}_2$ might shift the red curve in an upward direction, these higher values are disfavoured from Planck scale perturbativity of λ_2 and $\tilde{\lambda}_2$. Consideration of the self-quartic coupling of the leptoquark introduces positive contributions, indicating the need for a higher initial value of Y_ϕ to push λ_h to the negative region. However, for \tilde{R}_2 with three generations, we find little difference in the critical value of Y_ϕ .

4.2 Vacuum stability of S_3

Now, we discuss the stability of Higgs vacuum for the S_3 scenario. The one- and two-loop beta functions of λ_h in this case are as follows:

$$\beta(\lambda_h)_{S_3,1\text{-gen}}^{1\text{-loop}} = \beta(\lambda_h)_{SM}^{1\text{-loop}} + \Delta\beta(\lambda_h)_{S_3}^{1\text{-loop}}$$

$$\beta(\lambda_h)_{S_3,3\text{-gen}}^{1\text{-loop}} = \beta(\lambda_h)_{SM}^{1\text{-loop}} + \sum_{i=1}^3 \left[\Delta\beta(\lambda_h)_{S_3}^{1\text{-loop}} \right]_i$$

with $\Delta\beta(\lambda_h)_{S_3}^{1\text{-loop}} = \frac{9}{16\pi^2} \left(\lambda_3^2 + \lambda_3 \tilde{\lambda}_3 + \frac{5}{12} \tilde{\lambda}_3^2 \right)$,

(70)

$$\beta(\lambda_h)_{S_3,1\text{-gen}}^{2\text{-loop}} = \beta(\lambda_h)_{SM}^{2\text{-loop}} + \Delta\beta(\lambda_h)_{S_3}^{2\text{-loop}}$$

$$\beta(\lambda_h)_{S_3,3\text{-gen}}^{2\text{-loop}} = \beta(\lambda_h)_{SM}^{2\text{-loop}} + \sum_{i=1}^3 \left[\Delta\beta(\lambda_h)_{S_3}^{2\text{-loop}} \right]_i$$

with $\Delta\beta(\lambda_h)_{\tilde{R}_2,1\text{-gen}}^{2\text{-loop}} = \Delta\beta(\lambda_h)_{S_3}^{1\text{-loop}} + \frac{3}{(16\pi^2)^2} \left[-\frac{7}{2} \right.$

$$\times \left(\frac{3}{250} g_1^6 + \frac{1}{50} g^4 g_2^2 + \frac{1}{5} g_1^2 g_2^4 + g_2^6 \right) + 2\tilde{\lambda}_3 g_1^2 g_2^2$$

$$+ 30 \left(\frac{1}{50} g_1^4 + g_2^4 \right) \left(\lambda_3 + \frac{1}{2} \tilde{\lambda}_3 + \frac{11}{30} \lambda_h \right) - 8\tilde{\lambda}_3^2 \left(\lambda_3 \right.$$

$$+ \frac{1}{2} \tilde{\lambda}_3 + \frac{3}{8} g_2^2 + \frac{1}{4} \lambda_h \left. \right) + 48 \left(\frac{1}{30} g_1^2 + g_2^2 + \frac{2}{3} g_3^2 \right.$$

$$- \frac{1}{4} \lambda_3 - \frac{1}{8} \tilde{\lambda}_3 - \frac{5}{8} \lambda_h - \frac{1}{8} \text{Tr } X_3 \left. \right) \left(\lambda_3^2 + \lambda_3 \tilde{\lambda}_3 + \frac{5}{12} \tilde{\lambda}_3^2 \right)$$

$$- \frac{9}{2} \lambda_h \text{Tr} \left(\tilde{X}_3 \tilde{X}_\ell^T + X_3 \tilde{X}_d^T + X_3 \tilde{X}_u^T \right) + 3 \text{Tr} \left\{ \tilde{X}_3 \tilde{X}_\ell^2 \right.$$

$$\left. + X_3 (\tilde{X}_d^T)^2 + X_3 (\tilde{X}_u^T)^2 + \frac{4}{3} Y_3 \tilde{X}_\ell Y_3^\dagger (\tilde{X}_d^T + \frac{1}{2} \tilde{X}_u^T) \right\}.$$
(71)

The running of Higgs quartic coupling for the triplet leptoquark S_3 is displayed in Fig. 10 taking the EW value of λ_3 and $\tilde{\lambda}_3$ as 0.01. Here, blue, yellow and red curves denote the RG evolution of λ_h for SM, one generation of S_3 and three generations of S_3 , respectively, at two-loop order. As discussed in the previous section 4.1, gauge couplings and Higgs-leptoquark quartic couplings contribute positively in the running of λ_h , while the leptoquark Yukawa coupling brings in negative effects (see Eqs. (70) and (71)). Furthermore, since \tilde{R}_2 lies in fundamental representation of $SU(2)_L$, while S_3 stays in adjoint representation, the positive effects in the case of S_3 are very large compared to the same for

\tilde{R}_2 ; therefore, large Yukawa coupling for S_3 will be needed to make the vacuum unstable. We show the results for Y_ϕ of 1.29 and 3.9 in Fig. 10a, b, respectively. In the left panel, we see that both the case of S_3 with one generation and that with three generations show Planck scale stability for $Y_\phi = 1.29$, but the yellow curve touches the $\lambda_h = 0$ line, implying that a further increase in Y_ϕ will make the theory unstable before the Planck is reached. It is also interesting to note that the yellow curve touches the $\lambda_h = 0$ line at $\sim 10^{15}$ GeV and remains very flat up to the Planck scale as in the \tilde{R}_2 scenario with three generations. In the right panel, one can observe that the higher value of Y_ϕ , i.e. 3.9, has forced the red and yellow curves to move downward pushing the one-generation S_3 to the unstable region. However, the red curve touches the $\lambda_h = 0$ line at this Yukawa coupling, indicating that $Y_\phi \leq 3.9$ in order to preserve Planck scale stability with three generations of S_3 . It is worth mentioning that here the red curve just kisses the $\lambda_h = 0$ line at a lower energy scale of $\sim 10^{13.5}$ GeV, and then the positive contributions cause it to grow faster in the positive direction, unlike the previous cases. However, to ensure perturbativity of the model, $Y_\phi \leq \sqrt{4\pi} \approx 3.54$. Therefore, combining vacuum stability and perturbativity, one should consider $\sqrt{4\pi}$ as the upper limit of Y_ϕ for the three-generation scenario of S_3 . Like \tilde{R}_2 , in this case also, the behaviour of these plots does not show any notable alteration if λ_3 and $\tilde{\lambda}_3$ are increased to 0.1 from 0.01. The inclusion of leptoquark self-quartic coupling inserts huge positive effects for S_3 . Therefore, with three generations of S_3 , the critical initial value of 3.9 for Y_ϕ now goes beyond 5. However, since $\sqrt{4\pi} \leq 5$, the upper bound on Y_ϕ remains $\sqrt{4\pi}$ when considering combined constraint from vacuum stability and perturbativity.

4.3 Vacuum stability of $\tilde{R}_2 + S_3$ with 3-gen

The one-loop and two-loop beta functions for λ_h with three generations of $\tilde{R}_2 + S_3$ can be written as:

$$\begin{aligned} \beta(\lambda_h)_{\tilde{R}_2+S_3,3\text{-gen}}^{1\text{-loop}} &= \sum_{i=1}^3 \left[\beta(\lambda_h)_{\tilde{R}_2+S_3,1\text{-gen}}^{1\text{-loop}} \right]_i \\ \beta(\lambda_h)_{\tilde{R}_2+S_3,3\text{-gen}}^{2\text{-loop}} &= \sum_{i=1}^3 \left[\beta(\lambda_h)_{\tilde{R}_2+S_3,1\text{-gen}}^{2\text{-loop}} \right]_i \end{aligned} \tag{72}$$

The result at two-loop order for this scenario with all the leptoquark Yukawa couplings being 1.0 and all the Higgs-leptoquark couplings being 0.01 are shown in Fig. 11. We have already seen that in this model all the parameters blow up at the energy scale of $10^{14.4}$ GeV. The parameter λ_h is also no different from them. With any value of Higgs-leptoquark coupling or Yukawa coupling less than one, this divergence is unavoidable for this model. It is also noteworthy that λ_h

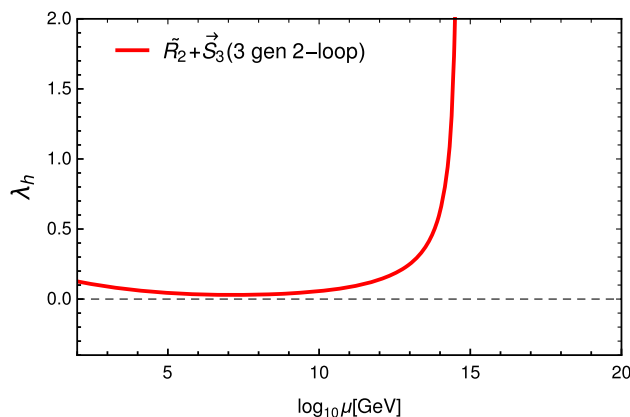


Fig. 11 Running of Higgs quartic coupling λ_h for three generations of $\tilde{R}_2 + S_3$ at the two-loop level. Here, all the leptoquark Yukawa couplings are assumed to be 1.0 and all the Higgs-leptoquark couplings are taken to be 0.01. In this model, λ_h diverges at an energy scale ($\sim 10^{14.4}$ GeV) far below the Planck scale at two-loop order

grows into the non-perturbative region before the emergence of instability in this model. Therefore, we will discuss the behaviour of λ_h for one generation of $\tilde{R}_2 + S_3$.

4.4 Vacuum stability of $\tilde{R}_2 + S_3$ with 1-gen

The one- and two-loop beta functions for λ_h for the combined scenario of $\tilde{R}_2 + S_3$ with one generation can simply be expressed as:

$$\begin{aligned} \beta(\lambda_h)_{\tilde{R}_2+S_3,1\text{-gen}}^{1\text{-loop}} &= \beta(\lambda_h)_{\text{SM}}^{1\text{-loop}} + \Delta\beta(\lambda_h)_{\tilde{R}_2}^{1\text{-loop}} \\ &\quad + \Delta\beta(\lambda_h)_{S_3}^{1\text{-loop}}, \\ \beta(\lambda_h)_{\tilde{R}_2+S_3,1\text{-gen}}^{2\text{-loop}} &= \beta(\lambda_h)_{\text{SM}}^{2\text{-loop}} + \Delta\beta(\lambda_h)_{\tilde{R}_2}^{2\text{-loop}} \\ &\quad + \Delta\beta(\lambda_h)_{S_3}^{2\text{-loop}}. \end{aligned} \tag{73}$$

The two-loop result for this case with all the leptoquark-Higgs coupling being 0.01 is displayed in Fig. 12, where the blue curve represents the SM and the yellow line denotes this particular model. As can be seen, with $Y_\phi = 1.0$, λ_h stays entirely in the positive region, whereas for $Y_\phi \geq 1.21$, this model no longer remains stable. With $Y_\phi = 1.21$, the orange curve touches the $\lambda_h = 0$ line at a relatively higher scale, $\sim 10^{16}$ GeV, and remains mostly flat up to Planck scale. Here, Y_ϕ includes the leptoquark Yukawa couplings for both \tilde{R}_2 and S_3 . The result remains almost the same with all the leptoquark-Higgs coupling being 0.1.

4.5 Bounds from effective potential stability constraints

Now, to study the stability, we follow the Coleman–Weinberg effective potential approach [145], where the one-loop contributions from all the particles at zero temperature with van-

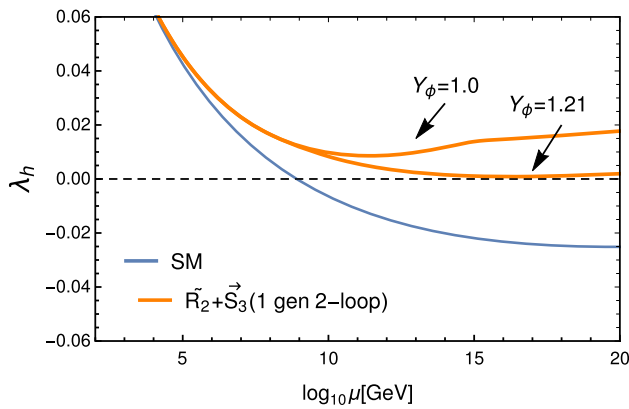


Fig. 12 Higgs quartic coupling running with scale is given for one generation of $\tilde{R}_2 + \tilde{S}_3$. Here, λ_h running for SM and one 0 of $\tilde{R}_2 + \tilde{S}_3$ are explained by blue and yellow curves, respectively. In order to maintain Planck scale stability, the upper bound on Y_ϕ for this model is 1.21. Here, Y_ϕ includes the leptoquark Yukawa couplings for both \tilde{R}_2 and \tilde{S}_3

ishing moments are included in effective coupling λ_{eff} . The effective potential for high field values in the h -direction can be defined as

$$V_{\text{eff}}(h, \mu) \simeq \lambda_{\text{eff}}(h, \mu) \frac{h^4}{4}, \quad \text{with } h \gg v, \quad (74)$$

The possibility of minima in the leptoquark direction can lead to charge- and colour-breaking minima, which is physically unwanted. However, such possibilities have little relevance in our case. Firstly, unlike the Higgs field, the bare mass term for the leptoquark is chosen sufficiently large and positive, ensuring a positive sign of the effective leptoquark mass term, i.e. for $\tilde{R}_2, m_2^2 + \lambda_2 \frac{v_2^2}{2}, m_2^2 + (\lambda_2 + \tilde{\lambda}_2) \frac{v_2^2}{2} > 0$, which gives $\langle \tilde{R}_2 \rangle = 0$, for both with and without self-leptoquark couplings at the tree level. The chances of a non-zero vacuum expectation value (VEV) at the loop level in the presence of the self-quartic coupling and with the negative Higgs-leptoquark quartic coupling, though possible, but for the choice of large positive bare leptoquark mass term, which is of the order of TeV, are diminished in our case. It should be noted that the possibility of the resultant negative mass gives rise to the unphysical solution.

Such observations have also been made in the context of 2HDM, that if $v_1 \gg v_2$, where $v_{1,2}$ are the two VEVs corresponding to the two Higgs doublets $\Phi_{1,2}$, the potential along the Φ_2 direction remains almost flat, and hence it is instructive to show the variation in the potential perpendicular to it, i.e. along Φ_1 [147, 111, 118]. Even at the one-loop ϕ_2 direction, it is not possible to have any deeper minima as compared to the ϕ_1 direction. Similarly, in our leptoquark case, as the tree-level VEV in the leptoquark direction is zero, the possibility of deeper minima in that direction also ceases to exist.

The total potential including tree-level potential and the one-loop contributions from SM particles and leptoquarks

Table 2 Different particles and the corresponding coefficients which contribute to the Coleman–Weinberg effective potential cf. Eq. (76). Here, the number of degrees of freedom for three generations of leptoquarks, i.e. 18, is shown outside the parentheses, while the same with one generation of leptoquark, i.e. 6, is listed inside the brackets

Particles	i	F	n_i	c_i	κ_i	κ'_i
SM	W^\pm	0	6	5/6	$g_2^2/4$	0
	Z	0	3	5/6	$(g_1^2 + g_2^2)/4$	0
	t	1	12	3/2	Y_t^2	0
	h	0	1	3/2	λ_h	m^2
	G^\pm	0	2	3/2	λ_h	m^2
	G^0	0	1	3/2	λ_h	m^2
\tilde{R}_2	$\tilde{R}_2^{2/3}$	0	18 (6)	3/2	$\lambda_2/2$	m_2^2
	$\tilde{R}_2^{1/3}$	0	18 (6)	3/2	$(\lambda_2 + \tilde{\lambda}_2)/2$	m_2^2
\tilde{S}_3	$\tilde{S}_3^{4/3}$	0	18 (6)	3/2	$\lambda_3/2$	m_3^2
	$\tilde{S}_3^{2/3}$	0	18 (6)	3/2	$(\lambda_3 + \tilde{\lambda}_3)/2$	m_3^2
	$\tilde{S}_3^{1/3}$	0	18 (6)	3/2	$(2\lambda_3 + \tilde{\lambda}_3)/4$	m_3^2

can be defined as:

$$V = V_0 + V_1^{\text{SM}} + V_1^{\tilde{R}_2/\tilde{S}_3/\tilde{R}_2+\tilde{S}_3}, \quad (75)$$

where V_0 is the tree-level potential of the model and V_1 is the one-loop effective potential which includes the contributions from the SM particles and the leptoquarks, and can be expressed as:

$$V_1(h, \mu) = \frac{1}{64\pi^2} \sum_i (-1)^F n_i \mathcal{M}_i^4(h) \left[\log \frac{\mathcal{M}_i^2(h)}{\mu^2} - c_i \right]. \quad (76)$$

Here, the summation includes all the particles which couple to Higgs field h at tree level, where n_i denotes the number of degrees of freedom for those particles, c_i is a constant taking value $\frac{5}{6}$ for gauge bosons and $\frac{3}{2}$ for fermions and scalars, and the quantity F is another constant which becomes 0 for bosons and 1 for fermions. The entity \mathcal{M}_i , which is given by

$$\mathcal{M}_i^2(h) = \kappa_i h^2 - \kappa'_i, \quad (77)$$

signifies the field-dependent masses for the particles in the model, with κ and κ' being two constants. All the particles relevant for this paper are listed in Table 2 along with all the corresponding constants. For the numerical analysis, we have considered $h = \mu$, since the potential remains invariant at this scale [147].

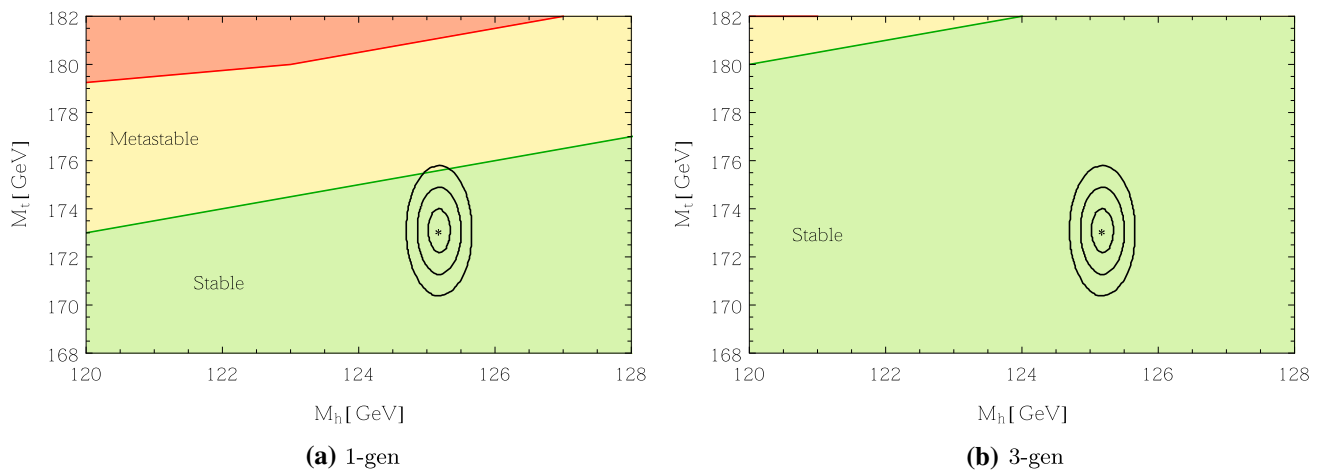


Fig. 13 Phase space diagram with Higgs mass M_h vs top mass M_t in GeV for \tilde{R}_2 . Green, yellow and red colours correspond to stable, metastable and unstable regions, respectively. The black dotted circles denote 1σ , 2σ and 3σ contours, and the black dot denotes the current Higgs mass and top mass value

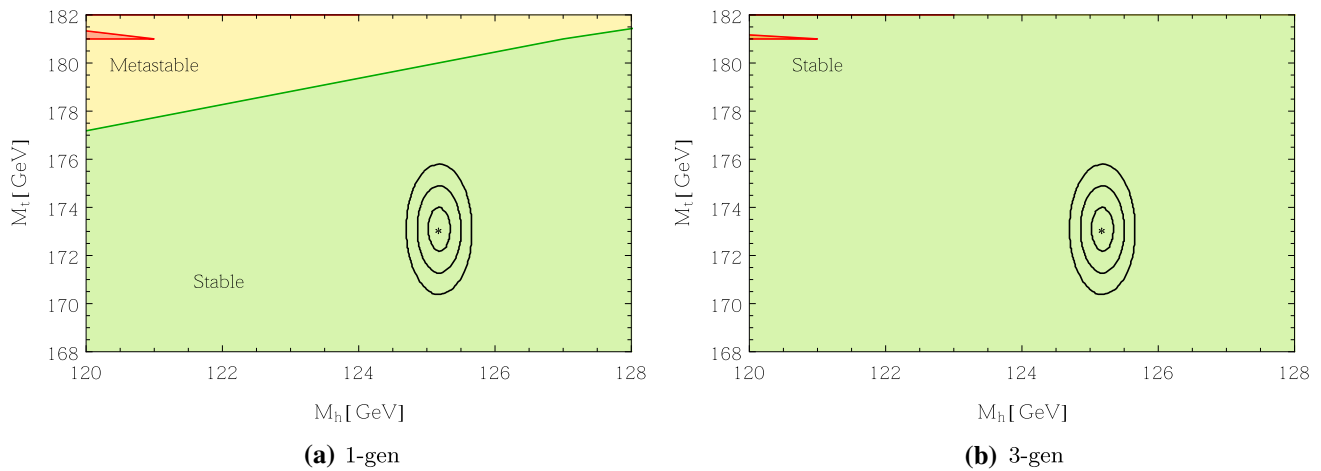


Fig. 14 Phase diagram for S_3 with M_h in GeV vs M_t in GeV. The stable, metastable and unstable regions are delineated by green, yellow and red colours, respectively. The black dot denotes the current values of Higgs mass and top mass in GeV, and black circles are 1σ , 2σ and 3σ contours

The full effective potential in (75) can be redefined in terms of an effective quartic coupling λ_{eff} , as in (74) using one-loop potential (76) as follows:

$$\lambda_{\text{eff}}(h, \mu) \simeq \underbrace{\lambda_h(\mu)}_{\text{tree-level}} + \underbrace{\frac{1}{16\pi^2} \sum_{\substack{i=W^\pm, Z, t, \\ h, G^\pm, G^0}} n_i \kappa_i^2 \left[\log \frac{\kappa_i h^2}{\mu^2} - c_i \right]}_{\text{Contribution from SM}} + \underbrace{\frac{1}{16\pi^2} \sum n_i \kappa_i^2 \left[\log \frac{\kappa_i h^2}{\mu^2} - c_i \right]}_{\text{Contribution from } \tilde{R}_2/S_3/\tilde{R}_2 + S_3}, \quad (78)$$

Now let us consider that there are two minima of the Higgs potential and we reside at the first one. If the second minimum is higher than the first one, the tunnelling from first minimum to the second one will be impossible, which in turn would

indicate that the first minimum lies in the stable region, denoted by $\lambda_{\text{eff}} > 0$. But if the height of the second minimum is lower than that of the first one, there would be a finite probability for the system to tunnel to the second one. In this scenario, if the tunnelling lifetime becomes greater than the age of the universe, we term the first minimum as metastable region.

The tunnelling probability in this scenario is given by:

$$P = T_0^4 \mu^4 e^{\frac{-8\pi^2}{3\lambda_{\text{eff}}(\mu)}}, \quad (79)$$

where μ is the scale at which the probability is maximum, i.e. $\frac{\partial P}{\partial \mu} = 0$, and T_0 is the age of the universe. Using condition $\frac{\partial P}{\partial \mu} = 0$ along with $\beta_\lambda = 0$, we can obtain the expression of λ_{eff} at different scales:

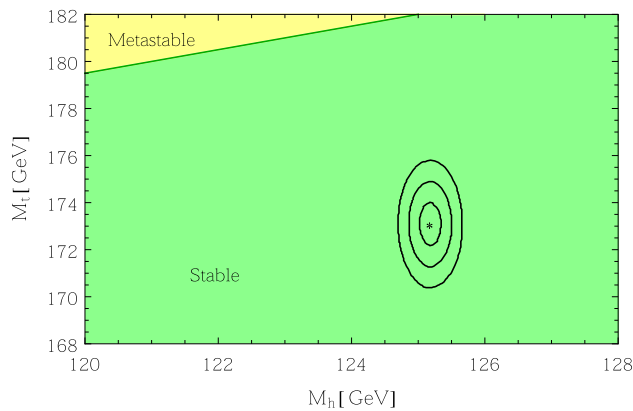


Fig. 15 Higgs mass M_h vs top quark mass M_t plot in GeV for one generation of \tilde{R}_2 and S_3 . The green and yellow colours represent stable and metastable regions. The black circles are 1σ , 2σ and 3σ contours, with the current experimental values of Higgs mass and top quark mass denoted by dots at the centre

$$\lambda_{\text{eff}}(\mu) = \frac{\lambda_{\text{eff}}(v)}{1 - \frac{3}{2\pi^2} \log\left(\frac{v}{\mu}\right) \lambda_{\text{eff}}(v)}. \quad (80)$$

Now, if we set $P = 1$, $T_0 = 10^{10}$ years and $\mu = v$, where $v \simeq 246$ GeV is the EW VEV in Eq. (79), then $\lambda_{\text{eff}}(v)$ comes out to be 0.0623. However, if we consider $P < 1$ with $T_0 = 10^{10}$ years, then it will be equivalent to demanding that the tunnelling probability from the first vacuum to the deeper one is greater than T_0 , and we will obtain the condition for metastability as [94]:

$$0 > \lambda_{\text{eff}}(\mu) \gtrsim \frac{-0.065}{1 - 0.01 \log\left(\frac{v}{\mu}\right)}. \quad (81)$$

Lastly, if the tunnelling probability from the first minimum to the deeper one is less than the age of the universe, i.e. $\lambda_{\text{eff}} < 0$, then the first minimum will be designated as the unstable region. We know that the SM vacuum lies in the metastable region. However, the presence of leptoquarks will exert extra effects in λ_{eff} , which will alter the metastability of the Higgs vacuum. Different regions with respect to stability, metastability and instability for \tilde{R}_2 , S_3 and one generation of $\tilde{R}_2 + S_3$ are presented in Figs. 13, 14 and 15. We refrain from three generations of $\tilde{R}_2 + S_3$, as it obtains serious constraints from Planck scale perturbativity and stability. We have plotted Higgs mass M_h (in GeV) versus top mass M_t (in GeV) in the above-mentioned figures along with the stable, metastable and unstable regions coloured by green, yellow and red, respectively. The black circles define 1σ , 2σ and 3σ contours, with a dot at the centre denoting the current Higgs mass and top mass values [144, 148, 149]. In Fig. 13a, b, the results for one generation and three generations of \tilde{R}_2 are illustrated. For this analysis, M_h is varied between 119 GeV and 135 GeV, whereas M_t is varied from 165 GeV to 185 GeV with fixed $\lambda_h = 0.1264$

and $Y_u^{33} = 0.9369$ at the EW scale. The other quartic couplings λ_2 and $\tilde{\lambda}_2$ are varied from 0.1 to 0.8. As can be seen, for one generation of \tilde{R}_2 , only the 3σ contour hits metastability while the three-generation scenario resides entirely inside the stable region, as the positive effects of gauge couplings and quartic couplings are very large. Again, the positive contributions forming gauge couplings in the triplet leptoquark case are even higher than in the \tilde{R}_2 scenario. Therefore, we obtain the complete stable region with both one generation and three generations of S_3 , shown in Fig. 14a, b. The positive gauge coupling contributions are higher for the $\tilde{R}_2 + S_3$ case, and hence we obtain a completely stable region for this case as well, see Fig. 15.

5 Phenomenology

In this section, we discuss different experimental bounds on the parameter space of scalar leptoquarks and compare them with the theoretical bounds arising from the demand of perturbativity and stability of the theory up to Planck scale. There are both direct and indirect bounds on leptoquarks. While the indirect limits are obtained using effective four-fermion interactions induced by leptoquarks at various low-energy experiments, the direct ones are drawn from the cross section involving their production (if any) at high energy colliders. B-anomalies in semi-leptonic B decays, lepton flavour non-universality, lepton flavour-violating decays, anomalous magnetic moment of muon and rare kaon decays are a few low-energy phenomena constraining leptoquarks. A comprehensive list containing all the indirect bounds on leptoquarks can be found in the ‘‘Indirect Limits for Leptoquarks’’ section of Ref. [149]. However, most of the indirect limits involve bounds on the product of one diagonal and one off-diagonal Yukawa coupling of the leptoquarks with quarks and leptons [92, 150, 151]. Since this coupling has been considered diagonal in our analysis, those indirect limits are automatically satisfied.

On the other hand, it is well known that leptoquarks coupling to multiple generations of quarks and leptons are capable of inducing flavour-changing neutral currents. For example, non-chiral leptoquarks, which can interact with both left- and right-handed leptons, obtain stringent constraints from muon $g - 2$ [153] and the ratio of partial decay rates $(\pi \rightarrow e\nu)/(\pi \rightarrow \mu\nu)$ [154] if they are allowed to interact with multiple generations of quarks and fermions. In our analysis, we neither force any leptoquark to couple to different generations of quarks and leptons, nor work with any non-chiral leptoquark.⁷ Therefore, the constraints arising from flavour-changing neutral currents will be much weaker in

⁷ Both \tilde{R}_2 and S_3 are chiral leptoquarks since they couple to left-handed leptons only.

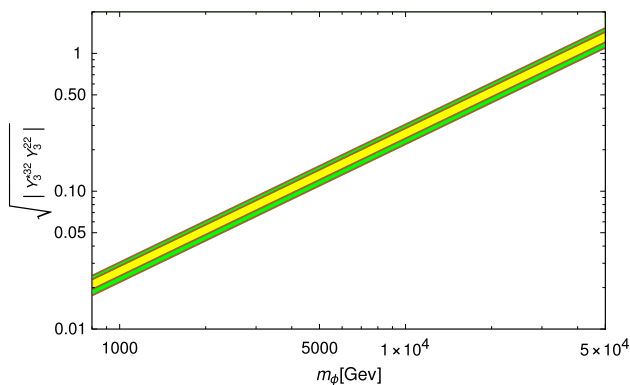


Fig. 16 Constraint on Yukawa coupling of S_3 as a function of its mass describing $R_{K^{(*)}}$ anomalies [15]. The yellow and green colours indicate 1σ and 2σ allowed regions

our scenarios. It is interesting to mention that the possibilities of larger Yukawa couplings of leptoquarks, i.e. $\mathcal{O}(1)$, are not completely ruled out by the low-energy observables [8, 22, 23, 25, 26, 73].

Now, it is impossible to find any single scalar leptoquark solution to all the flavour anomalies, and therefore combinations of different scalar leptoquarks are essential to take various flavour anomalies into account. For example, leptoquarks S_1 and R_2 can explain the observed anomalies in $R_{D^{(*)}}$, whereas leptoquark S_3 can account for $R_{K^{(*)}}$ anomalies [23]. So, in order to describe both the B-anomalies, one should consider $S_1 - S_3$ or $R_2 - S_3$ pairs.⁸ In Fig. 16, we depict the constraints on the parameter space of S_3 describing $R_{K^{(*)}}$ anomalies, where the yellow and green regions indicate 1σ and 2σ allowed ranges [15]. Again, To generate tiny neutrino masses through loops within the framework of leptoquark models, one has to combine S_1 or S_3 with \tilde{R}_2 [29, 155]. Moreover, although non-chiral leptoquarks S_1 and R_2 can accommodate muon and electron ($g - 2$), the masses of the leptoquarks required for illustrating the experimental values are ≈ 100 TeV considering the Yukawa couplings under perturbative limit [155]. Therefore, one should consider combinations of S_1 & S_3 , \tilde{S}_1 & S_3 or R_2 and \tilde{R}_2 mixing through the Higgs field [155]. However, the imposition of various flavour physics constraints along with LHC bounds and $\mu \rightarrow e\gamma$ result suggests that none of these scenarios can accommodate both muon and electron ($g - 2$). Therefore, to gain a complete picture regarding various low-energy observables, study of the bounds on the parameter space of different leptoquarks is indispensable.

We have already mentioned that we have considered only diagonal Yukawa couplings, whereas most of the indirect bounds involve off-diagonal elements as well. For instance, Fig. 16 shows the bound on $\sqrt{|Y_3^{*32} Y_3^{22}|}$ as a function of

⁸ Leptoquark \tilde{R}_2 cannot explain either of these two anomalies.

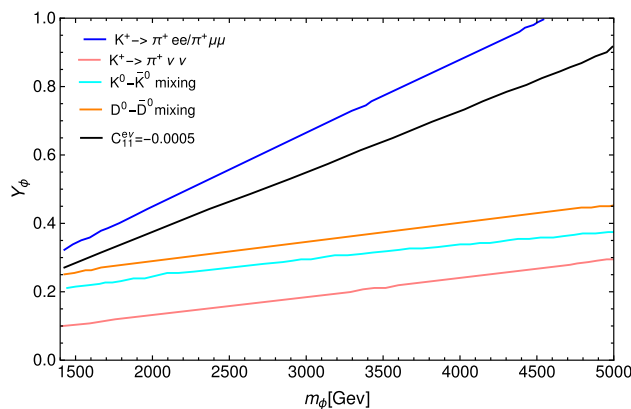


Fig. 17 Flavour constraint on Yukawa coupling of first-generation S_3 as a function of its mass [152]. The blue and red lines indicate the bounds from the ratio $B(K^+ \rightarrow \pi^+ ee)/B(K^+ \rightarrow \pi^+ \mu\mu)$ and the branching fraction $B(K^+ \rightarrow \pi^+ \nu\nu)$. The cyan and orange lines indicate constraints from neutral kaon and D-meson mixing, respectively. The black line signifies leptoquark (S_3) contribution of -0.0005 to the Wilson coefficient ($C_{11}^{e\nu}$) involved in the ratio $B(\pi \rightarrow \mu\nu)/B(\pi \rightarrow e\nu)$

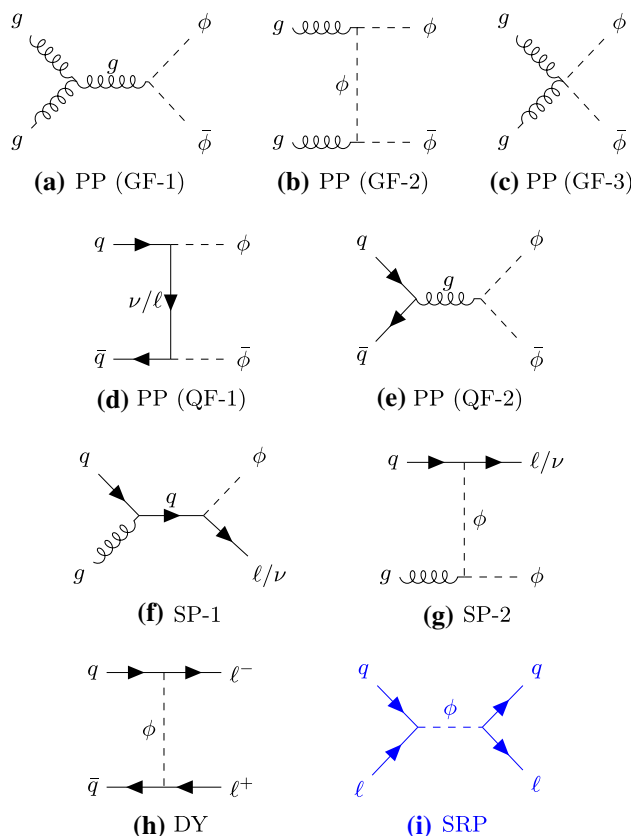


Fig. 18 Leading-order Feynman diagrams involving direct bounds on leptoquarks. The first two rows correspond to Leptoquark pair production (PP) at LHC, while the third and fourth rows signify single production (SP) of leptoquark associated with a quark, leptoquark contribution to Drell–Yan-like di-lepton process and single resonant production of leptoquark (SRP). Regarding pair production, the first three diagrams indicate gluon fusion (GF), while the last two illustrate quark fusion (QF). The photon and Z-mediated diagrams have been ignored due to the very small contribution

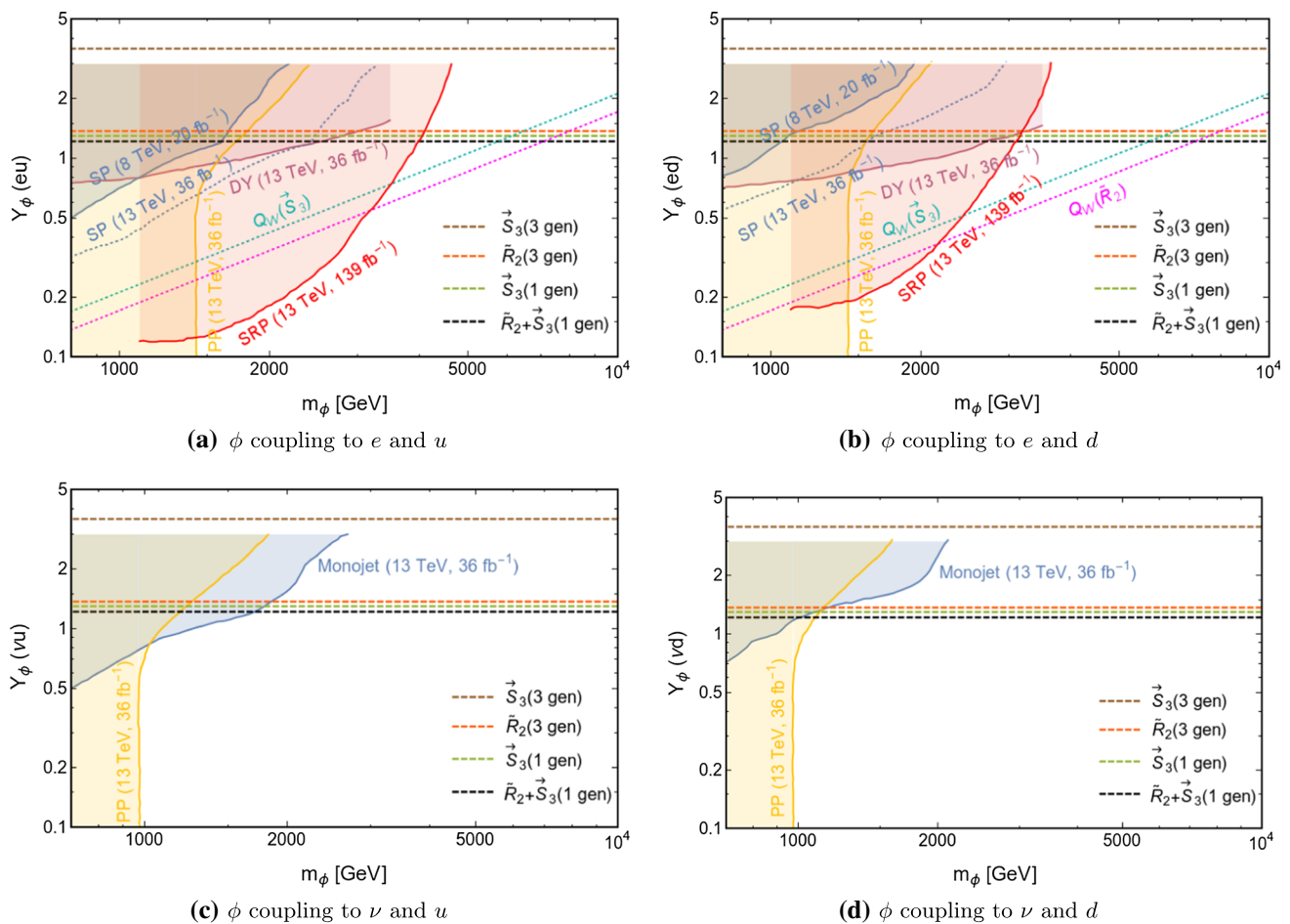


Fig. 19 Bounds on parameter space of scalar leptoquark coupling to first generation of quarks and leptons [156, 157]. The shaded regions are disallowed by direct detection. The limits from pair production involving charged leptons are recast from [158], while the same involving neutrinos are recast from [90]. These bounds are shown in yellow. The limits emerging from single production (SP), Drell–Yan (DY) and single resonant production (SRP), shown by bluish, maroonish purple and reddish portions, are based on Refs. [157, 159, 160]. On the other hand,

the mono-jet limits (bluish) are drawn from Ref. [161]. The dotted lines with magenta and sea green colours represent constraints from weak hypercharge measurements involving \tilde{R}_2 and S_3 , respectively. Finally, the dashed lines indicate theoretical upper bounds on the Yukawa coupling appearing from Planck scale stability up to two-loop order; the brown and red lines represent the limits for three generations of S_3 and \tilde{R}_2 , whereas the green and black lines portray the same for one generation of S_3 and $\tilde{R}_2 + S_3$

mass for S_3 to explain $R_{K^{(*)}}$ anomalies. Now, the upper limits on the diagonal Yukawa couplings derived from the demand of Planck scale stability and perturbativity are not expected to change much with the introduction of small off-diagonal couplings. However, these small off-diagonal couplings along with large diagonal elements can now be used to explain various flavour anomalies with respect to different indirect bounds. Again, there arise some additional flavour constraints on the parameter space of the first-generation scalar triplet leptoquark (S_3) [152], which are depicted in Fig. 17, but such bounds do not appear for \tilde{R}_2 . Moreover, different low-energy bounds on the Yukawa couplings of the $\tilde{R}_2 - S_3$ model are described in Ref. [29]. However, we are mostly interested in the constraints from the collider perspective.

When discussing the direct bounds on leptoquarks, we consider pair production (PP), single production (SP) associated with a quark, Drell–Yan processes (DY) and single resonant production of leptoquark (SRP). At the pp collider, like LHC, pair production of leptoquarks can occur through both gluon fusion (GF) and quark fusion (QF), whose corresponding Feynman diagrams are shown in the first and second rows of Fig. 18. The Feynman diagrams for single production of the leptoquark, contribution to Drell–Yan like dilepton processes and SRP are presented in the third and fourth rows of Fig. 18. Regarding the coupling of leptoquarks to charged leptons, we obtain the opposite-sign di-lepton (OSD) signature for DY processes, as shown in Fig 18(h), whereas PP and SP provide di-jet plus OSD and mono-jet plus OSD final states at the detector [43, 73]. Conversely, for leptoquarks

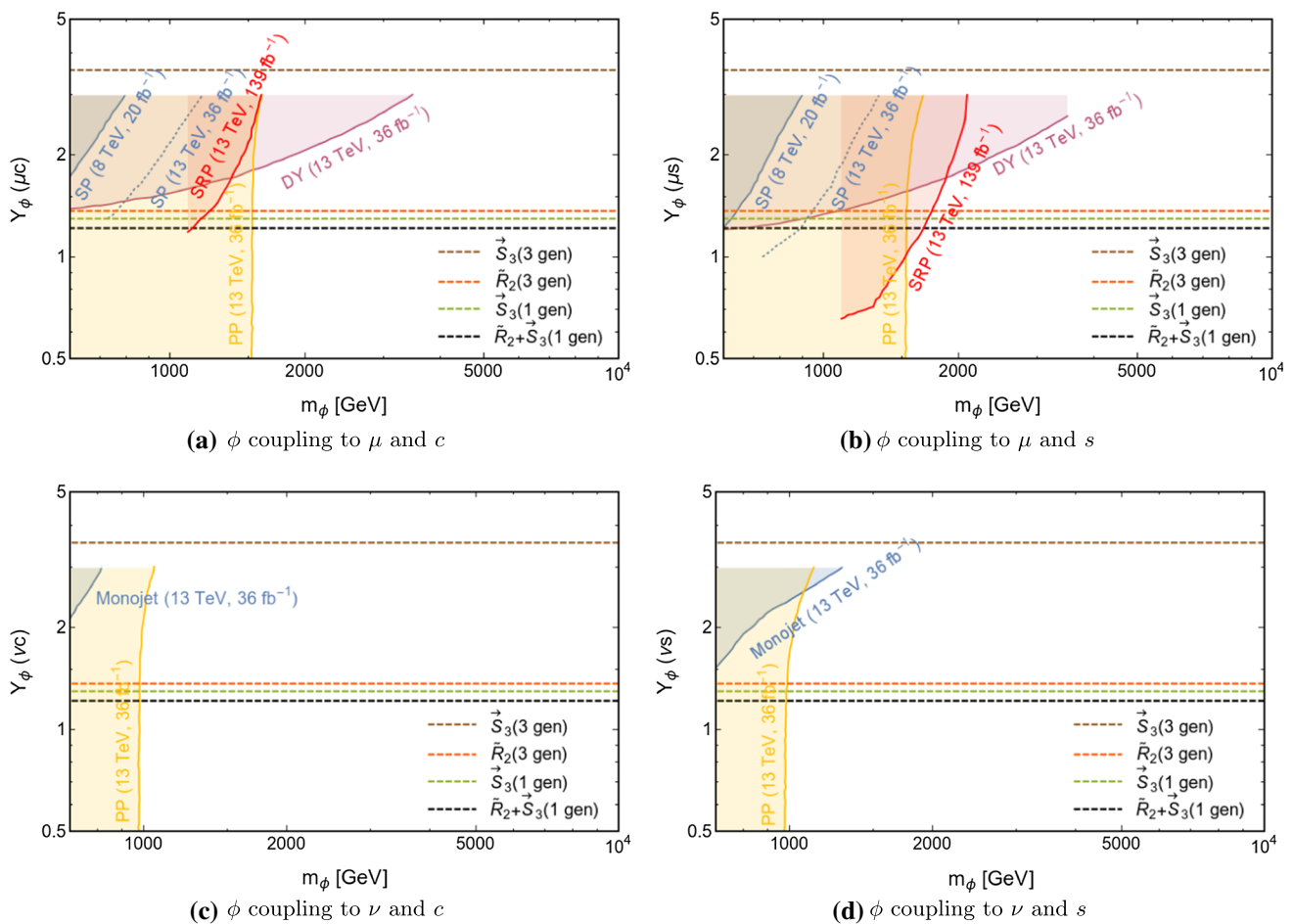


Fig. 20 Bounds on parameter space of scalar leptoquark coupling to second generation of quarks and leptons [156, 157]. The shaded regions are disallowed by direct detection. The limits from pair production involving charged leptons are recast from [162], while the same involving neutrinos are recast from [90]. These bounds are shown in yellow. The limits emerging from single production (SP), Drell–Yan (DY) and

single resonant production (SRP), shown by bluish, maroonish purple and reddish portions, are based on Refs. [157, 159, 160]. On the other hand, the mono-jet limits (bluish) are drawn from Ref. [161]. Finally, the dashed lines indicate theoretical upper bounds on the Yukawa coupling appearing from Planck scale stability up to two-loop order; the colour codes are as mentioned in Fig. 19

coupling to neutrinos, we have di-jet plus missing energy and mono-jet plus missing energy signatures only. The full data set collected at HERA in ep collision excluded the first generation of leptoquarks with mass up to 800 GeV at 95% confidence limits for coupling to be 0.3 [82]. In a more recent study they have modified Y_ϕ/m_ϕ limits for the first generation of leptoquarks [83]. The CMS collaboration at the LHC also searched for single production of leptoquarks which probe the high coupling region of leptoquarks [88, 160].

We depict different direct constraints on the parameter space of scalar leptoquarks in Figs. 19, 20 and 21. These bounds can be recast for different models of scalar leptoquarks depending on the cross sections and the corresponding decay branching fractions leading to the final states. Figure 19 summarizes the bounds for the first generation of leptoquarks, and Figs. 20 and 21 show the same for the second and

third generations of leptoquarks, respectively. All the plots presented in Figs. 19 and 20 are taken from Refs. [156, 157], which use Refs. [90, 158, 162] for PP, Ref. [159] for SP, Ref. [160] for DY, LHC Run II data for SRP and Ref. [161] for mono-jet signature with first and second generations of leptons to restrict the parameter space for leptoquark-quark-lepton coupling below 3.0 with leptoquark mass below 3 TeV. Conversely, Fig. 21a describing constraints on $\phi\tau b$ coupling is taken from Ref. [156], which use Refs. [163–165] for their analysis, and Fig. 21b illustrating limits on $\phi\nu b$ coupling is taken from Ref. [91]. For the final states involving charged leptons, the yellow, blueish, maroonish purple and reddish portions indicate the prohibited region from PP, SP, DY and SRP processes, respectively. On the contrary, for the final states involving missing energy, the yellow and bluish regions signify PP and mono-jet signals.

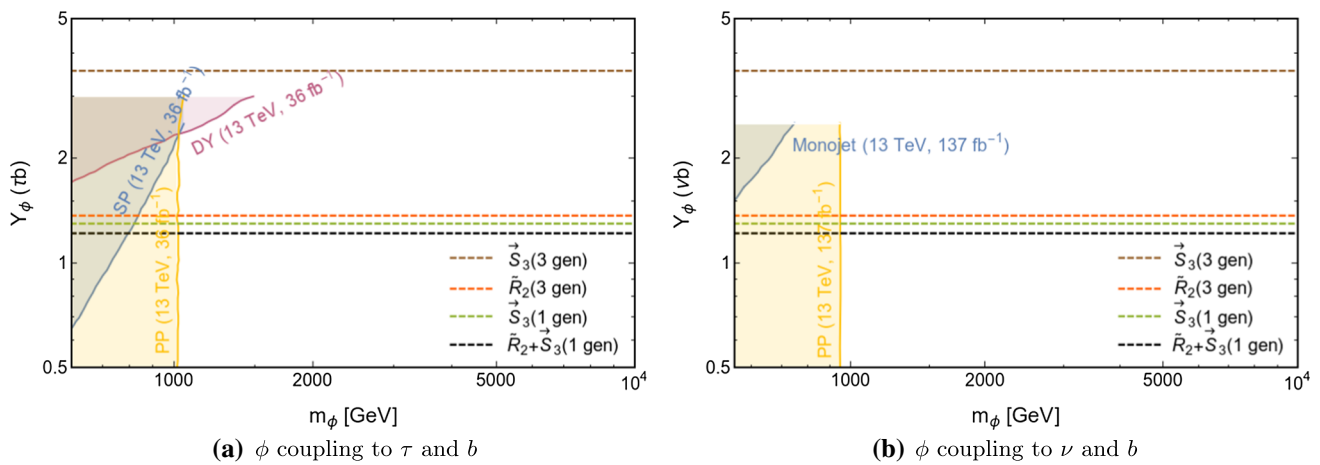


Fig. 21 Bounds on parameter space of scalar leptoquark coupling to third generation of quarks and leptons [91, 156]. The shaded regions are disallowed by direct detection. The limit from pair production involving charged leptons is recast from [163], which is shown in yellow. The limits emerging from single production (SP) and Drell–Yan (DY),

shown by bluish and maroonish purple portions, are based on Refs. [164, 165]. Finally, the dashed lines indicate theoretical upper bounds on the Yukawa coupling appearing from Planck scale stability up to two-loop order; the colour codes are as mentioned in Fig. 19

We impose the theoretical bounds obtained from the perturbative unitarity and the stability at the two-loop for the dimensionless couplings in the $m_\phi - Y_\phi$ plane for \tilde{R}_2 , S_3 and $\tilde{R}_2 + S_3$, respectively. The brown ($Y_\phi = 3.90$) and the red ($Y_\phi = 1.36$) dashed lines depict the theoretical upper limits on the Yukawa couplings of leptoquarks for three generations of S_3 and \tilde{R}_2 , respectively, considering Planck scale stability at the two-loop level. The same for one generation of S_3 and $\tilde{R}_2 + S_3$ are presented by the green ($Y_\phi = 1.29$) and the black ($Y_\phi = 1.21$) dashed lines.

At this point it is worth mentioning that we do not present the bounds on \tilde{R}_2 with one generation and $\tilde{R}_2 + S_3$ with three generations in these plots. Actually, as described earlier, \tilde{R}_2 with one generation cannot achieve Planck scale stability for any small value of Y_ϕ at two-loop order. On the other hand, although $\tilde{R}_2 + S_3$ with three generations shows stability for $Y_\phi \leq 1.0$, it loses perturbativity at an energy scale ($\sim 10^{14.4}$ GeV) far below the Planck scale at two-loop order.

For the first-generation leptoquark coupling to charged leptons, there exists another bound from measurement of the weak charge of proton and nuclei [156]. This quantity is measured through atomic parity violation and parity-violating electron scattering [149, 166]. For \tilde{R}_2 and S_3 , these measurements translate into $Y_\phi \leq 0.17 \left(\frac{m_\phi}{1\text{TeV}} \right)$ and $Y_\phi \leq 0.21 \left(\frac{m_\phi}{1\text{TeV}} \right)$, respectively, which are shown by the dotted lines in magenta and sea green colours, respectively. Since \tilde{R}_2 couples to the down-type quarks only, while S_3 interacts with both up-type and down-type quarks, we find the magenta line in Fig. 19b only, whereas the sea green line exists in both Fig. 19a and b. Because the nuclei do not contain other gen-

erations of quarks as valance quarks, this kind of limit does not appear for other generations of leptoquarks.

From these results it is evident that the theoretical limits coming from Planck scale stability and perturbative unitarity up to two-loop order might put stronger constraints on the parameter space of leptoquarks with higher mass range in particular for the second and third generations of the leptoquarks. On the other hand, bounds on the Higgs-leptoquark quartic coupling are not very well studied in the literature. In our analysis, we find that this coupling being larger than ~ 0.2 disturbs the perturbativity of the theory up to Planck scale.⁹

6 Conclusion

In this paper, we have studied the scalar doublet leptoquark \tilde{R}_2 , the scalar triplet leptoquark S_3 and their combination with both one generation and three generations with respect to the perturbativity and the stability of the Higgs vacuum. The extra contribution in the running of the gauge couplings at one-loop level mainly depends on the number of the leptoquark components present in the model, which is determined by its gauge structure. Although at the two-loop level they depend on the leptoquark Yukawa couplings, they do not depend on the Higgs-leptoquark couplings explicitly. With the two-loop effects, the gauge coupling g_2 for the leptoquark S_3 and the combined scenario of \tilde{R}_2 and S_3 with three gen-

⁹ To be more specific, for three generations of \tilde{R}_2 one needs $(\lambda_2, \tilde{\lambda}_2) \leq 0.22$, and for three generations of S_3 we require $(\lambda_3, \tilde{\lambda}_3) \leq 0.18$ in order to confirm Planck scale perturbativity.

erations diverges at $10^{19.7}$ GeV and $10^{14.4}$ GeV, respectively, which forces the other couplings to hit singularity at those scales. But at the one-loop level, all the leptoquark models considered in this paper achieve Planck scale perturbativity with gauge couplings. It is also noteworthy that no Landau pole emerges in the running of gauge couplings for two generations of these leptoquarks. The Higgs-leptoquark quartic couplings acquire severe constraints from Planck scale perturbativity. With larger EW values of these couplings (e.g. 0.3), the theories become non-perturbative at much lower energy scales than the Planck scale. These constraints do not change much due to alteration in the leptoquark Yukawa couplings. For the three-generation scenario with \tilde{R}_2 and S_3 combined, the Higgs-leptoquark quartic couplings diverge much below the Planck scale. On the other hand, the leptoquark Yukawa couplings obtain the upper bound from the Planck scale perturbativity and stability of the Higgs vacuum. In the running of λ_h , the gauge couplings exert positive contributions, whereas the Yukawa couplings of leptoquarks introduce negative effects. For three generations of \tilde{R}_2 with the Higgs-leptoquark quartic couplings being 0.1, the Yukawa coupling should be smaller than 1.36 for the theory maintaining stability up to Planck scale. This number becomes 1.29, 3.9¹⁰ and 1.21 for one generation of S_3 , three generations of S_3 and one generation of $\tilde{R}_2 + S_3$, respectively. Finally, regarding the Coleman–Weinberg effective potential approach, the presence of any of these leptoquarks with any number of generations pushes the metastable vacuum of SM to the stable region, although the 3σ contour of \tilde{R}_2 with one generation marginally touches the metastable region. The phenomenological bounds obtained mainly from the collider experiments are also drawn along with our theoretical bounds. We see that the Planck scale perturbativity and stability puts some theoretical additional restrictions on the parameter space of the leptoquarks in addition to the experimental bounds.

Acknowledgements The authors acknowledge SERB CORE Grant CRG/2018/ 004971 and MATRICS Grant MTR/2020/000668 for the financial support. SJ thanks DST/INSPIRES/03/2018/ 001207 for the financial support towards finishing this work. This work has also been supported in part by MCIN/ AEI/10.13039/501100011033 Grant No. PID2020-114473 GB-I00 and Grant PROMETEO/2021/071 (Generalitat Valenciana). The authors also thank Alexander Bednyakov for some useful comments.

Data Availability Statement This manuscript has no associated data or the data will not be deposited. [Authors’ comment: The results of this paper provide theoretical constraints on scalar and doublet leptoquarks arising from stability of vacuum and perturbativity. No experimental or astrophysical data has been analysed or produced in this article.]

¹⁰ The upper bound on Y_ϕ would be $\sqrt{4\pi}$ considering perturbative unitarity and Planck scale stability for three generations of S_3 .

Open Access This article is licensed under a Creative Commons Attribution 4.0 International License, which permits use, sharing, adaptation, distribution and reproduction in any medium or format, as long as you give appropriate credit to the original author(s) and the source, provide a link to the Creative Commons licence, and indicate if changes were made. The images or other third party material in this article are included in the article’s Creative Commons licence, unless indicated otherwise in a credit line to the material. If material is not included in the article’s Creative Commons licence and your intended use is not permitted by statutory regulation or exceeds the permitted use, you will need to obtain permission directly from the copyright holder. To view a copy of this licence, visit <http://creativecommons.org/licenses/by/4.0/>. Funded by SCOAP³.

Appendix A: Two-loop beta functions of g_3

Using SARAH, we generate the beta function of g_3 for different models up to two loops, which are given below:

$$\beta(g_3)_{SM}^{2-loop} = -7 \left(\frac{g_3^3}{16\pi^2} \right) + \frac{g_3^3}{(16\pi^2)^2} \left[\frac{11}{10} g_1^2 + \frac{9}{2} g_2^2 - 26 g_3^2 - 2 \text{Tr} \left(X_u + X_d \right) \right], \tag{82}$$

$$\beta(g_3)_{\tilde{R}_2, 1-gen}^{2-loop} = -\frac{20}{3} \left(\frac{g_3^3}{16\pi^2} \right) + \frac{g_3^3}{(16\pi^2)^2} \left[\frac{7}{6} g_1^2 + \frac{15}{2} g_2^2 - \frac{56}{3} g_3^2 - 2 \text{Tr} \left(X_u + X_d + \frac{1}{2} X_2 \right) \right], \tag{83}$$

$$\beta(g_3)_{\tilde{R}_2, 3-gen}^{2-loop} = -6 \left(\frac{g_3^3}{16\pi^2} \right) + \frac{g_3^3}{(16\pi^2)^2} \left[\frac{13}{10} g_1^2 + \frac{27}{2} g_2^2 - 4 g_3^2 - 2 \text{Tr} \left(X_u + X_d + \frac{1}{2} \sum_{i=1}^3 X_{2,i} \right) \right], \tag{84}$$

$$\beta(g_3)_{S_3, 1-gen}^{2-loop} = -\frac{13}{2} \left(\frac{g_3^3}{16\pi^2} \right) + \frac{g_3^3}{(16\pi^2)^2} \left[\frac{3}{2} g_1^2 + \frac{33}{2} g_2^2 - 15 g_3^2 - 2 \text{Tr} \left(X_u + X_d + \frac{3}{4} X_3 \right) \right], \tag{85}$$

$$\beta(g_3)_{S_3, 3-gen}^{2-loop} = -\frac{11}{2} \left(\frac{g_3^3}{16\pi^2} \right) + \frac{g_3^3}{(16\pi^2)^2} \left[\frac{23}{10} g_1^2 + \frac{81}{2} g_2^2 + 7 g_3^2 - 2 \text{Tr} \left(X_u + X_d + \frac{3}{4} \sum_{i=1}^3 X_{3,i} \right) \right], \tag{86}$$

$$\beta(g_3)_{\tilde{R}_2 + S_3, 1-gen}^{2-loop} = -\frac{37}{6} \left(\frac{g_3^3}{16\pi^2} \right) + \frac{g_3^3}{(16\pi^2)^2} \left[\frac{47}{30} g_1^2 + \frac{39}{2} g_2^2 - \frac{23}{3} g_3^2 - 2 \text{Tr} \left(X_u + X_d + \frac{1}{2} X_2 + \frac{3}{4} X_3 \right) \right], \tag{87}$$

$$\beta(g_3)_{\tilde{R}_2 + S_3, 3-gen}^{2-loop} = -\frac{9}{2} \left(\frac{g_3^3}{16\pi^2} \right) + \frac{g_3^3}{(16\pi^2)^2} \left[\frac{5}{2} g_1^2 + \frac{99}{2} g_2^2 + 29 g_3^2 - 2 \text{Tr} \left(X_u + X_d + \frac{1}{2} \sum_{i=1}^3 X_{2,i} + \frac{3}{4} \sum_{i=1}^3 X_{3,i} \right) \right]. \tag{88}$$

Appendix B: Two-loop beta functions of g_1

Now, with the help of SARAH, we show the two-loops beta function of g_1 for all the models as follows:

$$\beta(g_1)_{SM}^{2-loop} = \frac{41}{10} \left(\frac{g_1^3}{16\pi^2} \right) + \frac{g_1^3}{(16\pi^2)^2} \left[\frac{199}{50} g_1^2 + \frac{27}{10} g_2^2 + \frac{44}{5} g_3^2 - \frac{3}{2} \text{Tr} \left(X_l + \frac{17}{15} X_u + \frac{1}{3} X_d \right) \right], \tag{89}$$

$$\beta(g_1)_{\tilde{R}_{2,1-gen}}^{2-loop} = \frac{62}{15} \left(\frac{g_1^3}{16\pi^2} \right) + \frac{g_1^3}{(16\pi^2)^2} \left[\frac{299}{75} g_1^2 + 3 g_2^2 + \frac{28}{3} g_3^2 - \frac{3}{2} \text{Tr} \left(X_l + \frac{17}{15} X_u + \frac{1}{3} X_d + \frac{13}{15} X_2 \right) \right], \tag{90}$$

$$\beta(g_1)_{\tilde{R}_{2,3-gen}}^{2-loop} = \frac{21}{5} \left(\frac{g_1^3}{16\pi^2} \right) + \frac{g_1^3}{(16\pi^2)^2} \left[4 g_1^2 + \frac{18}{5} g_2^2 + \frac{52}{5} g_3^2 - \frac{3}{2} \text{Tr} \left(X_l + \frac{17}{15} X_u + \frac{1}{3} X_d + \frac{13}{15} \sum_{i=1}^3 X_{2,i} \right) \right], \tag{91}$$

$$\beta(g_1)_{S_{3,1-gen}}^{2-loop} = \frac{43}{10} \left(\frac{g_1^3}{16\pi^2} \right) + \frac{g_1^3}{(16\pi^2)^2} \left[\frac{207}{50} g_1^2 + \frac{15}{2} g_2^2 + 12 g_3^2 - \frac{3}{2} \text{Tr} \left(X_l + \frac{17}{15} X_u + \frac{1}{3} X_d + X_3 \right) \right], \tag{92}$$

$$\beta(g_1)_{S_{3,3-gen}}^{2-loop} = \frac{47}{10} \left(\frac{g_1^3}{16\pi^2} \right) + \frac{g_1^3}{(16\pi^2)^2} \left[\frac{223}{50} g_1^2 + \frac{171}{10} g_2^2 + \frac{92}{5} g_3^2 - \frac{3}{2} \text{Tr} \left(X_l + \frac{17}{15} X_u + \frac{1}{3} X_d + \sum_{i=1}^3 X_{3,i} \right) \right], \tag{93}$$

$$\beta(g_1)_{\tilde{R}_{2+S_{3,1-gen}}^{2-loop}} = \frac{13}{3} \left(\frac{g_1^3}{16\pi^2} \right) + \frac{g_1^3}{(16\pi^2)^2} \left[\frac{311}{75} g_1^2 + \frac{39}{5} g_2^2 + \frac{188}{15} g_3^2 - \frac{3}{2} \text{Tr} \left(X_l + \frac{17}{15} X_u + \frac{1}{3} X_d + \frac{13}{15} X_2 + X_3 \right) \right], \tag{94}$$

$$\beta(g_1)_{\tilde{R}_{2+S_{3,3-gen}}^{2-loop}} = \frac{24}{5} \left(\frac{g_1^3}{16\pi^2} \right) + \frac{g_1^3}{(16\pi^2)^2} \left[\frac{112}{25} g_1^2 + 18 g_2^2 + 20 g_3^2 - \frac{3}{2} \text{Tr} \left(X_l + \frac{17}{15} X_u + \frac{1}{3} X_d + \frac{13}{15} \sum_{i=1}^3 X_{2,i} + \sum_{i=1}^3 X_{3,i} \right) \right]. \tag{95}$$

Appendix C: Running of top Yukawa coupling

Top Yukawa coupling plays a very important role in the stability of the Higgs vacuum. Therefore, it is important to study the RG evolution of this parameter. As already mentioned

in Eq. (15), the absolute value for top Yukawa coupling at any energy scale must be less than $\sqrt{4\pi}$ in order to ensure the perturbativity of the model. It is worth mentioning that although the Yukawa couplings for leptons and other quarks also vary with the scale, their initial value at the EW scale are so small that they usually never cross the perturbativity bound unless some other parameter hits the divergence. Therefore, we restrict our discussion for the top Yukawa coupling only. Now, to investigate the running of the top Yukawa coupling, we study the RG evolution of Y_u (Yukawa matrix for up-type quarks) whose (3,3) component would provide us the desired result. The one-loop and two-loop beta functions of Y_u under SM are as follows:

$$\beta(Y_u)_{SM}^{1-loop} = \frac{Y_u}{16\pi^2} \left[\frac{3}{2} (\tilde{X}_u - \tilde{X}_d) - I_3 \left(\frac{17}{20} g_1^2 + \frac{9}{4} g_2^2 + 8 g_3^2 \right) + 3 I_3 \text{Tr} \left(X_u + X_d + \frac{1}{3} X_l \right) \right], \tag{96}$$

$$\begin{aligned} \beta(Y_u)_{SM}^{2-loop} = & \beta(Y_u)_{SM}^{1-loop} + \frac{Y_u}{(16\pi^2)^2} \left[\left(\frac{11}{4} \tilde{X}_d^2 - \tilde{X}_u \tilde{X}_d \right. \right. \\ & + \frac{3}{2} \tilde{X}_u^2 - \frac{1}{4} \tilde{X}_d \tilde{X}_u \left. \right) + \tilde{X}_u \left\{ \frac{223}{80} g_1^2 + \frac{135}{16} g_2^2 \right. \\ & + 16 g_3^2 - 12 \lambda_h - \frac{27}{4} \text{Tr} \left(X_u + X_d + \frac{1}{3} X_l \right) \left. \right\} \\ & - \tilde{X}_d \left\{ \frac{43}{80} g_1^2 - \frac{9}{16} g_2^2 + 16 g_3^2 - \frac{15}{4} \text{Tr} \left(X_u \right. \right. \\ & + X_d + \frac{1}{3} X_l \left. \right) \left. \right\} + I_3 \left(6 \lambda_h^2 + \frac{1187}{600} g_1^4 - \frac{23}{4} g_2^4 \right. \\ & - 108 g_3^4 - \frac{9}{20} g_1^2 g_2^2 + \frac{19}{15} g_1^2 g_3^2 + 9 g_2^2 g_3^2 \left. \right) \\ & + \frac{5}{8} I_3 \text{Tr} \left\{ \left(g_1^2 + 9 g_2^2 + 32 g_3^2 \right) X_d + \left(\frac{17}{5} g_1^2 \right. \right. \\ & + 9 g_2^2 + 32 g_3^2 \left. \right) X_u + 3 \left(g_1^2 + g_2^2 \right) X_l \left. \right\} \\ & - \frac{27}{4} I_3 \text{Tr} \left(X_u^2 + X_d^2 - \frac{2}{9} \tilde{X}_u \tilde{X}_d + \frac{1}{3} X_l^2 \right) \left. \right]. \tag{97} \end{aligned}$$

The above two expressions are matrix equations, with I_3 indicating the 3×3 identity matrix in the flavour space of up-type quarks.

Now, for leptoquark \tilde{R}_2 (with both one generation and three generations), the one-loop beta function of Y_u does not obtain any additional contribution at the one-loop level, i.e. $\Delta\beta(Y_u)_{\tilde{R}_2}^{1-loop} = 0$. Hence, it remains the same as that of SM:

$$\beta(Y_u)_{\tilde{R}_{2,1-gen}}^{1-loop} = \beta(Y_u)_{\tilde{R}_{2,3-gen}}^{1-loop} = \beta(Y_u)_{SM}^{1-loop}. \tag{98}$$

Nevertheless, there exist some non-vanishing two-loop contributions to it, and hence the full two-loop beta functions of Y_u for leptoquark \tilde{R}_2 with one both generation and

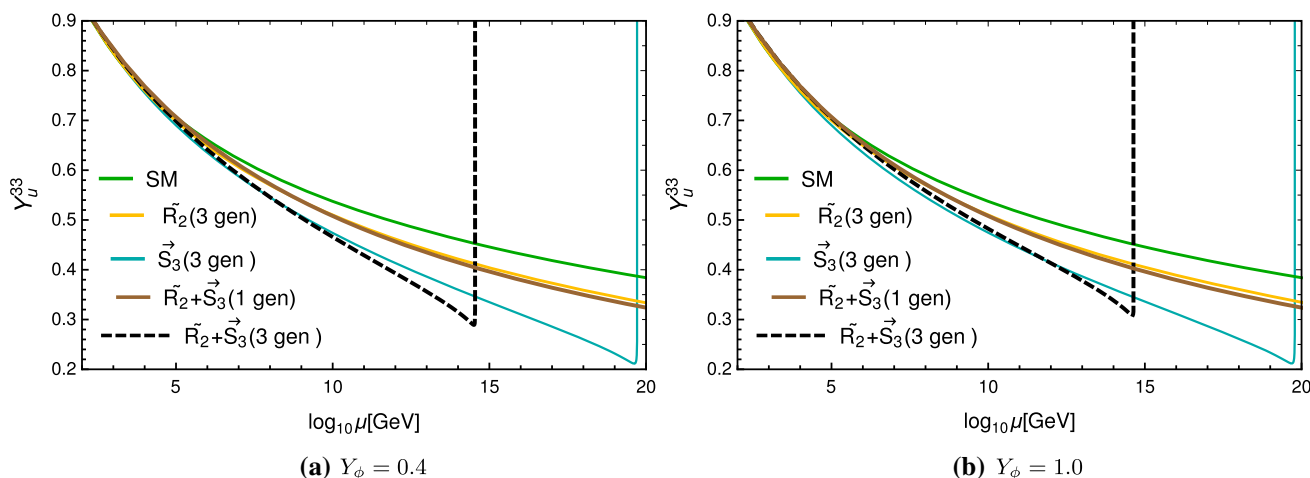


Fig. 22 Variation in top quark Yukawa with scale

three generations can be expressed as follows:¹¹

$$\beta(Y_u)_{\tilde{R}_2, 1\text{-gen}}^{2\text{-loop}} = \beta(Y_u)_{\text{SM}}^{2\text{-loop}} + \Delta\beta(Y_u)_{\tilde{R}_2}^{2\text{-loop}}$$

$$\beta(Y_u)_{\tilde{R}_2, 3\text{-gen}}^{2\text{-loop}} = \beta(Y_u)_{\text{SM}}^{2\text{-loop}} + \sum_{i=1}^3 \left[\Delta\beta(Y_u)_{\tilde{R}_2}^{2\text{-loop}} \right]_i$$

where $\Delta\beta(Y_u)_{\tilde{R}_2}^{2\text{-loop}} = \frac{Y_u}{(16\pi^2)^2} \left[\frac{7}{4} Y_d^\dagger X_2 Y_d + I_3 \left\{ \left(\frac{2}{45} g_1^4 + \frac{3}{2} g_2^4 + \frac{44}{9} g_3^4 \right) + 3 \left(\lambda_2^2 + \lambda_2 \tilde{\lambda}_2 + \tilde{\lambda}_2^2 \right) - \frac{9}{2} \text{Tr} \left(X_2 X_d + \frac{1}{2} \tilde{X}_2 \tilde{X}_l \right) \right\} \right]$. (99)

In the case of leptoquark S_3 , the correction to the one-loop beta function of Y_u contains only one term, and hence it looks like:

$$\beta(Y_u)_{S_3, 1\text{-gen}}^{1\text{-loop}} = \beta(Y_u)_{\text{SM}}^{1\text{-loop}} + \Delta\beta(Y_u)_{S_3}^{1\text{-loop}}$$

$$\beta(Y_u)_{S_3, 3\text{-gen}}^{1\text{-loop}} = \beta(Y_u)_{\text{SM}}^{1\text{-loop}} + \sum_{i=1}^3 \left[\Delta\beta(Y_u)_{S_3}^{1\text{-loop}} \right]_i$$

with $\Delta\beta(Y_u)_{S_3}^{1\text{-loop}} = \frac{3}{64\pi^2} Y_u X_3^T$. (100)

The full two-loop beta function for Y_u in this scenario becomes:

$$\beta(Y_u)_{S_3, 1\text{-gen}}^{2\text{-loop}} = \beta(Y_u)_{\text{SM}}^{2\text{-loop}} + \Delta\beta(Y_u)_{S_3}^{2\text{-loop}}$$

$$\beta(Y_u)_{S_3, 3\text{-gen}}^{2\text{-loop}} = \beta(Y_u)_{\text{SM}}^{2\text{-loop}} + \sum_{i=1}^3 \left[\Delta\beta(Y_u)_{S_3}^{2\text{-loop}} \right]_i$$

with

¹¹ It should be noted that when taking $\sum_{i=1}^3 \Delta\beta$ for any parameter, one has to change X_γ to $\sum_{i=1}^3 X_{\gamma,i}$ and $f(\lambda_\gamma, \tilde{\lambda}_\gamma)$ to $\sum_{i=1}^3 f(\lambda_\gamma^i, \tilde{\lambda}_\gamma^i)$, along with making all the other additive terms three times those of the one-generation case.

$$\Delta\beta(Y_u)_{S_3}^{2\text{-loop}} = \Delta\beta(Y_u)_{S_3}^{1\text{-loop}} + \frac{Y_u}{(16\pi^2)^2} \left[I_3 \left\{ \frac{4}{15} g_1^4 + 6g_2^4 + \frac{22}{3} g_3^4 + \frac{9}{2} \left(\lambda_3^2 + \lambda_3 \tilde{\lambda}_3 + \frac{3}{4} \tilde{\lambda}_3^2 \right) - \frac{27}{8} \text{Tr} \left(\tilde{X}_3 \tilde{X}_l + X_3 \tilde{X}_d^T + X_3 \tilde{X}_u^T \right) \right\} + \left(-3\lambda_3 - \frac{9}{2} \tilde{\lambda}_3 + \frac{43}{20} g_1^2 + \frac{45}{4} g_2^2 + \frac{11}{2} g_3^2 - \frac{9}{8} \text{Tr} X_3 \right) X_3^T - \frac{3}{16} Y_3^* \tilde{X}_l^T Y_3^T + \frac{3}{2} X_3^T \tilde{X}_d - \frac{3}{8} X_3^T \tilde{X}_u - \frac{27}{32} (X_3^T)^2 \right].$$
 (101)

Now, in the combined scenario of \tilde{R}_2 and S_3 , apart from the individual contributions of \tilde{R}_2 and S_3 to the running of Y_u , there emerges another at the two-loop level which contains effects of Y_2 and Y_3 simultaneously. Therefore, the beta function for Y_u up to two-loop order in this case can be expressed as:

$$\beta(Y_u)_{\tilde{R}_2 + S_3, 1\text{-gen}}^{2\text{-loop}} = \beta(Y_u)_{\text{SM}}^{2\text{-loop}} + \Delta\beta(Y_u)_{\tilde{R}_2}^{2\text{-loop}} + \Delta\beta(Y_u)_{S_3}^{2\text{-loop}} - \frac{9}{4096\pi^2} Y_u Y_3^* \tilde{X}_2^T Y_3^T,$$
 (102)

$$\beta(Y_u)_{\tilde{R}_2 + S_3, 3\text{-gen}}^{2\text{-loop}} = \beta(Y_u)_{\text{SM}}^{2\text{-loop}} + \sum_{i=1}^3 \left[\Delta\beta(Y_u)_{\tilde{R}_2}^{2\text{-loop}} \right]_i + \sum_{i=1}^3 \left[\Delta\beta(Y_u)_{S_3}^{2\text{-loop}} \right]_i - \frac{9 Y_u}{4096\pi^2} \sum_{(i,l)=1}^3 Y_{3,i}^* \tilde{X}_{2,l}^T Y_{3,i}^T.$$
 (103)

At this point, it is important to mention that for our choice of leptoquark couplings in the three-generation cases, $Y_{\gamma,i} Y_{\gamma',j} = 0$ for $i \neq j$, where $(\gamma, \gamma') \in \{2, 3\}$.

We depict the results for the variation in the top Yukawa coupling with the energy scale at the two-loop level under different models in Fig. 22, where the left and right panels show the leptoquark coupling with quarks and leptons (Y_ϕ) to be 0.4 and 1.0, respectively. The green curve explains the

SM scenario, while the yellow and blue lines illustrate \tilde{R}_2 and S_3 leptoquarks with three generations. As expected, the SM value of the top Yukawa coupling decreases with energy. With the inclusion of leptoquarks, this coupling shifts further down, and for the case of S_3 it achieves divergence at $10^{19.7}$ GeV. Since \tilde{R}_2 and S_3 with one generation do not show any abnormal behaviour, we do not present them here. On the other hand, the brown (solid) and black (dashed) curves represent the combined models of \tilde{R}_2 and S_3 with one and three generations, respectively. As anticipated, the case with three generations of both leptoquarks stays at the bottom of all the other lines for lower values of Y_ϕ (e.g. $Y_\phi = 0.4$, shown by the left panel of Fig. 22), although only this curve is noticeably affected if Y_ϕ is increased to some sufficiently higher value (e.g. $Y_\phi = 1.0$, as exhibited in the right panel of Fig. 22). Like all the other couplings for this scenario, it also diverges at $10^{14.4}$ GeV. The relative positions of the curves in the above-mentioned plot depend primarily on the negative contributions from the gauge couplings at the one-loop level, see Eqs. (96)–(100). With the increase in the number of leptoquark components, the values of gauge couplings are enhanced at any particular energy scale, which in turn will push the top Yukawa coupling downward.

Appendix D: Running of leptoquark Yukawa couplings

Now, let us discuss the evolution of leptoquark Yukawa couplings Y_2 and Y_3 . As mentioned in Eq. (15), these parameters should also have an upper bound of $\sqrt{4\pi}$ at any energy scale μ . For the \tilde{R}_2 scenario, the one-loop and two-loop beta functions for Y_2 are given by:

$$\begin{aligned} \beta(Y_2)_{\tilde{R}_2, 1\text{-gen}}^{1\text{-loop}} &= \frac{1}{16\pi^2} \left[X_d Y_2 + \frac{5}{2} X_2 Y_2 + \frac{1}{2} Y_2 \tilde{X}_l \right. \\ &\quad \left. - \left(\frac{13}{20} g_1^2 + \frac{9}{4} g_2^2 + 4g_3^2 - \text{Tr} X_2 \right) Y_2 \right], \quad (104) \\ \beta(Y_2)_{\tilde{R}_2, 1\text{-gen}}^{2\text{-loop}} &= \beta(Y_2)_{\tilde{R}_2, 1\text{-gen}}^{1\text{-loop}} + \frac{1}{(16\pi^2)^2} \left[Y_2 \tilde{X}_l \right. \\ &\quad \left. \left\{ \frac{117}{80} g_1^2 + \frac{33}{16} g_2^2 - 2\lambda_2 + 2\tilde{\lambda}_2 \right. \right. \\ &\quad \left. \left. - \frac{9}{4} \text{Tr} \left(X_u + X_d + \frac{1}{3} X_l \right) \right\} \right. \\ &\quad \left. + X_d Y_2 \left\{ \frac{61}{120} g_1^2 + \frac{51}{8} g_2^2 - \frac{16}{3} g_3^2 - 4\lambda_2 - 2\tilde{\lambda}_2 \right. \right. \\ &\quad \left. \left. - \frac{9}{2} \text{Tr} \left(X_u + X_d + \frac{1}{3} X_l \right) \right\} + \frac{1}{2} X_2^2 Y_2 - \frac{3}{4} X_2 X_d Y_2 \right. \\ &\quad \left. - \frac{1}{4} Y_2 \tilde{X}_l \tilde{X}_2 - \frac{1}{4} Y_2 \tilde{X}_l^2 + 2X_d Y_2 \tilde{X}_l \right. \\ &\quad \left. - \frac{1}{4} X_d^2 Y_2 - \frac{1}{4} Y_d \tilde{X}_u Y_d^\dagger Y_2 \right] \end{aligned}$$

$$\begin{aligned} &+ X_2 Y_2 \left(\frac{107}{48} g_1^2 + \frac{201}{16} g_2^2 + \frac{73}{3} g_3^2 - \frac{15}{4} \text{Tr} X_2 \right) \\ &+ Y_2 \left[\lambda_2^2 + \lambda_2 \tilde{\lambda}_2 + \tilde{\lambda}_2^2 + \frac{3961}{1800} g_1^4 \right. \\ &\quad \left. - \frac{17}{4} g_2^4 - \frac{173}{9} g_3^4 + \frac{9}{20} g_1^2 g_2^2 + \frac{17}{15} g_1^2 g_3^2 - 9g_2^2 g_3^2 \right. \\ &\quad \left. + \left(\frac{13}{24} g_1^2 + \frac{15}{8} g_2^2 + \frac{10}{3} g_3^2 \right) \text{Tr} X_2 \right. \\ &\quad \left. - \frac{3}{2} \text{Tr} \left(X_2 X_d + \frac{1}{2} \tilde{X}_l \tilde{X}_2 + \frac{5}{2} X_2^2 \right) \right] \Bigg\}. \quad (105) \end{aligned}$$

Now, for three generations of \tilde{R}_2 , we have three Yukawa matrices of leptoquark ($Y_{2,i}$) corresponding to three different generations of quarks and leptons. The running of each of these Yukawa matrices at the one-loop level can be expressed as:

$$\begin{aligned} \beta(Y_{2,i})_{\tilde{R}_2, 3\text{-gen}}^{1\text{-loop}} &= \left[\beta(Y_2)_{\tilde{R}_2, 1\text{-gen}}^{1\text{-loop}} \right]_i \\ &+ \frac{1}{16\pi^2} \sum_{j \neq i} \left[\frac{3}{2} Y_{2,i} \tilde{X}_{2,j} + X_{2,j} Y_{2,i} + Y_{2,j} \text{Tr} \left(Y_{2,i} Y_{2,j}^\dagger \right) \right]. \quad (106) \end{aligned}$$

At this point we remind the reader again that $[\beta]_i$ for any parameter indicates the beta function of that parameter with the replacement of $f(Y_\gamma, X_\gamma, \tilde{X}_\gamma, \lambda_\gamma, \tilde{\lambda}_\gamma)$ to $f(Y_{\gamma,i}, X_{\gamma,i}, \tilde{X}_{\gamma,i}, \lambda_\gamma^i, \tilde{\lambda}_\gamma^i)$ with $\gamma \in \{2, 3\}$ and i representing the generation. It is interesting to note that there appear some additional terms with inter-generation interactions. The beta function for the i -th generation of Y_2 at two-loop order is given by:

$$\begin{aligned} \beta(Y_{2,i})_{\tilde{R}_2, 3\text{-gen}}^{2\text{-loop}} &= \left\{ \beta(Y_{2,i})_{\tilde{R}_2, 3\text{-gen}}^{1\text{-loop}} - \left[\beta(Y_2)_{\tilde{R}_2, 1\text{-gen}}^{1\text{-loop}} \right]_i \right\} \\ &+ \left[\beta(Y_2)_{\tilde{R}_2, 1\text{-gen}}^{2\text{-loop}} \right]_i + \frac{Y_{2,i}}{(16\pi^2)^2} \left(\frac{7}{90} g_1^4 + 3g_2^4 + \frac{32}{9} g_3^4 \right) \\ &+ \frac{1}{(16\pi^2)^2} \sum_{j \neq i} \left[-\frac{3}{2} Y_{2,i} \text{Tr} \left(X_{2,i} X_{2,j} + \frac{3}{2} \tilde{X}_{2,i} \tilde{X}_{2,j} \right) \right. \\ &\quad \left. + \left(\frac{47}{80} g_1^2 + \frac{99}{16} g_2^2 + 17g_3^2 \right) Y_{2,i} \tilde{X}_{2,j} \right. \\ &\quad \left. + \left(\frac{197}{120} g_1^2 + \frac{51}{8} g_2^2 + \frac{22}{3} g_3^2 \right) X_{2,j} Y_{2,i} - \frac{3}{4} X_{2,i} X_{2,j} Y_{2,i} \right. \\ &\quad \left. - \frac{3}{4} Y_{2,i} Y_{2,j}^\dagger X_d Y_{2,j} + \frac{5}{4} Y_{2,i} Y_{2,j}^\dagger X_{2,i} Y_{2,j} \right. \\ &\quad \left. - \frac{3}{4} Y_{2,i} \tilde{X}_{2,j} \tilde{X}_{2,i} - \frac{3}{4} Y_{2,i} \tilde{X}_{2,j}^2 - \frac{1}{4} Y_{2,i} \tilde{X}_l Y_{2,j}^\dagger Y_{2,i} \right. \\ &\quad \left. + \frac{5}{4} Y_{2,j} \tilde{X}_{2,i} Y_{2,i}^\dagger + 2X_{2,j} Y_{2,i} \tilde{X}_{2,j} - \frac{3}{4} X_{2,j}^2 Y_{2,i} \right. \\ &\quad \left. + \sum_{k \neq \{i, j\}} \left(2Y_{2,j} Y_{2,k}^\dagger Y_{2,i} Y_{2,j}^\dagger Y_{2,k} - \frac{3}{4} Y_{2,j} \tilde{X}_{2,k} Y_{2,j}^\dagger Y_{2,i} \right. \right. \\ &\quad \left. \left. - \frac{3}{4} Y_{2,i} Y_{2,j}^\dagger X_{2,k} Y_{2,j} \right) + \left\{ \left(\frac{13}{24} g_1^2 + \frac{15}{8} g_2^2 + \frac{10}{3} g_3^2 \right) Y_{2,j} \right. \right. \end{aligned}$$

$$\begin{aligned}
 & -\frac{3}{2}Y_{2,j}\tilde{\chi}_{2,i} - \frac{9}{4}\tilde{\chi}_{2,i}Y_{2,j} \Big\} \text{Tr}\left(Y_{2,i}Y_{2,j}^\dagger\right) \\
 & + \frac{15}{4}Y_{2,i}Y_{2,j}^\dagger Y_{2,i} \text{Tr}\left(Y_{2,j}Y_{2,i}^\dagger\right) - \left(\frac{9}{4}Y_{2,i}\tilde{\chi}_{2,j} + \frac{3}{2}\mathcal{X}_{2,j}Y_{2,i}\right) \text{Tr}\tilde{\chi}_{2,j} \\
 & - \frac{3}{2} \sum_{k \notin \{i,j\}} \left\{ \left(\frac{3}{2}Y_{2,i}Y_{2,j}^\dagger Y_{2,k} + Y_{2,k}Y_{2,j}^\dagger Y_{2,i}\right) \text{Tr}\left(Y_{2,j}Y_{2,k}^\dagger\right) \right. \\
 & \left. + Y_{2,j} \text{Tr}\left(\frac{3}{2}Y_{2,i}\tilde{\chi}_{2,k}Y_{2,j}^\dagger + \mathcal{X}_{2,k}Y_{2,i}Y_{2,j}^\dagger\right) \right\} \\
 & - \frac{3}{2}Y_{2,j} \text{Tr}\left(\mathcal{X}_d Y_{2,i}Y_{2,j}^\dagger + \frac{1}{2}Y_{2,i}\tilde{\chi}_l Y_{2,j}^\dagger\right) \\
 & \left. + \frac{5}{2}\mathcal{X}_{2,i}Y_{2,i}Y_{2,j}^\dagger + \frac{5}{2}Y_{2,i}\tilde{\chi}_{2,j}Y_{2,j}^\dagger \right\}. \tag{107}
 \end{aligned}$$

The term within the curly brackets is added to the above expression in order to incorporate the extra contribution at one-loop order coming from the cross-generation interaction, as shown in Eq. (106). The rest of the terms arise from two-loop contributions.

In a similar fashion, the one-loop and two-loop beta functions for Y_3 in the case of leptoquark S_3 can be expressed as follows:

$$\begin{aligned}
 \beta(Y_3)_{S_3,1\text{-gen}}^{1\text{-loop}} &= \frac{1}{32\pi^2} \left[Y_3\tilde{\chi}_l + 6Y_3\tilde{\chi}_3 + \tilde{\chi}_d^T Y_3 \right. \\
 & \left. + \tilde{\chi}_u^T Y_3 - \left(g_1^2 + 9g_2^2 + 8g_3^2 - 2\text{Tr}\mathcal{X}_3\right) Y_3 \right], \tag{108} \\
 \beta(Y_3)_{S_3,1\text{-gen}}^{2\text{-loop}} &= \beta(Y_2)_{S_3,1\text{-gen}}^{1\text{-loop}} + \frac{1}{(16\pi^2)^2} \\
 & \left[Y_3\tilde{\chi}_l \left\{ \frac{69}{80}g_1^2 + \frac{33}{16}g_2^2 - 2\lambda_3 + \tilde{\lambda}_3 \right. \right. \\
 & \left. - \frac{9}{4}\text{Tr}\left(X_u + X_d + \frac{1}{3}X_l\right) \right\} \\
 & + \tilde{\chi}_d^T Y_3 \left\{ \frac{7}{240}g_1^2 + \frac{33}{16}g_2^2 - \frac{8}{3}g_3^2 - 2\lambda_3 + \tilde{\lambda}_3 \right. \\
 & \left. - \frac{9}{4}\text{Tr}\left(X_u + X_d + \frac{1}{3}X_l\right) \right\} \\
 & + \tilde{\chi}_u^T Y_3 \left\{ \frac{427}{240}g_1^2 + \frac{33}{16}g_2^2 - \frac{8}{3}g_3^2 \right. \\
 & \left. - 2\lambda_3 - 3\tilde{\lambda}_3 \right. \\
 & \left. - \frac{9}{4}\text{Tr}\left(X_u + X_d + \frac{1}{3}X_l\right) \right\} \\
 & + \mathcal{X}_3 Y_3 \left(\frac{23}{10}g_1^2 + 48g_2^2 + 31g_3^2 - \frac{9}{2}\text{Tr}\mathcal{X}_3 \right) \\
 & - \frac{1}{4}Y_3\tilde{\chi}_l^2 - \frac{3}{16}Y_3\tilde{\chi}_l\tilde{\chi}_3 \\
 & + \frac{13}{16}Y_3\tilde{\chi}_3^2 - \frac{9}{16}\mathcal{X}_3\tilde{\chi}_d Y_3 \\
 & - \frac{9}{16}\mathcal{X}_3\tilde{\chi}_u Y_3 + 2\tilde{X}_d Y_3\tilde{\chi}_l - \frac{1}{4}\tilde{\chi}_d^2 Y_3 - \frac{1}{4}\tilde{\chi}_u^2 Y_3 \\
 & \left. + Y_3 \left[\lambda_3^2 + \lambda_3\tilde{\lambda}_3 + \frac{3}{4}\tilde{\lambda}_3^2 \right. \right.
 \end{aligned}$$

$$\begin{aligned}
 & \left. + \frac{599}{400}g_1^4 - \frac{173}{16}g_2^4 - \frac{55}{3}g_3^4 - \frac{23}{40}g_1^2g_2^2 - 31g_2^2g_3^2 \right. \\
 & \left. - \frac{1}{15}g_1^2g_3^2 + \frac{5}{12}\left(g_1^2 + 9g_2^2 + 8g_3^2\right) \text{Tr}\mathcal{X}_3 \right. \\
 & \left. - \frac{3}{4}\text{Tr}\left(\tilde{\chi}_3\tilde{\chi}_l + \mathcal{X}_3\tilde{\chi}_d^T + \mathcal{X}_3\tilde{\chi}_u^T + 6\mathcal{X}_3^2\right) \right\}. \tag{109}
 \end{aligned}$$

For the three-generation case of S_3 , the one-loop beta of the i -th-generation leptoquark Yukawa coupling takes the form:

$$\begin{aligned}
 \beta(Y_{3,i})_{S_3,3\text{-gen}}^{1\text{-loop}} &= \left[\beta(Y_2)_{S_3,1\text{-gen}}^{1\text{-loop}} \right]_i + \frac{9}{64\pi^2} \\
 & \times \sum_{j \neq i} \left[Y_{3,i}\tilde{\chi}_{3,j} + \frac{1}{3}\mathcal{X}_{3,j}Y_{3,i} + \frac{4}{9}Y_{3,j} \text{Tr}\left(Y_{3,i}Y_{3,j}^\dagger\right) \right]. \tag{110}
 \end{aligned}$$

As in the case of \tilde{R}_2 , here also some new terms appear due to inter-generation interactions at the one-loop level. Encompassing these additional terms, the two-loop beta function can be written as:

$$\begin{aligned}
 \beta(Y_{3,i})_{S_3,3\text{-gen}}^{2\text{-loop}} &= \left\{ \beta(Y_{3,i})_{S_3,3\text{-gen}}^{2\text{-loop}} - \left[\beta(Y_3)_{S_3,1\text{-gen}}^{1\text{-loop}} \right]_i \right\} \\
 & + \left[\beta(Y_3)_{S_3,1\text{-gen}}^{2\text{-loop}} \right]_i \\
 & + \frac{Y_{3,i}}{(16\pi^2)^2} \left(\frac{49}{150}g_1^4 + 21g_2^4 + \frac{16}{3}g_3^4 \right) + \frac{1}{(16\pi^2)^2} \sum_{j \neq i} \\
 & \times \left[-\frac{9}{8}Y_{3,i} \text{Tr}\left(\mathcal{X}_{3,i}\mathcal{X}_{3,j} + 3\tilde{\chi}_{3,i}\tilde{\chi}_{3,j}\right) \right. \\
 & + Y_{3,i}\tilde{\chi}_{3,j} \left(\frac{3}{5}g_1^2 + 36g_2^2 + \frac{51}{2}g_3^2 \right) \mathcal{X}_{3,j}Y_{3,i} \left(\frac{17}{10}g_1^2 + 12g_2^2 \right. \\
 & \left. + \frac{11}{2}g_3^2 \right) - \frac{27}{32}\mathcal{X}_{3,i}\mathcal{X}_{3,j}Y_{3,i} \\
 & + \frac{53}{32}Y_{3,i}Y_{3,j}^\dagger\mathcal{X}_{3,i}Y_{3,j} - \frac{27}{32}Y_{3,i}\tilde{\chi}_{3,j}\tilde{\chi}_{3,i} - \frac{27}{32}Y_{3,i}\tilde{\chi}_{3,i}^2 \\
 & - \frac{27}{32}Y_{3,i}Y_{3,j}^\dagger\mathcal{X}_{3,k}Y_{3,j} \\
 & - \frac{9}{16}Y_{3,i}Y_{3,j}^\dagger\tilde{\chi}_d^T Y_{3,j} \\
 & - \frac{9}{16}Y_{3,i}Y_{3,j}^\dagger\tilde{\chi}_u^T Y_{3,j} - \frac{3}{16}Y_{3,j}\tilde{\chi}_l Y_{3,i}^\dagger Y_{3,i} \\
 & + \frac{53}{32}Y_{3,j}\tilde{\chi}_{3,i}Y_{3,i}^\dagger Y_{3,i} \\
 & + \frac{5}{2}\mathcal{X}_{3,j}Y_{3,i}\tilde{\chi}_{3,j} - \frac{27}{32}\mathcal{X}_{3,j}^2 Y_{3,i} \\
 & \left. + \left\{ \left(\frac{5}{12}g_1^2 + \frac{15}{4}g_2^2 + \frac{10}{3}g_3^2 \right) Y_{3,j} - \frac{9}{8}Y_{3,j}\tilde{\chi}_{3,i} \right. \right. \\
 & \left. - \frac{27}{8}\mathcal{X}_{3,i}Y_{3,j} \right\} \text{Tr}\left(Y_{3,i}Y_{3,j}^\dagger\right) \\
 & \left. - \frac{9}{2}Y_{3,i}Y_{3,j}^\dagger Y_{3,i} \text{Tr}\left(Y_{3,j}Y_{3,i}^\dagger\right) \right.
 \end{aligned}$$

$$\begin{aligned}
 & - \left(\frac{27}{8} Y_{3,i} \tilde{\mathcal{X}}_{3,j} + \frac{9}{8} X_{3,j} Y_{3,i} \right) \text{Tr} X_{3,j} \\
 & - \frac{3}{4} Y_{3,j} \text{Tr} \left(\tilde{\mathcal{X}}_l Y_{3,j}^\dagger Y_{3,i} \right) \\
 & - \frac{9}{2} Y_{3,j} \text{Tr} \left(X_{3,i} Y_{3,i} Y_{3,j}^\dagger \right) \\
 & - \frac{9}{2} Y_{3,j} \text{Tr} \left(Y_{3,i} \tilde{\mathcal{X}}_{3,j} Y_{3,j}^\dagger \right) \\
 & - \frac{3}{4} Y_{3,j} \text{Tr} \left(Y_{3,i} Y_{3,j}^\dagger \tilde{\mathcal{X}}_d^T \right) - \frac{3}{4} Y_{3,j} \text{Tr} \left(Y_{3,i} Y_{3,j}^\dagger \tilde{\mathcal{X}}_u^T \right) \\
 & + \sum_{k \neq \{i,j\}} \left\{ \frac{5}{2} Y_{3,j} Y_{3,k}^\dagger Y_{3,i} Y_{3,j}^\dagger Y_{3,k} \right. \\
 & - \frac{27}{32} Y_{3,j} \tilde{\mathcal{X}}_{3,k} Y_{3,j}^\dagger Y_{3,i} \\
 & - \left. \left(\frac{27}{8} Y_{3,i} Y_{3,j}^\dagger Y_{3,k} + \frac{9}{8} Y_{3,k} Y_{3,j}^\dagger Y_{3,i} \right) \text{Tr} \left(Y_{3,j} Y_{3,k}^\dagger \right) \right. \\
 & \left. - \frac{27}{8} Y_{3,j} \text{Tr} \left(Y_{3,i} \tilde{\mathcal{X}}_{3,k} Y_{3,j}^\dagger \right) - \frac{9}{8} Y_{3,j} \text{Tr} \left(Y_{3,i} Y_{3,j}^\dagger X_{3,k} \right) \right\}. \tag{111}
 \end{aligned}$$

Now, for the combined scenario of \tilde{R}_2 and S_3 , the above expressions are modified, and extra contributions from the interactions of doublet and triplet leptoquarks emerge at both the one- and two-loop levels. Thus, they can be written as follows:

$$\begin{aligned}
 \beta(Y_2)_{\tilde{R}_2+S_3,1\text{-gen}}^{2\text{-loop}} &= \frac{9}{64\pi^2} Y_2 \tilde{\mathcal{X}}_3 + \beta(Y_2)_{\tilde{R}_2,1\text{-gen}}^{2\text{-loop}} \\
 &+ \frac{1}{(16\pi^2)^2} \left[Y_2 \tilde{\mathcal{X}}_3 \left(\frac{21}{20} g_1^2 + \frac{135}{4} g_2^2 + \frac{51}{2} g_3^2 - \frac{27}{8} \text{Tr} X_3 \right) \right. \\
 &- \frac{9}{8} Y_2 \left(\tilde{\mathcal{X}}_3 \tilde{\mathcal{X}}_2 + \frac{3}{4} \tilde{\mathcal{X}}_3^2 + \frac{1}{2} Y_3^\dagger \tilde{\mathcal{X}}_d^T Y_3 \right. \\
 &+ \left. \frac{1}{2} Y_3^\dagger \tilde{\mathcal{X}}_u^T Y_3 \right) + 3 Y_d Y_3^* Y_2^T Y_d^* Y_3 - \frac{3}{8} Y_d X_3^T Y_d^\dagger Y_2 \\
 &+ \left. Y_2 \left\{ \frac{7}{30} g_1^4 + 6 g_2^4 + \frac{8}{3} g_3^4 - \frac{27}{8} \text{Tr} \left(\tilde{\mathcal{X}}_2 \tilde{\mathcal{X}}_3 \right) \right\} \right]. \tag{112}
 \end{aligned}$$

$$\begin{aligned}
 \beta(Y_3)_{\tilde{R}_2+S_3,1\text{-gen}}^{2\text{-loop}} &= \frac{3}{32\pi^2} Y_3 \tilde{\mathcal{X}}_2 + \beta(Y_3)_{\tilde{R}_2,1\text{-gen}}^{2\text{-loop}} \\
 &+ \frac{1}{(16\pi^2)^2} \left[- \frac{3}{4} Y_3 \left(\tilde{\mathcal{X}}_2^2 + \frac{3}{4} \tilde{\mathcal{X}}_2 \tilde{\mathcal{X}}_3 + Y_2^\dagger X_d Y_2 \right) \right. \\
 &- \frac{1}{4} Y_d^T X_2^T Y_d^* Y_3 + 2 Y_d^T Y_2^* Y_3^T Y_d^\dagger Y_2 \\
 &- \left. Y_3 \tilde{\mathcal{X}}_2 \left(\frac{1}{80} g_1^2 - \frac{99}{16} g_2^2 - 17 g_3^2 + \frac{9}{4} \text{Tr} X_2 \right) \right. \\
 &+ \left. Y_3 \left\{ \frac{49}{1800} g_1^4 + \frac{21}{8} g_2^4 + \frac{16}{9} g_3^4 \right. \right. \\
 &- \left. \left. \frac{9}{4} \text{Tr} \left(\tilde{\mathcal{X}}_2 \tilde{\mathcal{X}}_3 \right) \right\} \right]. \tag{113}
 \end{aligned}$$

$$\begin{aligned}
 \beta(Y_{2,i})_{\tilde{R}_2+S_3,3\text{-gen}}^{2\text{-loop}} &= \frac{9}{64\pi^2} \sum_{l=1}^3 Y_{2,i} \tilde{\mathcal{X}}_{3,l} + \beta(Y_{2,i})_{\tilde{R}_2,3\text{-gen}}^{2\text{-loop}} \\
 &+ \frac{Y_{2,i}}{(16\pi^2)^2} \left(\frac{7}{10} g_1^4 + 18 g_2^4 + 8 g_3^4 \right) \\
 &+ \frac{1}{(16\pi^2)^2} \sum_{l=1}^3 \left[- \frac{27}{8} Y_{2,i} \text{Tr} \left(\tilde{\mathcal{X}}_{2,i} \tilde{\mathcal{X}}_{3,l} \right) \right. \\
 &+ Y_{2,i} \tilde{\mathcal{X}}_{3,l} \left(\frac{21}{20} g_1^2 + \frac{135}{4} g_2^2 + \frac{51}{2} g_3^2 \right) \\
 &- \frac{9}{8} Y_{2,i} \left(\tilde{\mathcal{X}}_{3,l} \tilde{\mathcal{X}}_{2,i} + \frac{1}{2} Y_{3,l}^\dagger \tilde{\mathcal{X}}_d^T Y_{3,l} + \frac{1}{2} Y_{3,l}^\dagger \tilde{\mathcal{X}}_u^T Y_{3,l} \right. \\
 &+ \left. \frac{3}{4} \sum_{k=1}^3 Y_{3,l}^\dagger X_{3,k} Y_{3,l} \right) + \frac{9}{8} \sum_{j \neq i} Y_{2,j} \tilde{\mathcal{X}}_{3,l} Y_{2,j}^\dagger \\
 &+ 3 Y_d Y_{3,l}^* Y_{2,i}^T Y_d^* Y_{3,l} - \frac{3}{8} Y_d X_{3,l}^T Y_d^\dagger Y_{2,i} \\
 &- \left. \frac{27}{8} \sum_{k=1}^3 Y_{2,i} Y_{3,l}^\dagger Y_{3,k} \text{Tr} \left(Y_{3,l} Y_{3,k}^\dagger \right) \right]. \tag{114}
 \end{aligned}$$

$$\begin{aligned}
 \beta(Y_{3,i})_{\tilde{R}_2+S_3,3\text{-gen}}^{2\text{-loop}} &= \frac{3}{32\pi^2} \sum_{l=1}^3 Y_{3,i} \tilde{\mathcal{X}}_{2,l} + \beta(Y_{3,i})_{\tilde{R}_2,3\text{-gen}}^{2\text{-loop}} \\
 &+ \frac{Y_{3,i}}{(16\pi^2)^2} \left(\frac{49}{600} g_1^4 + \frac{63}{8} g_2^4 + \frac{16}{3} g_3^4 \right) \\
 &+ \frac{1}{(16\pi^2)^2} \sum_{l=1}^3 \left[- \frac{9}{4} Y_{3,i} \text{Tr} \left(\tilde{\mathcal{X}}_{2,l} \tilde{\mathcal{X}}_{3,i} \right) \right. \\
 &+ Y_{3,i} \tilde{\mathcal{X}}_{2,l} \left(- \frac{1}{80} g_1^2 + \frac{99}{16} g_2^2 + 17 g_3^2 \right) \\
 &- \frac{3}{4} Y_{3,i} \left(Y_{2,l}^\dagger X_d Y_{2,l} + \frac{3}{4} \tilde{\mathcal{X}}_{2,l} \tilde{\mathcal{X}}_{3,i} + \sum_{k=1}^3 Y_{2,l}^\dagger X_{2,k} Y_{2,l} \right) \\
 &- \frac{1}{4} Y_d^T X_{2,l}^T Y_d^* Y_{3,i} 2 Y_d^T Y_{2,l}^* Y_{3,i} Y_d^\dagger Y_{2,l} \\
 &- \frac{9}{4} \sum_{k=1}^3 Y_{3,i} Y_{2,l}^\dagger Y_{2,k} \text{Tr} \left(Y_{2,l} Y_{2,k}^\dagger \right) \\
 &- \left. \frac{9}{4} \sum_{j \neq i} Y_{3,j} \text{Tr} \left(\tilde{\mathcal{X}}_{2,l} Y_{3,j}^\dagger Y_{3,i} \right) \right]. \tag{115}
 \end{aligned}$$

In all of the above four expressions, the first term indicates the extra contribution at one-loop order due to the presence of both doublet and triplet leptoquarks.

Since one-generation cases do not show any irregularities, we depict the variations in Y_2 and Y_3 in three-generation scenarios of the leptoquarks in Fig. 23. Figure 23a, b in the first row illustrate the variations in any diagonal element of Y_2 starting from 0.4 and 1.0, respectively, while Fig. 23c, d in the second row demonstrate the similar situation for Y_3 . As can be observed, for low Yukawa, the combined scenarios stay below the individual cases, whereas the situation flips

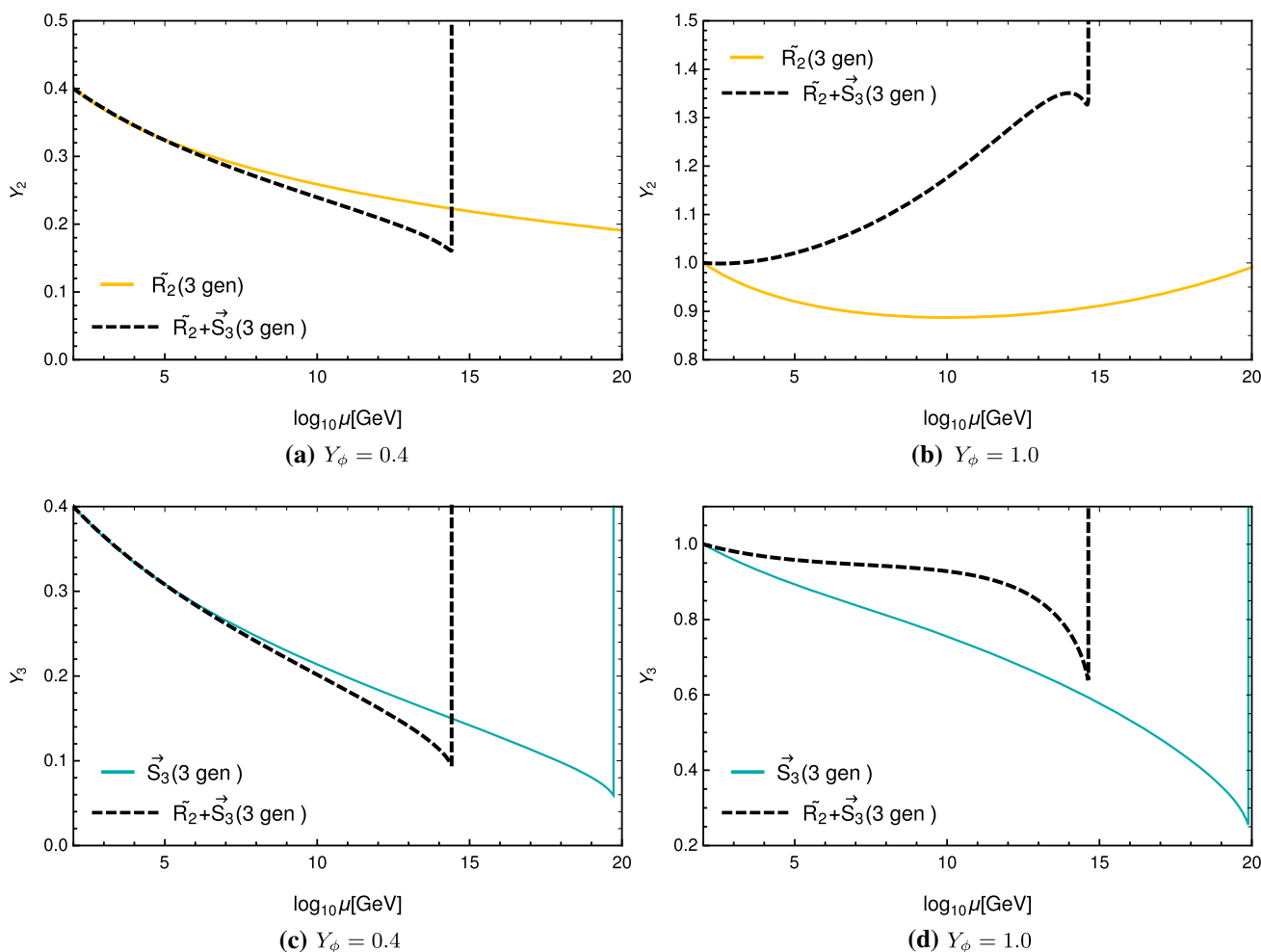


Fig. 23 Variation in leptoquark Yukawa with scale

for higher Yukawa cases due to the large effects from the combined terms of Y_2 and Y_3 . As expected, Y_3 for three generations of S_3 decreases monotonically with energy and hits the divergence at $10^{19.7}$ GeV, while both Y_2 and Y_3 diverge at $10^{14.4}$ GeV for the three-generation $\tilde{R}_2 + S_3$ case. However, Y_2 shows different behaviour for large Yukawa. For the \tilde{R}_2 case, as can be observed from Fig. 23b, it initially decreases with scale, then reaches a minimum and gradually starts increasing. For the $\tilde{R}_2 + S_3$ case, it increases with energy from the beginning, then reaches a maximum and starts to fall off, but suddenly blows up at $10^{14.4}$ GeV.

Appendix E: Two-loop beta functions of Higgs-leptoquark quartic couplings for \tilde{R}_2

$$\beta(\lambda_2)_{\tilde{R}_2, 1\text{-gen}}^{2\text{-loop}} = \beta(\lambda_2)_{\tilde{R}_2, 1\text{-gen}}^{1\text{-loop}} + \frac{1}{(16\pi^2)^2} \left[-\frac{1091}{3000}g_1^6 + \frac{263}{8}g_2^6 + \frac{1031}{600}g_1^4g_2^2 \right]$$

$$\begin{aligned} & -\frac{1}{5}g_1^4g_3^2 - \frac{29}{120}g_1^2g_2^4 - 15g_2^4g_3^2 \\ & + 2g_1^2g_2^2g_3^2 + \lambda_h \left(\frac{3}{10}g_1^4 - g_1^2g_2^2 + \frac{45}{4}g_2^4 \right) \\ & - 16 \left(\lambda_2^3 + \frac{1}{2}\lambda_2^2\tilde{\lambda}_2 + \frac{5}{4}\lambda_2\tilde{\lambda}_2^2 + \tilde{\lambda}_2^3 \right) + \lambda_2 \left(\frac{929}{200}g_1^4 + \frac{53}{8}g_2^4 \right) \\ & - \frac{254}{9}g_3^4 + \frac{21}{20}g_1^2g_2^2 + \frac{2}{9}g_1^2g_3^2 + 10g_2^2g_3^2 \\ & + \frac{72}{5}g_1^2\lambda_h + 72g_2^2\lambda_h - 60\lambda_h^2 \\ & + \tilde{\lambda}_2 \left(\frac{7}{15}g_1^4 + 15g_2^4 + \frac{40}{3}g_3^4 \right) \\ & - \frac{22}{15}g_1^2g_2^2 + \frac{8}{3}g_2^2g_3^2 + \frac{24}{5}g_1^2\lambda_h + 36g_2^2\lambda_h - 16\lambda_h^2 \\ & + \lambda_2^2 \left(\frac{2}{3}g_1^2 + 6g_2^2 + \frac{16}{3}g_3^2 - 72\lambda_h \right) \\ & + \tilde{\lambda}_2^2 \left(-\frac{4}{15}g_1^2 + 6g_2^2 + \frac{8}{3}g_3^2 - 28\lambda_h \right) - \lambda_2\tilde{\lambda}_2 \left(12g_2^2 + 32\lambda_h \right) \\ & - \left\{ \frac{73}{100}g_1^4 + \frac{3}{4}g_2^4 - \frac{13}{10}g_1^2g_2^2 + 4\lambda_2^2 + 2\tilde{\lambda}_2^2 \right\} \end{aligned}$$

$$\begin{aligned}
 & -\lambda_2 \left(\frac{13}{12} g_1^2 + \frac{15}{4} g_2^2 + \frac{20}{3} g_3^2 \right) \left\{ \text{Tr} \mathcal{X}_2 \right. \\
 & - \left[12\lambda_2^2 + 6\tilde{\lambda}_2^2 - \frac{1}{20} g_1^4 + \frac{9}{4} g_2^4 + 32g_3^4 + \frac{9}{10} g_1^2 g_2^2 + 24\lambda_h \tilde{\lambda}_2 \right. \\
 & - 5\lambda_2 \left(\frac{1}{4} g_1^2 + \frac{9}{4} g_2^2 + 8g_3^2 - \frac{72}{5} \lambda_h \right) \left. \right\} \text{Tr} \mathcal{X}_d \\
 & - \left[\frac{1}{4} g_1^4 + \frac{3}{4} g_2^4 + \frac{11}{10} g_1^2 g_2^2 + 4\lambda_2^2 + 2\tilde{\lambda}_2^2 + 8\lambda_h \tilde{\lambda}_2 \right. \\
 & - \left. \frac{15}{4} \lambda_2 \left(g_1^2 + g_2^2 - \frac{32}{5} \lambda_h \right) \right] \text{Tr} \mathcal{X}_l \\
 & - \left[12\lambda_2^2 + 6\tilde{\lambda}_2^2 + \frac{19}{100} g_1^4 + \frac{9}{4} g_2^4 + 32g_3^4 + \frac{21}{10} g_1^2 g_2^2 + 24\lambda_h \tilde{\lambda}_2 \right. \\
 & - \lambda_2 \left(\frac{17}{4} g_1^2 + \frac{45}{4} g_2^2 + 40g_3^2 - 72\lambda_h \right) \left. \right\} \text{Tr} \mathcal{X}_u \\
 & - \text{Tr} \left\{ \left(\frac{8}{15} g_1^2 + \frac{32}{3} g_3^2 \right) \mathcal{X}_2 \mathcal{X}_d \right. \\
 & + \frac{16}{5} g_1^2 \tilde{\mathcal{X}}_l \tilde{\mathcal{X}}_2 \\
 & + \left(21\lambda_2 + 24\tilde{\lambda}_2 \right) \tilde{\mathcal{X}}_u \tilde{\mathcal{X}}_d \\
 & + \lambda_2 \left(\frac{15}{2} \mathcal{X}_2^2 + 4\mathcal{X}_2 \mathcal{X}_d - 2\tilde{\mathcal{X}}_l \tilde{\mathcal{X}}_2 + \frac{9}{2} \mathcal{X}_l^2 + \frac{27}{2} \mathcal{X}_u^2 \right. \\
 & \left. + \frac{27}{2} \mathcal{X}_d^2 \right) \left. \right\} \\
 & + \text{Tr} \left(26\mathcal{X}_2^2 \mathcal{X}_d + 20\tilde{\mathcal{X}}_2^2 \tilde{\mathcal{X}}_l + 14\mathcal{X}_2 \mathcal{X}_d^2 + 12\tilde{\mathcal{X}}_2 \tilde{\mathcal{X}}_l^2 \right. \\
 & \left. - 2\mathcal{X}_2 Y_d \tilde{\mathcal{X}}_u Y_d^\dagger + 14Y_2 \tilde{\mathcal{X}}_l Y^\dagger \mathcal{X}_d \right). \tag{116}
 \end{aligned}$$

$$\begin{aligned}
 \beta(\tilde{\lambda}_2)_{\tilde{R}_2, 1\text{-gen}}^{2\text{-loop}} &= \beta(\tilde{\lambda}_2)_{\tilde{R}_2, 1\text{-gen}}^{1\text{-loop}} + \frac{1}{(16\pi^2)^2} \\
 & \times \left[27g_2^6 - \frac{583}{150} g_1^4 g_2^2 \right. \\
 & - \frac{49}{15} g_1^2 g_2^4 - 4g_1^2 g_2^2 g_3^2 + 2g_1^2 g_2^2 \lambda_h + \frac{2}{5} g_1^2 g_2^2 \lambda_2 \\
 & + 4 \left(\tilde{\lambda}_2^3 - 8\lambda_2 \tilde{\lambda}_2^2 - 8\lambda_2^2 \tilde{\lambda}_2 \right) + \tilde{\lambda}_2 \left(\frac{2227}{600} g_1^4 \right. \\
 & - \frac{187}{8} g_2^4 - \frac{494}{9} g_3^4 + \frac{287}{60} g_1^2 g_2^2 + \frac{2}{9} g_1^2 g_3^2 + \frac{14}{3} g_2^2 g_3^2 \\
 & + \frac{24}{5} g_1^2 \lambda_h - 28\lambda_h^2 \left. \right) + 2\tilde{\lambda}_2^2 \left(\frac{14}{15} g_1^2 + 9g_2^2 + \frac{8}{3} g_3^2 \right. \\
 & \left. - 20\lambda_h \right) + 4\lambda_2 \tilde{\lambda}_2 \left(\frac{1}{3} g_1^2 + 9g_2^2 + \frac{8}{3} g_3^2 - 20\lambda_h \right) \\
 & + \left\{ \frac{13}{5} g_1^2 g_2^2 + \tilde{\lambda}_2 \left(\frac{13}{12} g_1^2 + \frac{15}{4} g_2^2 + \frac{20}{3} g_3^2 - 8\lambda_2 - 4\tilde{\lambda}_2 \right) \right\} \text{Tr} \mathcal{X}_2 \\
 & + \left\{ -\frac{9}{5} g_1^2 g_2^2 + \tilde{\lambda}_2 \left(\frac{5}{4} g_1^2 + \frac{45}{4} g_2^2 + 40g_3^2 \right. \right. \\
 & \left. \left. - 24\lambda_h - 24\lambda_2 - 12\tilde{\lambda}_2 \right) \right\} \text{Tr} \mathcal{X}_d + \left\{ -\frac{21}{5} g_1^2 g_2^2 + \tilde{\lambda}_2 \left(\frac{17}{4} g_1^2 \right. \right. \\
 & \left. \left. + \frac{45}{4} g_2^2 + 40g_3^2 - 24\lambda_h - 24\lambda_2 - 12\tilde{\lambda}_2 \right) \right\} \text{Tr} \mathcal{X}_u \\
 & + \left\{ -\frac{11}{5} g_1^2 g_2^2 + \tilde{\lambda}_2 \left(\frac{15}{4} g_1^2 + \frac{15}{4} g_2^2 - 8\lambda_h - 8\lambda_2 - 4\tilde{\lambda}_2 \right) \right\} \text{Tr} \mathcal{X}_l \\
 & - \text{Tr} \left\{ 8 \left(\lambda_2 + \frac{7}{4} \tilde{\lambda}_2 - \frac{2}{5} g_1^2 \right) \tilde{\mathcal{X}}_2 \tilde{\mathcal{X}}_l \right.
 \end{aligned}$$

$$\begin{aligned}
 & + \frac{27}{2} \tilde{\lambda}_2 \left(\frac{5}{9} \mathcal{X}_2^2 + \mathcal{X}_u^2 + \mathcal{X}_d^2 + \frac{1}{3} \mathcal{X}_l^2 + \frac{8}{27} \mathcal{X}_2 \mathcal{X}_d - 2\tilde{\mathcal{X}}_u \tilde{\mathcal{X}}_d \right) \left. \right\} \\
 & - 16 \text{Tr} \left\{ \tilde{\mathcal{X}}_2^2 \tilde{\mathcal{X}}_l + \frac{1}{2} \tilde{\mathcal{X}}_2 \tilde{\mathcal{X}}_l^2 + \frac{3}{4} Y_2 \tilde{\mathcal{X}}_l Y_2^\dagger \mathcal{X}_d \right\}. \tag{117}
 \end{aligned}$$

$$\begin{aligned}
 \beta(\lambda_2^{ij})_{\tilde{R}_2, 3\text{-gen}}^{2\text{-loop}} &= \left[\beta(\lambda_2)_{\tilde{R}_2, 1\text{-gen}}^{2\text{-loop}} \right]_i + \frac{1}{(16\pi^2)^2} \left\{ -\frac{7}{750} g_1^6 \right. \\
 & + \frac{7}{150} g_1^4 g_2^2 + \frac{7}{10} g_1^2 g_2^4 - \frac{21}{2} g_2^6 \\
 & + \lambda_2^{ii} \left(\frac{11}{90} g_1^4 + \frac{33}{2} g_2^4 + \frac{88}{9} g_3^4 \right) \left. \right\} + \frac{1}{(16\pi^2)^2} \\
 & \times \sum_{j \neq i} \left[-6\lambda_2^{ij} \left\{ \left(\lambda_2^{jj} \right)^2 \right. \right. \\
 & + \lambda_2^{jj} \tilde{\lambda}_2^{jj} + \left(\tilde{\lambda}_2^{jj} \right)^2 \left. \right\} - 6\tilde{\lambda}_2^{ij} \left(\tilde{\lambda}_2^{jj} \right)^2 \\
 & + \left(\lambda_2^{jj} + \frac{1}{2} \tilde{\lambda}_2^{jj} \right) \left(\frac{1}{30} g_1^4 + \frac{45}{2} g_2^4 + \frac{80}{3} g_3^4 \right) - \frac{1}{2} \tilde{\lambda}_2^{jj} g_1^2 g_2^2 \\
 & - \frac{9}{2} \lambda_2^{ii} \text{Tr} \left\{ 2\mathcal{X}_d \mathcal{X}_{2,j} + \tilde{\mathcal{X}}_l \tilde{\mathcal{X}}_{2,j} + \frac{2}{3} \mathcal{X}_{2,i} \mathcal{X}_{2,j} \right. \\
 & + \tilde{\mathcal{X}}_{2,i} \tilde{\mathcal{X}}_{2,j} \left. \right\} + 4 \text{Tr} \left\{ \mathcal{X}_d \left(\mathcal{X}_{2,i} \mathcal{X}_{2,j} + \mathcal{X}_{2,j} \mathcal{X}_{2,i} \right. \right. \\
 & \left. \left. + \frac{3}{2} Y_{2,i} \tilde{\mathcal{X}}_{2,j} Y_{2,i}^\dagger + 3Y_{2,j} \tilde{\mathcal{X}}_{2,i} Y_{2,j}^\dagger \right) \right\} \\
 & + 6 \text{Tr} \left\{ \tilde{\mathcal{X}}_l \left(\tilde{\mathcal{X}}_{2,i} \tilde{\mathcal{X}}_{2,j} + \tilde{\mathcal{X}}_{2,j} \tilde{\mathcal{X}}_{2,i} + \frac{2}{3} Y_{2,i}^\dagger \mathcal{X}_{2,j} Y_{2,i} \right. \right. \\
 & \left. \left. + \frac{2}{3} Y_{2,j}^\dagger \mathcal{X}_{2,i} Y_{2,j} \right) \right\} \left. \right]. \tag{118}
 \end{aligned}$$

$$\begin{aligned}
 \beta(\tilde{\lambda}_2^{ij})_{\tilde{R}_2, 3\text{-gen}}^{2\text{-loop}} &= \left[\beta(\tilde{\lambda}_2)_{\tilde{R}_2, 1\text{-gen}}^{2\text{-loop}} \right]_i \\
 & + \frac{1}{(16\pi^2)^2} \left\{ \tilde{\lambda}_2^{ii} \left(\frac{11}{90} g_1^4 + \frac{33}{2} g_2^4 \right. \right. \\
 & \left. \left. + \frac{88}{9} g_3^4 \right) - \frac{7}{75} g_1^4 g_2^2 - \frac{7}{5} g_1^2 g_2^4 \right\} \\
 & + \frac{1}{(16\pi^2)^2} \sum_{j \neq i} \left[-6\tilde{\lambda}_2^{ij} \left\{ \left(\lambda_2^{jj} \right)^2 \right. \right. \\
 & + \lambda_2^{jj} \tilde{\lambda}_2^{jj} + \left(\tilde{\lambda}_2^{jj} \right)^2 \left. \right\} \\
 & + \tilde{\lambda}_2^{jj} g_1^2 g_2^2 - \frac{9}{2} \tilde{\lambda}_2^{ii} \text{Tr} \left\{ 2\mathcal{X}_d \mathcal{X}_{2,j} + \tilde{\mathcal{X}}_l \tilde{\mathcal{X}}_{2,j} \right. \\
 & + \frac{2}{3} \mathcal{X}_{2,i} \mathcal{X}_{2,j} + \tilde{\mathcal{X}}_{2,i} \tilde{\mathcal{X}}_{2,j} \left. \right\} - 6 \text{Tr} \left\{ \tilde{\mathcal{X}}_l \left(\tilde{\mathcal{X}}_{2,i} \tilde{\mathcal{X}}_{2,j} + \tilde{\mathcal{X}}_{2,j} \tilde{\mathcal{X}}_{2,i} \right. \right. \\
 & \left. \left. + \frac{2}{3} Y_{2,i}^\dagger \mathcal{X}_{2,j} Y_{2,i} \right) \right\} \left. \right]. \tag{119}
 \end{aligned}$$

Appendix F: Two-loop beta functions of Higgs-leptoquark quartic couplings for S_3

$$\begin{aligned}
 \beta(\lambda_3)_{S_3, 1\text{-gen}}^{2\text{-loop}} &= \beta(\lambda_3)_{S_3}^{1\text{-loop}} + \frac{1}{(16\pi^2)^2} \\
 & \times \left[-\frac{789}{500} g_1^6 + \frac{689}{100} g_1^4 g_2^2 + \frac{176}{15} g_1^2 g_2^4 + \frac{49}{6} g_2^6 \right. \\
 & - \frac{4}{5} g_1^4 g_3^2 + 8g_1^2 g_2^2 g_3^2 \\
 & \left. - 40g_2^4 g_3^2 + \frac{6}{5} g_1^4 \lambda_h - 4g_1^2 g_2^2 \lambda_h + 60g_2^4 \lambda_h \right.
 \end{aligned}$$

$$\begin{aligned}
 & + \lambda_3 \left(\frac{25067}{3600} g_1^4 + \frac{199}{120} g_1^2 g_2^2 \right. \\
 & + \frac{12661}{48} g_2^4 + \frac{8}{9} g_1^2 g_3^2 + \frac{80}{3} g_2^2 g_3^2 \\
 & - \frac{112}{9} g_3^4 + \frac{72}{5} g_1^2 \lambda_h + 72 g_2^2 \lambda_h - 60 \lambda_h^2 \Big) \\
 & + \tilde{\lambda}_3 \left(\frac{17}{20} g_1^4 - \frac{26}{3} g_1^2 g_2^2 + \frac{505}{4} g_2^4 \right. \\
 & + \frac{8}{3} g_2^2 g_3^2 + 20 g_3^4 + \frac{24}{5} g_1^2 \lambda_h \\
 & + 36 g_2^2 \lambda_h - 16 \lambda_h^2 \Big) + \lambda_3^2 \left(\frac{13}{15} g_1^2 + 11 g_2^2 + \frac{16}{3} g_3^2 - 72 \lambda_h \right) \\
 & + \tilde{\lambda}_3^2 \left(-\frac{23}{60} g_1^2 + \frac{11}{4} g_2^2 + \frac{4}{3} g_3^2 - 18 \lambda_h \right) \\
 & + \lambda_3 \tilde{\lambda}_3 \left(-12 g_2^2 - 32 \lambda_h \right) - \left(19 \lambda_3^3 + 11 \lambda_3^2 \tilde{\lambda}_3 + \frac{57}{4} \lambda_3 \tilde{\lambda}_3^2 \right. \\
 & + \frac{19}{2} \tilde{\lambda}_3^3 \Big) + \left\{ \frac{1}{5} g_1^4 - \frac{18}{5} g_1^2 g_2^2 - 6 g_2^4 - 32 g_3^4 \right. \\
 & + \lambda_3 \left(\frac{5}{4} g_1^2 + \frac{45}{4} g_2^2 + 40 g_3^2 - 72 \lambda_h \right) - 24 \tilde{\lambda}_3 \lambda_h \\
 & - 12 \lambda_3^2 - 3 \tilde{\lambda}_3^2 \Big\} \text{Tr} X_d + \left\{ -\frac{19}{25} g_1^4 - \frac{42}{5} g_1^2 g_2^2 - 6 g_2^4 \right. \\
 & - 32 g_3^4 + \lambda_3 \left(\frac{17}{4} g_1^2 + \frac{45}{4} g_2^2 + 40 g_3^2 - 72 \lambda_h \right) - 24 \tilde{\lambda}_3 \lambda_h \\
 & - 12 \lambda_3^2 - 3 \tilde{\lambda}_3^2 \Big\} \text{Tr} X_u + \left\{ -\frac{2}{5} g_1^4 - \frac{4}{5} g_1^2 g_2^2 + g_2^4 \right. \\
 & + \lambda_3 \left(\frac{5}{6} g_1^2 + \frac{15}{2} g_2^2 + \frac{20}{3} g_3^2 \right) - 4 \lambda_3^2 - \tilde{\lambda}_3^2 \Big\} \text{Tr} X_3 \\
 & + \left\{ -2 g_2^4 - g_1^4 - \frac{22}{5} g_1^2 g_2^2 + \frac{3}{4} \lambda_3 (5 g_1^2 + 5 g_2^2 - 32 \lambda_h) \right. \\
 & - 8 \tilde{\lambda}_3 \lambda_h - 4 \lambda_3^2 - \tilde{\lambda}_3^2 \Big\} \text{Tr} X_l - \text{Tr} \left\{ \frac{27}{2} \lambda_3 \tilde{X}_d^2 \right. \\
 & + 21 \lambda_3 \tilde{X}_u \tilde{X}_d + 24 \tilde{\lambda}_3 \tilde{X}_u \tilde{X}_d \Big\} - \frac{9}{2} \lambda_3 \text{Tr} X_l^2 - 9 \lambda_3 \text{Tr} X_3^2 \\
 & + \text{Tr} \left(\tilde{X}_3 \tilde{X}_l \right) \left(-\frac{1}{4} \lambda_3 - \frac{14}{5} g_1^2 + 2 g_2^2 \right) \\
 & - \text{Tr} \left(X_3 \tilde{X}_d^T \right) \left(\frac{1}{4} \lambda_3 + \frac{2}{15} g_1^2 - 2 g_2^2 + \frac{32}{3} g_3^2 \right) \\
 & - \text{Tr} \left(X_3 \tilde{X}_u^T \right) \left(\frac{33}{4} \lambda_3 - 4 \tilde{\lambda}_3 \right) \\
 & + \text{Tr} \left(-\frac{27}{2} \lambda_3 X_u^2 + 12 \tilde{X}_l^2 \tilde{X}_3 \right. \\
 & + 25 \tilde{X}_3^2 \tilde{X}_l + 12 Y_3^\dagger \tilde{X}_d^T Y_3 \tilde{X}_l + 2 Y_3^\dagger \tilde{X}_u^T Y_3 \tilde{X}_l \\
 & + 27 X_3^2 \tilde{X}_d^T + 6 X_3^2 \tilde{X}_u^T + 12 \tilde{X}_d^T X_3 \tilde{X}_d^T - 2 X_3 \tilde{X}_d^T \tilde{X}_u^T \\
 & \left. - 2 X_3 \tilde{X}_u^T \tilde{X}_d^T + 4 \tilde{X}_u^T X_3 \tilde{X}_u^T \right). \tag{120}
 \end{aligned}$$

$$\begin{aligned}
 \beta(\tilde{\lambda}_3)_{S_3, 1\text{-gen}}^{2\text{-loop}} &= \beta(\tilde{\lambda}_3)_{S_3}^{1\text{-loop}} + \frac{1}{(16\pi^2)^2} \left[-\frac{427}{25} g_1^4 g_2^2 \right. \\
 & - \frac{547}{15} g_1^2 g_2^4 - 16 g_1^2 g_2^2 g_3^2 + 8 g_1^2 g_2^2 \left(\lambda_h + \frac{1}{5} \lambda_3 \right) \\
 & \left. + \tilde{\lambda}_3 \left(\frac{18947}{3600} g_1^4 + \frac{541}{48} g_2^4 - \frac{472}{9} g_3^4 \right. \right.
 \end{aligned}$$

$$\begin{aligned}
 & + \frac{2567}{120} g_1^2 g_2^2 + \frac{8}{9} g_1^2 g_3^2 + \frac{64}{3} g_2^2 g_3^2 \\
 & + \frac{24}{5} g_1^2 \lambda_h - 28 \lambda_h^2 \Big) + \tilde{\lambda}_3^2 \left(\frac{31}{15} g_1^2 - \frac{13}{4} \tilde{\lambda}_3 \right) \\
 & + \lambda_3 \tilde{\lambda}_3 \left(\frac{26}{15} g_1^2 - 35 \lambda_3 - 35 \tilde{\lambda}_3 \right) \\
 & + \tilde{\lambda}_3 \left(\lambda_3 + \frac{1}{2} \tilde{\lambda}_3 \right) \left(46 g_2^2 + \frac{32}{3} g_3^2 - 80 \lambda_h \right) \\
 & + \left\{ \frac{36}{5} g_1^2 g_2^2 + \tilde{\lambda}_3 \left(\frac{5}{4} g_1^2 + \frac{45}{4} g_2^2 \right. \right. \\
 & + 40 g_3^2 - 24 \lambda_h - 24 \lambda_3 - 12 \tilde{\lambda}_3 \Big) \Big\} \text{Tr} X_d + \left\{ \frac{44}{5} g_1^2 g_2^2 \right. \\
 & + \tilde{\lambda}_3 \left(\frac{15}{4} g_1^2 + \frac{15}{4} g_2^2 - 8 \lambda_h - 8 \lambda_3 - 4 \tilde{\lambda}_3 \right) \Big\} \text{Tr} X_l \\
 & + \left\{ \frac{8}{5} g_1^2 g_2^2 + \tilde{\lambda}_3 \left(\frac{5}{6} g_1^2 + \frac{15}{2} g_2^2 + \frac{20}{3} g_3^2 - 8 \lambda_3 - 4 \tilde{\lambda}_3 \right) \right\} \text{Tr} X_3 \\
 & \times \left\{ \frac{84}{5} g_1^2 g_2^2 + \tilde{\lambda}_3 \left(\frac{17}{4} g_1^2 + \frac{45}{4} g_2^2 + 40 g_3^2 \right. \right. \\
 & - 24 \lambda_h - 24 \lambda_3 - 12 \tilde{\lambda}_3 \Big) \Big\} \text{Tr} X_u \\
 & + \tilde{\lambda}_3 \text{Tr} \left\{ -\frac{27}{2} X_u^2 - \frac{27}{2} X_d^2 + 27 \tilde{X}_d \tilde{X}_u - \frac{9}{2} X_l^2 - 9 X_3^2 \right\} \\
 & + \left\{ \frac{14}{5} g_1^2 - 2 g_2^2 - 8 \lambda_3 - \frac{49}{4} \tilde{\lambda}_3 \right\} \text{Tr} \left(\tilde{X}_l \tilde{X}_3 \right) + \left\{ \frac{2}{15} g_1^2 - 2 g_2^2 \right. \\
 & + \frac{32}{3} g_3^2 - 8 \lambda_3 - \frac{49}{4} \tilde{\lambda}_3 \Big\} \text{Tr} \left(X_3 \tilde{X}_d^T \right) \\
 & - \left\{ \frac{14}{15} g_1^2 - 2 g_2^2 + \frac{32}{3} g_3^2 - 8 \lambda_3 + \frac{17}{4} \tilde{\lambda}_3 \right\} \text{Tr} \left(X_3 \tilde{X}_u^T \right) \\
 & - \text{Tr} \left(8 \tilde{X}_3 \tilde{X}_l^2 + 23 \tilde{X}_3^2 \tilde{X}_l + 12 \tilde{X}_l Y_3^\dagger \tilde{X}_d Y_3 \right. \\
 & \left. + 21 X_3^2 \tilde{X}_d^T - 21 X_3^2 \tilde{X}_u^T + 8 \tilde{X}_d^T X_3 \tilde{X}_d^T - 8 \tilde{X}_u^T X_3 \tilde{X}_u^T \right). \tag{121}
 \end{aligned}$$

$$\begin{aligned}
 \beta(\lambda_3^i)_{S_2, 3\text{-gen}}^{2\text{-loop}} &= \left[\beta(\lambda_3)_{S_3, 1\text{-gen}}^{2\text{-loop}} \right]_i \\
 & + \frac{1}{(16\pi^2)^2} \left\{ + \lambda_3^{ii} \left(\frac{143}{150} g_1^4 + 121 g_2^4 \right. \right. \\
 & + \frac{44}{3} g_3^4 \Big) - \frac{28}{125} g_1^6 - 112 g_2^6 \\
 & + \frac{28}{25} g_1^4 g_2^2 + \frac{56}{5} g_1^2 g_2^4 \Big\} + \frac{1}{(16\pi^2)^2} \sum_{j \neq i} \left[-9 \lambda_3^{ij} \left\{ \left(\lambda_3^{jj} \right)^2 \right. \right. \\
 & + \lambda_3^{jj} \tilde{\lambda}_3^{jj} + \frac{3}{4} \left(\tilde{\lambda}_3^{jj} \right)^2 \Big\} - 6 \tilde{\lambda}_3^{ii} \left(\tilde{\lambda}_3^{jj} \right)^2 \\
 & - 8 \tilde{\lambda}_3^{ij} g_1^2 g_2^2 + \left(\lambda_3^{jj} + \frac{1}{2} \tilde{\lambda}_3^{jj} \right) \left(\frac{4}{5} g_1^4 + 240 g_2^4 + 40 g_3^4 \right) \\
 & - \frac{27}{4} \lambda_3^{ii} \text{Tr} \left\{ \tilde{X}_l \tilde{X}_{3,j} + \frac{1}{3} X_{3,i} X_{3,j} + \tilde{X}_{3,i} \tilde{X}_{3,j} \right. \\
 & + X_{3,j} \tilde{X}_u^T + X_{3,j} \tilde{X}_d^T \Big\} + 9 \text{Tr} \left\{ \tilde{X}_l \left(\tilde{X}_{3,i} \tilde{X}_{3,j} + \tilde{X}_{3,j} \tilde{X}_{3,i} \right. \right. \\
 & \left. \left. + \frac{1}{3} Y_{3,i}^\dagger X_{3,j} Y_{3,i} + \frac{4}{9} Y_{3,j}^\dagger X_{3,i} Y_{3,j} \right) \right\}
 \end{aligned}$$

$$\begin{aligned}
 &+ 3\text{Tr}\left\{\tilde{\chi}_d^T\left(\mathcal{X}_{3,i}\mathcal{X}_{3,j} + \mathcal{X}_{3,j}\mathcal{X}_{3,i} + 3Y_{3,i}\tilde{\chi}_{3,j}^TY_{3,i}^\dagger\right)\right. \\
 &\left.+ 4\left(\tilde{\chi}_d^T + \frac{1}{2}\tilde{\chi}_u^T\right)Y_{3,j}\tilde{\chi}_{3,i}Y_{3,j}^\dagger\right\}. \tag{122}
 \end{aligned}$$

$$\begin{aligned}
 \beta(\tilde{\lambda}_3)_{S_2,3\text{-gen}}^{2\text{-loop}} &= \left[\beta(\tilde{\lambda}_3)_{S_3,1\text{-gen}}^{2\text{-loop}}\right]_i \\
 &+ \frac{1}{(16\pi^2)^2}\left\{\tilde{\lambda}_3^{ii}\left(\frac{143}{150}g_1^4 + 121g_2^4\right.\right. \\
 &\left.\left.+ \frac{44}{3}g_3^4\right) - \frac{56}{25}g_1^4g_2^2 - \frac{112}{5}g_1^2g_2^4\right\} \\
 &+ \frac{1}{(16\pi^2)^2}\sum_{j\neq i}\left[-9\tilde{\lambda}_3^{ii}\left\{\left(\lambda_3^{jj}\right)^2 + \lambda_3^{jj}\tilde{\lambda}_3^{jj} - \frac{7}{12}\left(\tilde{\lambda}_3^{jj}\right)^2\right\}\right. \\
 &\left.+ 16\tilde{\lambda}_3^{jj}g_1^2g_2^2 - \frac{27}{4}\tilde{\lambda}_3^{ii}\text{Tr}\left\{\tilde{\chi}_l\tilde{\chi}_{3,j} + \frac{1}{3}\mathcal{X}_{3,i}\mathcal{X}_{3,j}\right.\right. \\
 &\left.\left.+ \tilde{\chi}_{3,i}\tilde{\chi}_{3,j} + \mathcal{X}_{3,j}\tilde{\chi}_d^T + \mathcal{X}_{3,j}\tilde{\chi}_u^T\right\}\right. \\
 &\left.- 9\text{Tr}\left\{\tilde{\chi}_l\left(\tilde{\chi}_{3,i}\tilde{\chi}_{3,j} + \tilde{\chi}_{3,j}\tilde{\chi}_{3,i}\right.\right.\right. \\
 &\left.\left.\left.+ \frac{1}{3}Y_{3,i}^\dagger\mathcal{X}_{3,j}Y_{3,i} + \frac{2}{9}Y_{3,j}^\dagger\mathcal{X}_{3,i}Y_{3,j}\right)\right\}\right. \\
 &\left.+ 3\text{Tr}\left\{\left(\tilde{\chi}_u^T - \tilde{\chi}_d^T\right)\left(\mathcal{X}_{3,i}\mathcal{X}_{3,j} + \mathcal{X}_{3,j}\mathcal{X}_{3,i}\right.\right.\right. \\
 &\left.\left.\left.+ 3Y_{3,i}\tilde{\chi}_{3,j}Y_{3,i}^\dagger + 2Y_{3,j}\tilde{\chi}_{3,i}Y_{3,j}^\dagger\right)\right\}\right]. \tag{123}
 \end{aligned}$$

Appendix G: Two-loop beta functions of Higgs-leptoquark quartic couplings for $\tilde{R}_2 + S_3$

$$\begin{aligned}
 \beta(\lambda_2)_{\tilde{R}_2+S_3,1\text{-gen}}^{2\text{-loop}} &= \beta(\lambda_2)_{\tilde{R}_2,1\text{-gen}}^{2\text{-loop}} \\
 &+ \frac{1}{(16\pi^2)^2}\left[-9\lambda_2\left(\lambda_3^2 + \lambda_3\tilde{\lambda}_3 + \frac{3}{4}\tilde{\lambda}_3^2\right)\right. \\
 &\left.- 6\tilde{\lambda}_2\tilde{\lambda}_3^2 - 2\tilde{\lambda}_3g_1^2g_2^2\right. \\
 &\left.+ \left(\lambda_3 + \frac{1}{2}\tilde{\lambda}_3\right)\left(\frac{1}{5}g_1^4 + 90g_2^4 + 40g_3^4\right)\right. \\
 &\left.- \frac{7}{5}\left(\frac{1}{50}g_1^6 - \frac{1}{10}g_1^4g_2^2 - g_1^2g_2^4 + 15g_2^6\right)\right. \\
 &\left.+ 11\lambda_2\left(\frac{1}{30}g_1^4 + 3g_2^4 + \frac{2}{3}g_3^4\right)\right. \\
 &\left.- \frac{27}{4}\lambda_2\text{Tr}\left(\tilde{\chi}_3\tilde{\chi}_2 + \tilde{\chi}_3\tilde{\chi}_l + \mathcal{X}_3\tilde{\chi}_d^T + \mathcal{X}_3\tilde{\chi}_u^T\right)\right. \\
 &\left.+ 9\text{Tr}\left\{Y_2\tilde{\chi}_3Y_2^\dagger\mathcal{X}_d\right.\right. \\
 &\left.\left.+ \tilde{\chi}_2\tilde{\chi}_3\tilde{\chi}_l + \tilde{\chi}_3\tilde{\chi}_2\tilde{\chi}_l + \frac{4}{3}\tilde{\chi}_2Y_3^\dagger\tilde{\chi}_d^TY_3\right.\right. \\
 &\left.\left.+ \frac{2}{3}\tilde{\chi}_2Y_3^\dagger\tilde{\chi}_u^TY_3 + \frac{4}{9}Y_2Y_3^\daggerY_d^TY_2Y_3^\daggerY_d^\dagger\right.\right. \\
 &\left.\left.+ \frac{1}{3}\mathcal{X}_3Y_d^T\mathcal{X}_2^TY_d^*\right\}\right], \tag{124}
 \end{aligned}$$

$$\beta(\tilde{\lambda}_2)_{\tilde{R}_2+S_3,1\text{-gen}}^{2\text{-loop}} = \beta(\tilde{\lambda}_2)_{\tilde{R}_2,1\text{-gen}}^{2\text{-loop}}$$

$$\begin{aligned}
 &+ \frac{1}{(16\pi^2)^2}\left[-9\tilde{\lambda}_2\left(\lambda_3^2 + \lambda_3\tilde{\lambda}_3 + \frac{7}{12}\tilde{\lambda}_3^2\right)\right. \\
 &\left.+ 4\tilde{\lambda}_3g_1^2g_2^2 - \frac{7}{25}g_1^4g_2^2 - \frac{14}{5}g_1^2g_2^4\right. \\
 &\left.+ 11\tilde{\lambda}_2\left(\frac{1}{30}g_1^4 + 3g_2^4 + \frac{2}{3}g_3^4\right)\right. \\
 &\left.- \frac{27}{4}\tilde{\lambda}_2\text{Tr}\left(\tilde{\chi}_3\tilde{\chi}_2 + \tilde{\chi}_3\tilde{\chi}_l\right.\right. \\
 &\left.\left.+ \mathcal{X}_3\tilde{\chi}_d^T + \mathcal{X}_3\tilde{\chi}_u^T\right) - 9\text{Tr}\left\{\tilde{\chi}_2\tilde{\chi}_3\tilde{\chi}_l + \tilde{\chi}_3\tilde{\chi}_2\tilde{\chi}_l\right.\right. \\
 &\left.\left.+ \frac{2}{9}Y_2Y_3^\daggerY_d^TY_2^*Y_3^TY_d^\dagger\right.\right. \\
 &\left.\left.+ \frac{2}{3}\tilde{\chi}_2Y_3^\dagger\tilde{\chi}_d^TY_3 - \frac{2}{3}\tilde{\chi}_2Y_3^\dagger\tilde{\chi}_u^TY_3\right\}\right], \tag{125}
 \end{aligned}$$

$$\begin{aligned}
 \beta(\lambda_3)_{\tilde{R}_2+S_3,1\text{-gen}}^{2\text{-loop}} &= \beta(\lambda_3)_{S_3,1\text{-gen}}^{2\text{-loop}} \\
 &+ \frac{1}{(16\pi^2)^2}\left[-6\left(\lambda_2^2\lambda_3 + \lambda_2\tilde{\lambda}_2\lambda_3 + \tilde{\lambda}_2^2\lambda_3 + \tilde{\lambda}_2^2\tilde{\lambda}_3\right)\right. \\
 &\left.- \frac{7}{5}\left(\frac{1}{75}g_1^6 - \frac{1}{15}g_1^4g_2^2\right.\right. \\
 &\left.\left.- g_1^2g_2^4 + 10g_2^6\right) - 2\tilde{\lambda}_2g_1^2g_2^2\right. \\
 &\left.+ \left(\lambda_2 + \frac{1}{2}\tilde{\lambda}_2\right)\left(\frac{2}{15}g_1^4 + 60g_2^4 + \frac{80}{3}g_3^4\right)\right. \\
 &\left.+ 11\lambda_3\left(\frac{13}{1800}g_1^4 + \frac{11}{8}g_2^4 + \frac{4}{9}g_3^4\right)\right. \\
 &\left.- \frac{9}{2}\lambda_3\text{Tr}\left\{2\mathcal{X}_2\mathcal{X}_d + \tilde{\chi}_2\tilde{\chi}_3 + \tilde{\chi}_2\tilde{\chi}_l\right\}\right. \\
 &\left.+ 6\text{Tr}\left\{2Y_2\tilde{\chi}_3Y_2^\dagger\mathcal{X}_d + \tilde{\chi}_2\tilde{\chi}_3\tilde{\chi}_l + \tilde{\chi}_3\tilde{\chi}_2\tilde{\chi}_l\right.\right. \\
 &\left.\left.+ \frac{2}{3}Y_2Y_3^\daggerY_d^TY_2^*Y_3^TY_d^\dagger\right.\right. \\
 &\left.\left.+ \tilde{\chi}_2Y_3^\dagger\tilde{\chi}_d^TY_3 + \frac{2}{3}\mathcal{X}_3Y_d^T\mathcal{X}_2^TY_d^*\right\}\right], \tag{126}
 \end{aligned}$$

$$\begin{aligned}
 \beta(\tilde{\lambda}_3)_{\tilde{R}_2+S_3,1\text{-gen}}^{2\text{-loop}} &= \beta(\tilde{\lambda}_3)_{S_3,1\text{-gen}}^{2\text{-loop}} \\
 &+ \frac{1}{(16\pi^2)^2}\left[-6\tilde{\lambda}_3\left(\lambda_2^2 + \lambda_2\tilde{\lambda}_2 - \tilde{\lambda}_2^2\right)\right. \\
 &\left.+ 4\tilde{\lambda}_2g_1^2g_2^2 - \frac{14}{75}g_1^4g_2^2 - \frac{14}{5}g_1^2g_2^4\right. \\
 &\left.+ 11\tilde{\lambda}_3\left(\frac{13}{1800}g_1^4 + \frac{11}{8}g_2^4 + \frac{4}{9}g_3^4\right)\right. \\
 &\left.- \frac{9}{2}\tilde{\lambda}_3\text{Tr}\left\{2\mathcal{X}_2\mathcal{X}_d + \tilde{\chi}_2\tilde{\chi}_3 + \tilde{\chi}_2\tilde{\chi}_l\right\}\right. \\
 &\left.- 6\text{Tr}\left\{\tilde{\chi}_2\tilde{\chi}_3\tilde{\chi}_l + \tilde{\chi}_3\tilde{\chi}_2\tilde{\chi}_l\right.\right. \\
 &\left.\left.+ \frac{2}{3}Y_2Y_3^\daggerY_d^TY_2^*Y_3^TY_d^\dagger + \tilde{\chi}_2Y_3^\dagger\tilde{\chi}_d^TY_3 - \tilde{\chi}_2Y_3^\dagger\tilde{\chi}_u^TY_3\right.\right. \\
 &\left.\left.+ \frac{2}{3}\mathcal{X}_3Y_d^T\mathcal{X}_2^TY_d^*\right\}\right]. \tag{127}
 \end{aligned}$$

$$\begin{aligned}
 \beta(\lambda_2)_{\tilde{R}_2+S_3,3\text{-gen}}^{2\text{-loop}} &= \beta(\lambda_2)_{\tilde{R}_2,3\text{-gen}}^{2\text{-loop}} \\
 &+ \frac{1}{(16\pi^2)^2}\left\{11\lambda_2^{ii}\left(\frac{1}{10}g_1^4 + 9g_2^4 + 2g_3^4\right)\right.
 \end{aligned}$$

$$\begin{aligned}
 & -\frac{21}{250}g_1^6 + \frac{21}{50}g_1^4g_2^2 \\
 & + \frac{21}{5}g_1^2g_2^4 - 63g_2^6 \left\} + \frac{1}{(16\pi^2)^2} \sum_{l=1}^3 \left[-6\tilde{\lambda}_2^{ii} \left(\tilde{\lambda}_3^l \right)^2 \right. \right. \\
 & - 2\tilde{\lambda}_2^{ll}g_1^2g_2^2 - 9\lambda_2^{ii} \left\{ \left(\lambda_3^l \right)^2 + \lambda_3^l \tilde{\lambda}_3^l + \frac{3}{4} \left(\tilde{\lambda}_3^l \right)^2 \right\} \\
 & + \left(\lambda_3^l + \frac{1}{2}\tilde{\lambda}_3^l \right) \left(\frac{1}{5}g_1^4 + 90g_2^4 + 40g_3^4 \right) \\
 & - \frac{27}{4}\lambda_2^{ii} \text{Tr} \left(\tilde{\mathcal{X}}_{2,i} \tilde{\mathcal{X}}_{3,l} + \mathcal{X}_{3,l} \tilde{\mathcal{X}}_d^T + \mathcal{X}_{3,l} \tilde{\mathcal{X}}_u^T + \tilde{\mathcal{X}}_{3,l} \tilde{\mathcal{X}}_l \right) \\
 & + 9\text{Tr} \left\{ Y_{2,i} \tilde{\mathcal{X}}_{3,l} Y_{2,i}^\dagger \mathcal{X}_d + \tilde{\mathcal{X}}_{2,i} \tilde{\mathcal{X}}_{3,l} \tilde{\mathcal{X}}_l + \frac{4}{9} Y_{2,i} Y_{3,l}^\dagger Y_d^T Y_{2,i}^* Y_{3,l}^\dagger Y_d^T \right. \\
 & + \frac{4}{3} \tilde{\mathcal{X}}_{2,i} Y_{3,l}^\dagger \tilde{\mathcal{X}}_d^T Y_{3,l} \\
 & + \frac{2}{3} \tilde{\mathcal{X}}_{2,i} Y_{3,l}^\dagger \tilde{\mathcal{X}}_u^T Y_{3,l} \\
 & + Y_{2,i} \tilde{\mathcal{X}}_{3,l} Y_{2,i}^\dagger \mathcal{X}_d + \tilde{\mathcal{X}}_{2,i} \tilde{\mathcal{X}}_{3,i} \tilde{\mathcal{X}}_l \\
 & \left. + \frac{1}{3} \mathcal{X}_{3,l} Y_d^T \mathcal{X}_{2,i}^T Y_d^* \right\}, \tag{128}
 \end{aligned}$$

$$\begin{aligned}
 \beta(\tilde{\lambda}_2^{ii})_{\tilde{R}_2+S_3,3\text{-gen}}^{2\text{-loop}} & = \beta(\tilde{\lambda}_2^{ii})_{\tilde{R}_2,3\text{-gen}}^{2\text{-loop}} \\
 & + \frac{1}{(16\pi^2)^2} \left\{ 11\tilde{\lambda}_2^{ii} \left(\frac{1}{10}g_1^4 + 9g_2^4 + 2g_3^4 \right) \right. \\
 & - \frac{21}{25}g_1^4g_2^2 - \frac{42}{5}g_1^2g_2^4 \left. \right\} \\
 & + \frac{1}{(16\pi^2)^2} \sum_{l=1}^3 \left[9\tilde{\lambda}_2^{ii} \left\{ \frac{7}{12} \left(\tilde{\lambda}_3^l \right)^2 - \lambda_3^l \tilde{\lambda}_3^l \right. \right. \\
 & - \left. \left(\lambda_3^l \right)^2 \right\} + 4\tilde{\lambda}_3^l g_1^2 g_2^2 - \frac{27}{4} \tilde{\lambda}_2^{ii} \text{Tr} \left\{ \tilde{\mathcal{X}}_{2,i} \tilde{\mathcal{X}}_{3,l} + \tilde{\mathcal{X}}_l \tilde{\mathcal{X}}_{3,l} \right. \\
 & + \mathcal{X}_{3,l} \tilde{\mathcal{X}}_u^T + \mathcal{X}_{3,l} \tilde{\mathcal{X}}_d^T \left. \right\} - 9\text{Tr} \left\{ \tilde{\mathcal{X}}_{2,i} \tilde{\mathcal{X}}_{3,l} \tilde{\mathcal{X}}_l + \tilde{\mathcal{X}}_{2,i} \tilde{\mathcal{X}}_l \tilde{\mathcal{X}}_{3,l} \right. \\
 & + \frac{2}{9} Y_{2,i} Y_{3,l}^\dagger Y_d^T Y_{2,i}^* Y_{3,l}^\dagger Y_d^T \\
 & + \frac{2}{3} \tilde{\mathcal{X}}_{2,i} Y_{3,l}^\dagger \tilde{\mathcal{X}}_d^T Y_{3,l} \\
 & \left. - \frac{2}{3} \tilde{\mathcal{X}}_{2,i} Y_{3,l}^\dagger \tilde{\mathcal{X}}_u^T Y_{3,l} \right\}, \tag{129}
 \end{aligned}$$

$$\begin{aligned}
 \beta(\lambda_3^{ii})_{\tilde{R}_2+S_3,3\text{-gen}}^{2\text{-loop}} & = \beta(\lambda_3^{ii})_{S_3,3\text{-gen}}^{2\text{-loop}} \\
 & + \frac{1}{(16\pi^2)^2} \left\{ 11\lambda_3^{ii} \left(\frac{13}{600}g_1^4 + \frac{33}{8}g_2^4 + \frac{4}{3}g_3^4 \right) \right. \\
 & - \frac{7}{125}g_1^6 + \frac{7}{25}g_1^4g_2^2 \\
 & + \frac{21}{5}g_1^2g_2^4 - 42g_2^6 \left. \right\} + \frac{1}{(16\pi^2)^2} \sum_{l=1}^3 \\
 & \times \left[-6\tilde{\lambda}_3^{ii} \left(\tilde{\lambda}_2^l \right)^2 - 2\tilde{\lambda}_2^{ll}g_1^2g_2^2 \right. \\
 & - 6\lambda_3^{ii} \left\{ \left(\tilde{\lambda}_2^l \right)^2 + \lambda_2^l \tilde{\lambda}_2^l + \left(\lambda_2^l \right)^2 \right\} \\
 & + \left(\lambda_2^l + \frac{1}{2}\tilde{\lambda}_2^l \right) \left(\frac{2}{15}g_1^4 + 60g_2^4 + \frac{80}{3}g_3^4 \right)
 \end{aligned}$$

$$\begin{aligned}
 & - \frac{9}{2}\lambda_3^{ii} \text{Tr} \left\{ 2\mathcal{X}_{2,l} \mathcal{X}_d + \tilde{\mathcal{X}}_{3,i} \tilde{\mathcal{X}}_{2,l} + \tilde{\mathcal{X}}_l \tilde{\mathcal{X}}_{2,l} \right\} \\
 & + 6\text{Tr} \left\{ 2Y_{2,l} \tilde{\mathcal{X}}_{3,i} Y_{2,l}^\dagger \mathcal{X}_d + \tilde{\mathcal{X}}_{2,l} \tilde{\mathcal{X}}_{3,i} \tilde{\mathcal{X}}_l \right. \\
 & + \frac{2}{3} Y_{2,l} Y_{3,i}^\dagger Y_d^T Y_{2,l}^* Y_{3,i}^\dagger Y_d^T + \tilde{\mathcal{X}}_{2,l} Y_{3,i}^\dagger \tilde{\mathcal{X}}_d^T Y_{3,i} + \tilde{\mathcal{X}}_{2,l} \tilde{\mathcal{X}}_l \tilde{\mathcal{X}}_{3,i} \\
 & \left. + \frac{2}{3} \mathcal{X}_{3,i} Y_d^T \mathcal{X}_{2,l}^T Y_d^* \right\}, \tag{130}
 \end{aligned}$$

$$\begin{aligned}
 \beta(\tilde{\lambda}_3^{ii})_{\tilde{R}_2+S_3,3\text{-gen}}^{2\text{-loop}} & = \beta(\tilde{\lambda}_3^{ii})_{S_3,3\text{-gen}}^{2\text{-loop}} \\
 & + \frac{1}{(16\pi^2)^2} \left\{ -\frac{14}{25}g_1^4g_2^2 - \frac{42}{5}g_1^2g_2^4 \right. \\
 & + 11\lambda_3^{ii} \left(\frac{13}{600}g_1^4 + \frac{33}{8}g_2^4 + \frac{4}{3}g_3^4 \right) \left. \right\} \\
 & + \frac{1}{(16\pi^2)^2} \sum_{l=1}^3 \left[6\tilde{\lambda}_3^{ii} \left\{ \left(\tilde{\lambda}_2^l \right)^2 \right. \right. \\
 & - \lambda_2^l \tilde{\lambda}_2^l - \left. \left(\lambda_2^l \right)^2 \right\} + 4\tilde{\lambda}_2^{ll}g_1^2g_2^2 \\
 & - \frac{9}{2}\tilde{\lambda}_3^{ii} \text{Tr} \left\{ 2\mathcal{X}_{2,l} \mathcal{X}_d + \tilde{\mathcal{X}}_{3,i} \tilde{\mathcal{X}}_{2,l} + \tilde{\mathcal{X}}_l \tilde{\mathcal{X}}_{2,l} \right\} \\
 & - 6\text{Tr} \left(\tilde{\mathcal{X}}_{2,l} \tilde{\mathcal{X}}_{3,i} \tilde{\mathcal{X}}_l + \tilde{\mathcal{X}}_{3,i} \tilde{\mathcal{X}}_{2,l} \tilde{\mathcal{X}}_l + \frac{2}{3} Y_{2,l} Y_{3,i}^\dagger Y_d^T Y_{2,l}^* Y_{3,i}^\dagger Y_d^T \right. \\
 & + \tilde{\mathcal{X}}_{2,l} Y_{3,i}^\dagger \tilde{\mathcal{X}}_d^T Y_{3,i} - \tilde{\mathcal{X}}_{2,l} Y_{3,i}^\dagger \tilde{\mathcal{X}}_u^T Y_{3,i} \\
 & \left. + \frac{2}{3} \mathcal{X}_{3,i} Y_d^T \mathcal{X}_{2,l}^T Y_d^* \right). \tag{131}
 \end{aligned}$$

References

1. ATLAS Collaboration, G. Aad et al., Observation of a new particle in the search for the Standard Model Higgs boson with the ATLAS detector at the LHC. *Phys. Lett. B* **716**. <https://doi.org/10.1016/j.physletb.2012.08.020>. arXiv:1207.7214
2. CMS Collaboration, S. Chatrchyan et al., Observation of a New Boson at a Mass of 125 GeV with the CMS Experiment at the LHC. *Phys. Lett. B* **716**. <https://doi.org/10.1016/j.physletb.2012.08.021>. arXiv:1207.7235
3. I. Doršner, S. Fajfer, A. Greljo, J. Kamenik, N. Košnik, Physics of leptoquarks in precision experiments and at particle colliders. *Phys. Rep.* **641**, 1–68 (2016). <https://doi.org/10.1016/j.physrep.2016.06.001>. arXiv:1603.04993
4. J.C. Pati, A. Salam, Unified lepton-hadron symmetry and a Gauge theory of the basic interactions. *Phys. Rev. D* **8**, 1240–1251 (1973). <https://doi.org/10.1103/PhysRevD.8.1240>
5. J.C. Pati, A. Salam, Lepton number as the fourth color. *Phys. Rev. D* **10**, 275–289 (1974). <https://doi.org/10.1103/PhysRevD.10.275> [Erratum: *Phys. Rev. D* **11**, 703–703 (1975)]
6. D. Marzocca, Addressing the B-physics anomalies in a fundamental composite Higgs model. *JHEP* **07**, 121 (2018). [https://doi.org/10.1007/JHEP07\(2018\)121](https://doi.org/10.1007/JHEP07(2018)121). arXiv:1803.10972
7. V. Gherardi, D. Marzocca, E. Venturini, Low-energy phenomenology of scalar leptoquarks at one-loop accuracy. *JHEP* **01**, 138 (2021). [https://doi.org/10.1007/JHEP01\(2021\)138](https://doi.org/10.1007/JHEP01(2021)138) arXiv:2008.09548
8. A. Crivellin, D. Müller, T. Ota, Simultaneous explanation of $R(D^{(*)})$ and $b \rightarrow s\mu^+\mu^-$: the last scalar leptoquarks standing. *JHEP* **09**, 040 (2017). [https://doi.org/10.1007/JHEP09\(2017\)040](https://doi.org/10.1007/JHEP09(2017)040) arXiv:1703.09226

9. A. Crivellin, D. Müller, F. Saturnino, Flavor phenomenology of the leptoquark singlet-triplet model. *JHEP* **06**, 020 (2020). [https://doi.org/10.1007/JHEP06\(2020\)020](https://doi.org/10.1007/JHEP06(2020)020) arXiv:1912.04224
10. U. Aydemir, T. Mandal, S. Mitra, Addressing the $R_{D^{(*)}}$ anomalies with an S_1 leptoquark from $SO(10)$ grand unification. *Phys. Rev. D* **101**(2020). <https://doi.org/10.1103/PhysRevD.101.015011> arXiv:1902.08108
11. D. Bečirević, I. Doršner, S. Fajfer, N. Košnik, D.A. Faroughy, O. Sumensari, Scalar leptoquarks from grand unified theories to accommodate the B -physics anomalies. *Phys. Rev. D* **98**(2018). <https://doi.org/10.1103/PhysRevD.98.055003> arXiv:1806.05689
12. I. Bigaran, J. Gargalionis, R.R. Volkas, A near-minimal leptoquark model for reconciling flavour anomalies and generating radiative neutrino masses. *JHEP* **10**, 106 (2019). [https://doi.org/10.1007/JHEP10\(2019\)106](https://doi.org/10.1007/JHEP10(2019)106) arXiv:1906.01870
13. T. Mandal, S. Mitra, S. Raz, $R_{D^{(*)}}$ motivated S_1 leptoquark scenarios: impact of interference on the exclusion limits from LHC data. *Phys. Rev. D* **99**(2019). <https://doi.org/10.1103/PhysRevD.99.055028> arXiv:1811.03561
14. S. Iguro, M. Takeuchi, R. Watanabe, Testing leptoquark/EFT in $\bar{B} \rightarrow D^{(*)}\bar{\nu}$ at the LHC. *Eur. Phys. J. C* **81**, 406 (2021). <https://doi.org/10.1140/epjc/s10052-021-09125-5> arXiv:2011.02486
15. H.M. Lee, Leptoquark option for B-meson anomalies and leptonic signatures. *Phys. Rev. D* **104**(2021). <https://doi.org/10.1103/PhysRevD.104.015007> arXiv:2104.02982
16. M. Bordone, O. Catà, T. Feldmann, R. Mandal, Constraining flavour patterns of scalar leptoquarks in the effective field theory. *JHEP* **03**, 122 (2021). [https://doi.org/10.1007/JHEP03\(2021\)122](https://doi.org/10.1007/JHEP03(2021)122) arXiv:2010.03297
17. C. Borschensky, B. Fuks, A. Kulesza, D. Schwartzländer, Scalar leptoquark pair production at the LHC: precision predictions in the era of flavour anomalies. arXiv:2108.11404
18. T.E. Browder, N.G. Deshpande, R. Mandal, R. Sinha, Impact of $B \rightarrow K^* \nu \bar{\nu}$ measurements on beyond the Standard Model theories. *Phys. Rev. D* **104**(2021). <https://doi.org/10.1103/PhysRevD.104.053007> arXiv:2107.01080
19. J.-H. Sheng, J. Zhu, Q.-Y. Hu, Investigation on the New Physics effects of the vector leptoquark on semileptonic $\bar{B}^* \rightarrow V \tau^- \bar{\nu}_\tau$ decays. *Eur. Phys. J. C* **81**, 524 (2021). <https://doi.org/10.1140/epjc/s10052-021-09322-2>
20. C. Cornella, D.A. Faroughy, J. Fuentes-Martin, G. Isidori, M. Neubert, Reading the footprints of the B-meson flavor anomalies. *JHEP* **08**, 050 (2021). [https://doi.org/10.1007/JHEP08\(2021\)050](https://doi.org/10.1007/JHEP08(2021)050) arXiv:2103.16558
21. A. Crivellin, J. F. Eguren, J. Virto, Next-to-leading-order QCD matching for $\Delta F = 2$ processes in scalar leptoquark models. arXiv:2109.13600
22. A. Angelescu, D. Bečirević, D.A. Faroughy, O. Sumensari, Closing the window on single leptoquark solutions to the B -physics anomalies. *JHEP* **10**, 183 (2018). [https://doi.org/10.1007/JHEP10\(2018\)183](https://doi.org/10.1007/JHEP10(2018)183) arXiv:1808.08179
23. A. Angelescu, D. Bečirević, D.A. Faroughy, F. Jaffredo, O. Sumensari, Single leptoquark solutions to the B-physics anomalies. *Phys. Rev. D* **104**(2021). <https://doi.org/10.1103/PhysRevD.104.055017> arXiv:2103.12504
24. P. Anan, D. Bečirević, F. Mescia, O. Sumensari, Probing low energy scalar leptoquarks by the leptonic W and Z couplings. *JHEP* **02**, 109 (2019). [https://doi.org/10.1007/JHEP02\(2019\)109](https://doi.org/10.1007/JHEP02(2019)109) arXiv:1901.06315
25. E. Coluccio Leskow, G. D'Ambrosio, A. Crivellin, D. Müller, $(g - 2)_\mu$, lepton flavor violation, and Z decays with leptoquarks: correlations and future prospects. *Phys. Rev. D* **95**(2017). <https://doi.org/10.1103/PhysRevD.95.055018> arXiv:1612.06858
26. A. Crivellin, C. Greub, D. Müller, F. Saturnino, Scalar leptoquarks in leptonic processes. *JHEP* **02**, 182 (2021). [https://doi.org/10.1007/JHEP02\(2021\)182](https://doi.org/10.1007/JHEP02(2021)182) arXiv:2010.06593
27. S. Saad, Combined explanations of $(g - 2)_\mu$, $R_{D^{(*)}}$, $R_{K^{(*)}}$ anomalies in a two-loop radiative neutrino mass model. *Phys. Rev. D* **102**(2020). <https://doi.org/10.1103/PhysRevD.102.015019> arXiv:2005.04352
28. S. Saad, A. Thapa, Common origin of neutrino masses and $R_{D^{(*)}}$, $R_{K^{(*)}}$ anomalies. *Phys. Rev. D* **102**(2020). <https://doi.org/10.1103/PhysRevD.102.015014> arXiv:2004.07880
29. K.S. Babu, P.S.B. Dev, S. Jana, A. Thapa, Unified framework for B -anomalies, muon $g - 2$ and neutrino masses. *JHEP* **03**, 179 (2021). [https://doi.org/10.1007/JHEP03\(2021\)179](https://doi.org/10.1007/JHEP03(2021)179) arXiv:2009.01771
30. W.-F. Chang, One colorful resolution to the neutrino mass generation, three lepton flavor universality anomalies, and the Cabibbo angle anomaly. *JHEP* **09**, 043 (2021). [https://doi.org/10.1007/JHEP09\(2021\)043](https://doi.org/10.1007/JHEP09(2021)043) arXiv:2105.06917
31. D. Zhang, Radiative neutrino masses, lepton flavor mixing and muon $g - 2$ in a leptoquark model. *JHEP* **07**, 069 (2021). [https://doi.org/10.1007/JHEP07\(2021\)069](https://doi.org/10.1007/JHEP07(2021)069) arXiv:2105.08670
32. H. Georgi, The state of the art—gauge theories. *AIP Conf. Proc.* **23**, 575–582 (1975). <https://doi.org/10.1063/1.2947450>
33. H. Georgi, S. Glashow, Unity of all elementary particle forces. *Phys. Rev. Lett.* **32**, 438–441 (1974). <https://doi.org/10.1103/PhysRevLett.32.438>
34. S. Dimopoulos, L. Susskind, Mass Without Scalars. *Nucl. Phys. B.* **155**, 237–252 (1979). [https://doi.org/10.1016/0550-3213\(79\)90364-X4](https://doi.org/10.1016/0550-3213(79)90364-X4)
35. E. Farhi, L. Susskind, Technicolor. *Phys. Rep.* **74**, 277 (1981). [https://doi.org/10.1016/0370-1573\(81\)90173-3](https://doi.org/10.1016/0370-1573(81)90173-3)
36. B. Schrempp, F. Schrempp, Light leptoquarks. *Phys. Lett. B* **153**, 101–107 (1985). [https://doi.org/10.1016/0370-2693\(85\)91450-9](https://doi.org/10.1016/0370-2693(85)91450-9)
37. J. Wudka, Composite leptoquarks. *Phys. Lett. B* **167**, 337–342 (1986). [https://doi.org/10.1016/0370-2693\(86\)90356-4](https://doi.org/10.1016/0370-2693(86)90356-4)
38. H.P. Nilles, Supersymmetry, supergravity and particle physics. *Phys. Rep.* **110**, 1–162 (1984). [https://doi.org/10.1016/0370-1573\(84\)90008-5](https://doi.org/10.1016/0370-1573(84)90008-5)
39. H.E. Haber, G.L. Kane, The search for supersymmetry: probing physics beyond the Standard Model. *Phys. Rep.* **117**, 75–263 (1985). [https://doi.org/10.1016/0370-1573\(85\)90051-1](https://doi.org/10.1016/0370-1573(85)90051-1)
40. N. Assad, B. Fornal, B. Grinstein, Baryon number and lepton universality violation in leptoquark and diquark models. *Phys. Lett. B* **777**, 324–331 (2018). <https://doi.org/10.1016/j.physletb.2017.12.042> arXiv:1708.06350
41. P.F. Perez, C. Murgui, A.D. Plascencia, Leptoquarks and matter unification: flavor anomalies and the muon $g-2$. *Phys. Rev. D* **104**(2021). <https://doi.org/10.1103/PhysRevD.104.035041> arXiv:2104.11229
42. C. Murgui, M.B. Wise, Scalar leptoquarks, baryon number violation, and Pati–Salam symmetry. *Phys. Rev. D* **104**(2021). <https://doi.org/10.1103/PhysRevD.104.035017> arXiv:2105.14029
43. P. Bandyopadhyay, R. Mandal, Revisiting scalar leptoquark at the LHC. *Eur. Phys. J. C* **78**, 491 (2018). <https://doi.org/10.1140/epjc/s10052-018-5959-x> arXiv:1801.04253
44. A. Bhaskar, T. Mandal, S. Mitra, Boosting vector leptoquark searches with boosted tops. *Phys. Rev. D* **101**(2020). <https://doi.org/10.1103/PhysRevD.101.115015> arXiv:2004.01096
45. A. Bhaskar, D. Das, T. Mandal, S. Mitra, C. Neeraj, Precise limits on the charge- $2/3$ U_1 vector leptoquark. arXiv:2101.12069
46. A. Bhaskar, T. Mandal, S. Mitra, M. Sharma, Improving third-generation leptoquark searches with combined signals and boosted top. arXiv:2106.07605
47. L. Da Rold, M. Epele, A. Medina, N.I. Mileo, A. Szykman, Enhancement of the double Higgs production via leptoquarks at the LHC. arXiv:2105.06309
48. G. Hiller, D. Loose, I. Nišandžić, Flavorful leptoquarks at the LHC and beyond: spin 1. *JHEP* **06**, 080 (2021). [https://doi.org/10.1007/JHEP06\(2021\)080](https://doi.org/10.1007/JHEP06(2021)080) arXiv:2103.12724

49. U. Haisch, G. Polesello, Resonant third-generation leptoquark signatures at the Large Hadron Collider. *JHEP* **05**, 057 (2021). [https://doi.org/10.1007/JHEP05\(2021\)057](https://doi.org/10.1007/JHEP05(2021)057) arXiv:2012.11474
50. K. Chandak, T. Mandal, S. Mitra, Hunting for scalar leptoquarks with boosted tops and light leptons. *Phys. Rev. D* **100**(2019). <https://doi.org/10.1103/PhysRevD.100.075019> arXiv:1907.11194
51. A. Bhaskar, D. Das, B. De, S. Mitra, Enhancing scalar productions with leptoquarks at the LHC. *Phys. Rev. D* **102**(2020). <https://doi.org/10.1103/PhysRevD.102.035002> arXiv:2002.12571
52. A. Alves, O.J.T. Eboli, G. Grilli Di Cortona, R.R. Moreira, Indirect and monojet constraints on scalar leptoquarks. *Phys. Rev. D* **99**(2019). <https://doi.org/10.1103/PhysRevD.99.095005> arXiv:1812.08632
53. I. Doršner, S. Fajfer, M. Patra, A comparative study of the S_1 and U_1 leptoquark effects in the light quark regime. *Eur. Phys. J. C* **80**, 204 (2020). <https://doi.org/10.1140/epjc/s10052-020-7754-8> arXiv:1906.05660
54. S. Mandal, M. Mitra, N. Sinha, Probing leptoquarks and heavy neutrinos at the LHeC. *Phys. Rev. D* **98**(2018). <https://doi.org/10.1103/PhysRevD.98.095004> arXiv:1807.06455
55. R. Padhan, S. Mandal, M. Mitra, N. Sinha, Signatures of \tilde{R}_2 class of Leptoquarks at the upcoming ep colliders. *Phys. Rev. D* **101**(2020). <https://doi.org/10.1103/PhysRevD.101.075037> arXiv:1912.07236
56. M.J. Baker, J. Fuentes-Martín, G. Isidori, M. König, High- p_T signatures in vector-leptoquark models. *Eur. Phys. J. C* **79**, 334 (2019). <https://doi.org/10.1140/epjc/s10052-019-6853-x> arXiv:1901.10480
57. H. Nadeau, D. London, Leptoquarks at e gamma colliders. *Phys. Rev. D* **47**, 3742–3749 (1993). <https://doi.org/10.1103/PhysRevD.47.3742> arXiv:hep-ph/9303238
58. S. Atag, O. Cakir, Pair production of scalar leptoquarks at TeV energy gamma p colliders. *Phys. Rev. D* **49**, 5769–5772 (1994). <https://doi.org/10.1103/PhysRevD.49.5769>
59. S. Atag, A. Celikel, S. Sultansoy, Scalar leptoquark production at TeV energy gamma p colliders. *Phys. Lett. B* **326**, 185–189 (1994). [https://doi.org/10.1016/0370-2693\(94\)91212-2](https://doi.org/10.1016/0370-2693(94)91212-2)
60. W. Buchmuller, R. Ruckl, D. Wyler, Leptoquarks in lepton–quark collisions. *Phys. Lett. B* **191**, 442–448 (1987). [https://doi.org/10.1016/0370-2693\(87\)90637-X](https://doi.org/10.1016/0370-2693(87)90637-X) [Erratum: *Phys. Lett. B* 448, 320–320 (1999)]
61. J. Hewett, S. Pakvasa, Leptoquark production in hadron colliders. *Phys. Rev. D* **37**, 3165 (1988). <https://doi.org/10.1103/PhysRevD.37.3165>
62. J. Hewett, T. Rizzo, Leptoquark signals at e^+e^- colliders. *Phys. Rev. D* **36**, 3367 (1987). <https://doi.org/10.1103/PhysRevD.36.3367>
63. F. Cuypers, Leptoquark production in $e^- \gamma$ scattering. *Nucl. Phys. B* **474**, 57–71 (1996). [https://doi.org/10.1016/0550-3213\(96\)00270-2](https://doi.org/10.1016/0550-3213(96)00270-2) arXiv:hep-ph/9508397
64. J. Blumlein, E. Boos, A. Kryukov, Leptoquark pair production in hadronic interactions. *Z. Phys. C* **76**, 137–153 (1997). <https://doi.org/10.1007/s002880050538> arXiv:hep-ph/9610408
65. A. Belyaev, C. Leroy, R. Mehdiyev, A. Pukhov, Leptoquark single and pair production at LHC with CalcHEP/CompHEP in the complete model. *JHEP* **09**, 005 (2005). <https://doi.org/10.1088/1126-6708/2005/09/005> arXiv:hep-ph/0502067
66. M. Kramer, T. Plehn, M. Spira, P. Zerwas, Pair production of scalar leptoquarks at the Tevatron. *Phys. Rev. Lett.* **79**, 341–344 (1997). <https://doi.org/10.1103/PhysRevLett.79.341> arXiv:hep-ph/9704322
67. T. Plehn, H. Spiesberger, M. Spira, P. Zerwas, Formation and decay of scalar leptoquarks/squarks in ep collisions. *Z. Phys. C* **74**, 611–614 (1997). <https://doi.org/10.1007/s002880050426> arXiv:hep-ph/9703433
68. O.J.P. Eboli, R. Zukanovich Funchal, T.L. Lungov, Signal and backgrounds for leptoquarks at the CERN LHC. *Phys. Rev. D* **57**, 1715–1729 (1998). <https://doi.org/10.1103/PhysRevD.57.1715> arXiv:hep-ph/9709319
69. M. Kramer, T. Plehn, M. Spira, P.M. Zerwas, Pair production of scalar leptoquarks at the CERN LHC. *Phys. Rev. D* **71**(2005). <https://doi.org/10.1103/PhysRevD.71.057503> arXiv:hep-ph/0411038
70. J.B. Hammett, D.A. Ross, NLO leptoquark production and decay: the narrow-width approximation and beyond. *JHEP* **07**, 148 (2015). [https://doi.org/10.1007/JHEP07\(2015\)148](https://doi.org/10.1007/JHEP07(2015)148) arXiv:1501.06719
71. T. Mandal, S. Mitra, S. Seth, Single productions of colored particles at the LHC: an example with scalar leptoquarks. *JHEP* **07**, 028 (2015). [https://doi.org/10.1007/JHEP07\(2015\)028](https://doi.org/10.1007/JHEP07(2015)028) arXiv:1503.04689
72. P. Asadi, R. Capdevilla, C. Cesarotti, S. Homiller, Searching for leptoquarks at future muon colliders. arXiv:2104.05720
73. P. Bandyopadhyay, A. Karan, R. Mandal, Distinguishing signatures of scalar leptoquarks at hadron and muon colliders. arXiv:2108.06506
74. P. Bandyopadhyay, S. Dutta, A. Karan, Zeros of amplitude in the associated production of photon and leptoquark at $e - p$ collider. *Eur. Phys. J. C* **81**, 315 (2021). <https://doi.org/10.1140/epjc/s10052-021-09090-z> arXiv:2012.13644
75. P. Bandyopadhyay, S. Dutta, A. Karan, Investigating the production of leptoquarks by means of zeros of amplitude at photon electron collider. *Eur. Phys. J. C* **80**, 573 (2020). <https://doi.org/10.1140/epjc/s10052-020-8083-7> arXiv:2003.11751
76. P. Bandyopadhyay, S. Dutta, M. Jakkapu, A. Karan, Distinguishing leptoquarks at the LHC/FCC. *Nucl. Phys. B* **971**(2021). <https://doi.org/10.1016/j.nuclphysb.2021.115524> arXiv:2007.12997
77. S. Dutta, P. Bandyopadhyay, A. Karan, Distinguishing different BSM signatures at present and future colliders. arXiv:2105.00893
78. CELLO Collaboration, H. Behrend et al., Search for light leptoquark bosons. *Phys. Lett. B* **178**, 452–456 (1986). [https://doi.org/10.1016/0370-2693\(86\)91410-3](https://doi.org/10.1016/0370-2693(86)91410-3) [Addendum: *Phys. Lett. B* 184, 417 (1987)]
79. JADE Collaboration, W. Bartel et al., Search for leptoquarks and other new particles with lepton-hadron signature in e^+e^- interactions. *Z. Phys. C* **36**, 15 (1987). <https://doi.org/10.1007/BF01556160>
80. AMY Collaboration, G. Kim et al., A search for leptoquark and colored lepton pair production in e^+e^- annihilations at TRISTAN. *Phys. Lett. B* **240**, 243–249 (1990). [https://doi.org/10.1016/0370-2693\(90\)90442-9](https://doi.org/10.1016/0370-2693(90)90442-9)
81. DELPHI Collaboration, P. Abreu et al., Search for leptoquarks and FCNC in e^+e^- annihilations at $\sqrt{s} = 183$ GeV. *Phys. Lett. B* **446**, 62–74 (1999). [https://doi.org/10.1016/S0370-2693\(98\)01525-1](https://doi.org/10.1016/S0370-2693(98)01525-1). arXiv:hep-ex/9903072
82. H1 Collaboration, F. Aaron et al., Search for first generation leptoquarks in ep collisions at HERA. *Phys. Lett. B* **704**, 388–396 (2011). <https://doi.org/10.1016/j.physletb.2011.09.017>. arXiv:1107.3716
83. ZEUS Collaboration, H. Abramowicz et al., Limits on contact interactions and leptoquarks at HERA. *Phys. Rev. D* **99**, 092006 (2019). <https://doi.org/10.1103/PhysRevD.99.092006>. arXiv:1902.03048
84. UA2 Collaboration, J. Alitti et al., A Search for scalar leptoquarks at the CERN $\bar{p}p$ collider. *Phys. Lett. B* **274**, 507–512 (1992). [https://doi.org/10.1016/0370-2693\(92\)92024-B](https://doi.org/10.1016/0370-2693(92)92024-B)
85. D0 Collaboration, V.M. Abazov et al., Search for first generation leptoquark pair production in the electron + missing energy + jets final state. *Phys. Rev. D* **84**, 071104 (2011). <https://doi.org/10.1103/PhysRevD.84.071104>. arXiv:1107.1849

86. CDF Collaboration, T. Aaltonen et al., Search for Third Generation Vector Leptoquarks in $p\bar{p}$ Collisions at $\sqrt{s} = 1.96$ TeV. *Phys. Rev. D* **77**, 091105 (2008). <https://doi.org/10.1103/PhysRevD.77.091105>. arXiv:0706.2832
87. ATLAS Collaboration, G. Aad et al., Search for pairs of scalar leptoquarks decaying into quarks and electrons or muons in $\sqrt{s} = 13$ TeV pp collisions with the ATLAS detector. *JHEP* **10**, 112 (2020). [https://doi.org/10.1007/JHEP10\(2020\)112](https://doi.org/10.1007/JHEP10(2020)112). arXiv:2006.05872
88. CMS Collaboration, A.M. Sirunyan et al., Search for singly and pair-produced leptoquarks coupling to third-generation fermions in proton-proton collisions at $\sqrt{s} = 13$ TeV. *Phys. Lett. B* **819**, 136446 (2021). <https://doi.org/10.1016/j.physletb.2021.136446>. arXiv:2012.04178
89. ATLAS Collaboration, G. Aad et al., Search for pair production of third-generation scalar leptoquarks decaying into a top quark and a τ -lepton in pp collisions at $\sqrt{s} = 13$ TeV with the ATLAS detector. *JHEP* **06**, 179 (2021). [https://doi.org/10.1007/JHEP06\(2021\)179](https://doi.org/10.1007/JHEP06(2021)179). arXiv: 2101.11582
90. CMS Collaboration, A.M. Sirunyan et al., Constraints on models of scalar and vector leptoquarks decaying to a quark and a neutrino at $\sqrt{s} = 13$ TeV. *Phys. Rev. D* **98**, 032005 (2018). <https://doi.org/10.1103/PhysRevD.98.032005>. arXiv:1805.10228
91. CMS Collaboration, A.M. Sirunyan et al., Search for singly and pair-produced leptoquarks coupling to third-generation fermions in proton-proton collisions at $\sqrt{s}=13$ TeV. *Phys. Lett. B* **819**, 136446 (2021). <https://doi.org/10.1016/j.physletb.2021.136446>. arXiv:2012.04178
92. R. Mandal, A. Pich, Constraints on scalar leptoquarks from lepton and kaon physics. *JHEP* **12**, 089 (2019). [https://doi.org/10.1007/JHEP12\(2019\)089](https://doi.org/10.1007/JHEP12(2019)089) arXiv:1908.11155
93. S. Davidson, D.C. Bailey, B.A. Campbell, Model independent constraints on leptoquarks from rare processes. *Z. Phys. C* **61**, 613–644 (1994). <https://doi.org/10.1007/BF01552629> arXiv:hep-ph/9309310
94. G. Isidori, G. Ridolfi, A. Strumia, On the metastability of the standard model vacuum. *Nucl. Phys. B* **609**, 387–409 (2001). [https://doi.org/10.1016/S0550-3213\(01\)00302-9](https://doi.org/10.1016/S0550-3213(01)00302-9) arXiv:hep-ph/0104016
95. M. Gonderinger, H. Lim, M.J. Ramsey-Musolf, Complex scalar singlet dark matter: vacuum stability and phenomenology. *Phys. Rev. D* **86**(2012). <https://doi.org/10.1103/PhysRevD.86.043511> arXiv:1202.1316
96. M. Gonderinger, Y. Li, H. Patel, M.J. Ramsey-Musolf, Vacuum stability, perturbativity, and scalar singlet dark matter. *JHEP* **01**, 053 (2010). [https://doi.org/10.1007/JHEP01\(2010\)053](https://doi.org/10.1007/JHEP01(2010)053) arXiv:0910.3167
97. R. Costa, A.P. Morais, M.O.P. Sampaio, R. Santos, Two-loop stability of a complex singlet extended Standard Model. *Phys. Rev. D* **92**(2015). <https://doi.org/10.1103/PhysRevD.92.025024> arXiv:1411.4048
98. N. Haba, Y. Yamaguchi, Vacuum stability in the $U(1)_\chi$ extended model with vanishing scalar potential at the Planck scale. *PTEP* **2015** 093B05 (2015). <https://doi.org/10.1093/ptep/ptv121>. arXiv:1504.05669
99. W.-L. Guo, Y.-L. Wu, The real singlet scalar dark matter model. *JHEP* **10**, 083 (2010). [https://doi.org/10.1007/JHEP10\(2010\)083](https://doi.org/10.1007/JHEP10(2010)083) arXiv:1006.2518
100. V. Barger, P. Langacker, M. McCaskey, M. Ramsey-Musolf, G. Shaughnessy, Complex singlet extension of the Standard Model. *Phys. Rev. D* **79**(2009). <https://doi.org/10.1103/PhysRevD.79.015018> arXiv:0811.0393
101. N. Khan, S. Rakshit, Study of electroweak vacuum metastability with a singlet scalar dark matter. *Phys. Rev. D* **90**(2014). <https://doi.org/10.1103/PhysRevD.90.113008> arXiv:1407.6015
102. S. Baek, P. Ko, W.-I. Park, E. Senaha, Vacuum structure and stability of a singlet fermion dark matter model with a singlet scalar messenger. *JHEP* **11**, 116 (2012). [https://doi.org/10.1007/JHEP11\(2012\)116](https://doi.org/10.1007/JHEP11(2012)116) arXiv:1209.4163
103. P. Bandyopadhyay, E.J. Chun, R. Mandal, F.S. Queiroz, Scrutinizing right-handed neutrino portal dark matter With Yukawa effect. *Phys. Lett. B* **788**, 530–534 (2019). <https://doi.org/10.1016/j.physletb.2018.12.003> arXiv:1807.05122
104. P. Bandyopadhyay, E.J. Chun, R. Mandal, Implications of right-handed neutrinos in $B - L$ extended standard model with scalar dark matter. *Phys. Rev. D* **97**(2018). <https://doi.org/10.1103/PhysRevD.97.015001> arXiv:1707.00874
105. N. Chakrabarty, B. Mukhopadhyaya, High-scale validity of a two Higgs doublet scenario: metastability included. *Eur. Phys. J. C* **77**, 153 (2017). <https://doi.org/10.1140/epjc/s10052-017-4705-0> arXiv:1603.05883
106. N. Chakrabarty, D.K. Ghosh, B. Mukhopadhyaya, I. Saha, Dark matter, neutrino masses and high scale validity of an inert Higgs doublet model. *Phys. Rev. D* **92**(2015). <https://doi.org/10.1103/PhysRevD.92.015002> arXiv:1501.03700
107. B. Swiezewska, Inert scalars and vacuum metastability around the electroweak scale. *JHEP* **07**, 118 (2015). [https://doi.org/10.1007/JHEP07\(2015\)118](https://doi.org/10.1007/JHEP07(2015)118) arXiv:1503.07078
108. S. Gopalakrishna, T.S. Mukherjee, S. Sadhukhan, Extra neutral scalars with vectorlike fermions at the LHC. *Phys. Rev. D* **93**(2016). <https://doi.org/10.1103/PhysRevD.93.055004> arXiv:1504.01074
109. L. LopezHonorez, C.E. Yaguna, The inert doublet model of dark matter revisited. *JHEP* **09**, 046 (2010). [https://doi.org/10.1007/JHEP09\(2010\)046](https://doi.org/10.1007/JHEP09(2010)046) arXiv:1003.3125
110. P. Bandyopadhyay, E.J. Chun, R. Mandal, Scalar dark matter in leptophilic two-Higgs-doublet model. *Phys. Lett. B* **779**, 201–205 (2018). <https://doi.org/10.1016/j.physletb.2018.01.071> arXiv:1709.08581
111. N. Khan, S. Rakshit, Constraints on inert dark matter from the metastability of the electroweak vacuum. *Phys. Rev. D* **92**(2015). <https://doi.org/10.1103/PhysRevD.92.055006> arXiv:1503.03085
112. A. Datta, N. Ganguly, N. Khan, S. Rakshit, Exploring collider signatures of the inert Higgs doublet model. *Phys. Rev. D* **95**(2017). <https://doi.org/10.1103/PhysRevD.95.015017> arXiv:1610.00648
113. S. Yaser Ayazi, S.M. Firouzabadi, Footprint of triplet scalar dark matter in direct, indirect search and invisible Higgs decay. *Cogent Phys.* **2**, 1047559 (2015). <https://doi.org/10.1080/23311940.2015.1047559> arXiv:1501.06176
114. N. Khan, Exploring the hyperchargeless Higgs triplet model up to the Planck scale. *Eur. Phys. J. C* **78**, 341 (2018). <https://doi.org/10.1140/epjc/s10052-018-5766-4> arXiv:1610.03178
115. C. Coriano, L. Delle Rose, C. Marzo, Vacuum stability in $U(1)$ -prime extensions of the Standard Model with TeV scale right handed neutrinos. *Phys. Lett. B* **738**, 13–19 (2014). <https://doi.org/10.1016/j.physletb.2014.09.001> arXiv:1407.8539
116. C. Coriano, L. Delle Rose, C. Marzo, Constraints on abelian extensions of the Standard Model from two-loop vacuum stability and $U(1)_{B-L}$. *JHEP* **02**, 135 (2016). [https://doi.org/10.1007/JHEP02\(2016\)135](https://doi.org/10.1007/JHEP02(2016)135) arXiv:1510.02379
117. L. DelleRose, C. Marzo, A. Urbano, On the stability of the electroweak vacuum in the presence of low-scale seesaw models. *JHEP* **12**, 050 (2015). [https://doi.org/10.1007/JHEP12\(2015\)050](https://doi.org/10.1007/JHEP12(2015)050) arXiv:1506.03360
118. S. Jangid, P. Bandyopadhyay, P.S. Bhupal Dev, A. Kumar, Vacuum stability in inert Higgs doublet model with right-handed neutrinos. *JHEP* **08**, 154 (2020). [https://doi.org/10.1007/JHEP08\(2020\)154](https://doi.org/10.1007/JHEP08(2020)154) arXiv:2001.01764
119. I. Garg, S. Goswami, K.N. Vishnudath, N. Khan, Electroweak vacuum stability in presence of singlet scalar dark matter in TeV scale seesaw models. *Phys. Rev. D* **96**(2017). <https://doi.org/10.1103/PhysRevD.96.055020> arXiv:1706.08851

120. P. Bandyopadhyay, S. Jangid, M. Mitra, Scrutinizing vacuum stability in IDM with type-III inverse seesaw. *JHEP* **02**, 075 (2021). [https://doi.org/10.1007/JHEP02\(2021\)075](https://doi.org/10.1007/JHEP02(2021)075) arXiv:2008.11956
121. P. Bandyopadhyay, R. Mandal, Vacuum stability in an extended standard model with a leptoquark. *Phys. Rev. D* **95**(2017). <https://doi.org/10.1103/PhysRevD.95.035007> arXiv:1609.03561
122. D. Aristizabal Sierra, M. Hirsch, S.G. Kovalenko, Leptoquarks: neutrino masses and accelerator phenomenology. *Phys. Rev. D* **77**(2008). <https://doi.org/10.1103/PhysRevD.77.055011> arXiv:0710.5699
123. I. Doršner, S. Fajfer, N. Košnik, Leptoquark mechanism of neutrino masses within the grand unification framework. *Eur. Phys. J. C* **77**, 417 (2017). <https://doi.org/10.1140/epjc/s10052-017-4987-2> arXiv:1701.08322
124. K.S. Babu, P.S.B. Dev, S. Jana, A. Thapa, Non-standard interactions in radiative neutrino mass models. *JHEP* **03**, 006 (2020). [https://doi.org/10.1007/JHEP03\(2020\)006](https://doi.org/10.1007/JHEP03(2020)006) arXiv:1907.09498
125. H. Päs, E. Schumacher, Common origin of R_K and neutrino masses. *Phys. Rev. D* **92**(2015). <https://doi.org/10.1103/PhysRevD.92.114025> arXiv:1510.08757
126. C.-K. Chua, X.-G. He, W.-Y.P. Hwang, Neutrino mass induced radiatively by supersymmetric leptoquarks. *Phys. Lett. B* **479**, 224–229 (2000). [https://doi.org/10.1016/S0370-2693\(00\)00325-7](https://doi.org/10.1016/S0370-2693(00)00325-7) arXiv:hep-ph/9905340
127. U. Mahanta, Neutrino masses and mixing angles from leptoquark interactions. *Phys. Rev. D* **62**(2000). <https://doi.org/10.1103/PhysRevD.62.073009> arXiv:hep-ph/9909518
128. K.S. Babu, J. Julio, Two-loop neutrino mass generation through leptoquarks. *Nucl. Phys. B* **841**, 130–156 (2010). <https://doi.org/10.1016/j.nuclphysb.2010.07.022> arXiv:1006.1092
129. J.M. Arnold, B. Fornal, M.B. Wise, Simplified models with baryon number violation but no proton decay. *Phys. Rev. D* **87**(2013). <https://doi.org/10.1103/PhysRevD.87.075004> arXiv:1212.4556
130. S. Kovalenko, I. Schmidt, Proton stability in leptoquark models. *Phys. Lett. B* **562**, 104–108 (2003). [https://doi.org/10.1016/S0370-2693\(03\)00544-6](https://doi.org/10.1016/S0370-2693(03)00544-6) arXiv:hep-ph/0210187
131. S.M. Barr, E.M. Freire, ϵ'/ϵ in leptoquark and diquark models of CP violation. *Phys. Rev. D* **41**, 2129 (1990). <https://doi.org/10.1103/PhysRevD.41.2129>
132. P. Nath, P. Fileviez Perez, Proton stability in grand unified theories, in strings and in branes. *Phys. Rep.* **441**, 191–317 (2007). <https://doi.org/10.1016/j.physrep.2007.02.010> arXiv:hep-ph/0601023
133. I. Dorsner, P. Fileviez Perez, Unification without supersymmetry: neutrino mass, proton decay and light leptoquarks. *Nucl. Phys. B* **723**, 53–76 (2005). <https://doi.org/10.1016/j.nuclphysb.2005.06.016> arXiv:hep-ph/0504276
134. F. Staub, SARAH 4: a tool for (not only SUSY) model builders. *Comput. Phys. Commun.* **185**, 1773–1790 (2014). <https://doi.org/10.1016/j.cpc.2014.02.018> arXiv:1309.7223
135. F. Staub, Exploring new models in all detail with SARAH. *Adv. High Energy Phys.* **2015**(2015). <https://doi.org/10.1155/2015/840780> arXiv:1503.04200
136. G.'t Hooft, M.J.G. Veltman, Regularization and renormalization of gauge fields. *Nucl. Phys. B* **44**, 189–213 (1972). [https://doi.org/10.1016/0550-3213\(72\)90279-9](https://doi.org/10.1016/0550-3213(72)90279-9)
137. M.E. Machacek, M.T. Vaughn, Two loop renormalization group equations in a general quantum field theory. 2. Yukawa couplings. *Nucl. Phys. B* **236**, 221–232 (1984). [https://doi.org/10.1016/0550-3213\(84\)90533-9](https://doi.org/10.1016/0550-3213(84)90533-9)
138. M.E. Machacek, M.T. Vaughn, Two loop renormalization group equations in a general quantum field theory. 1. Wave function renormalization. *Nucl. Phys. B* **222**, 83–103 (1983). [https://doi.org/10.1016/0550-3213\(83\)90610-7](https://doi.org/10.1016/0550-3213(83)90610-7)
139. M.E. Machacek, M.T. Vaughn, Two loop renormalization group equations in a general quantum field theory. 3. Scalar quartic couplings. *Nucl. Phys. B* **249**, 70–92 (1985). [https://doi.org/10.1016/0550-3213\(85\)90040-9](https://doi.org/10.1016/0550-3213(85)90040-9)
140. S.P. Martin, M.T. Vaughn, Two loop renormalization group equations for soft supersymmetry breaking couplings. *Phys. Rev. D* **50**, 2282 (1994). <https://doi.org/10.1103/PhysRevD.50.2282> arXiv:hep-ph/9311340 [Erratum: *Phys. Rev. D* **78**, 039903 (2008)]
141. K.G. Chetyrkin, M.F. Zoller, Three-loop β -functions for top-Yukawa and the Higgs self-interaction in the Standard Model. *JHEP* **06**, 033 (2012). [https://doi.org/10.1007/JHEP06\(2012\)033](https://doi.org/10.1007/JHEP06(2012)033) arXiv:1205.2892
142. S.R. Juárez, W.P. Kielanowski, G. Mora, A. Bohm, Renormalization group: new relations between the parameters of the Standard Model. *Phys. Lett. B* **772**, 294–299 (2017). <https://doi.org/10.1016/j.physletb.2017.06.059> arXiv:1703.01523
143. G. Degrossi, S. Di Vita, J. Elias-Miro, J.R. Espinosa, G.F. Giudice, G. Isidori et al., Higgs mass and vacuum stability in the Standard Model at NNLO. *JHEP* **08**, 098 (2012). [https://doi.org/10.1007/JHEP08\(2012\)098](https://doi.org/10.1007/JHEP08(2012)098) arXiv:1205.6497
144. D. Buttazzo, G. Degrossi, P.P. Giardino, G.F. Giudice, F. Sala, A. Salvio et al., Investigating the near-criticality of the Higgs boson. *JHEP* **12**, 089 (2013). [https://doi.org/10.1007/JHEP12\(2013\)089](https://doi.org/10.1007/JHEP12(2013)089) arXiv:1307.3536
145. S. Coleman, E. Weinberg, Radiative corrections as the origin of spontaneous symmetry breaking. *Phys. Rev. D* **7**, 1888–1910 (1973). <https://doi.org/10.1103/PhysRevD.7.1888>
146. J. Elias-Miro, J.R. Espinosa, G.F. Giudice, G. Isidori, A. Riotto, A. Strumia, Higgs mass implications on the stability of the electroweak vacuum. *Phys. Lett. B* **709**, 222–228 (2012). <https://doi.org/10.1016/j.physletb.2012.02.013> arXiv:1112.3022
147. J.A. Casas, J.R. Espinosa, M. Quiros, A. Riotto, The lightest Higgs boson mass in the minimal supersymmetric standard model. *Nucl. Phys. B* **436**, 3–29 (1995). [https://doi.org/10.1016/0550-3213\(94\)00508-C](https://doi.org/10.1016/0550-3213(94)00508-C) arXiv:hep-ph/9407389 [Erratum: *Nucl. Phys. B* **439**, 466–468 (1995)]
148. I. Masina, Higgs boson and top quark masses as tests of electroweak vacuum stability. *Phys. Rev. D* **87**(2013). <https://doi.org/10.1103/PhysRevD.87.053001> arXiv:1209.0393
149. Particle Data Group, P.A. Zyla et al., Review of particle physics. *Prog. Theor. Exp. Phys.* **2020**, 083C01 (2020). <https://doi.org/10.1093/ptep/ptaa104>
150. M. Carpentier, S. Davidson, Constraints on two-lepton, two quark operators. *Eur. Phys. J. C* **70**, 1071–1090 (2010). <https://doi.org/10.1140/epjc/s10052-010-1482-4> arXiv:1008.0280
151. S. Davidson, A. Saporta, Constraints on $2\ell 2q$ operators from $\mu - e$ flavour-changing meson decays. *Phys. Rev. D* **99**(2019). <https://doi.org/10.1103/PhysRevD.99.015032> arXiv:1807.10288
152. A. Crivellin, D. Müller, L. Schnell, Combined constraints on first generation leptoquarks. *Phys. Rev. D* **103**(2021). <https://doi.org/10.1103/PhysRevD.103.115023> arXiv:2104.06417
153. K.-M. Cheung, Muon anomalous magnetic moment and leptoquark solutions. *Phys. Rev. D* **64**(2001). <https://doi.org/10.1103/PhysRevD.64.033001> arXiv:hep-ph/0102238
154. O.U. Shanker, $\pi \ell 2$, $K \ell 3$ and $K^0 - \bar{K}^0$ constraints on leptoquarks and supersymmetric particles. *Nucl. Phys. B* **204**, 375–386 (1982). [https://doi.org/10.1016/0550-3213\(82\)90196-1](https://doi.org/10.1016/0550-3213(82)90196-1)
155. I. Doršner, S. Fajfer, O. Sumensari, Muon $g - 2$ and scalar leptoquark mixing. *JHEP* **06**, 089 (2020). [https://doi.org/10.1007/JHEP06\(2020\)089](https://doi.org/10.1007/JHEP06(2020)089) arXiv:1910.03877
156. M. Schmaltz, Y.-M. Zhong, The leptoquark Hunter's guide: large coupling. *JHEP* **01**, 132 (2019). [https://doi.org/10.1007/JHEP01\(2019\)132](https://doi.org/10.1007/JHEP01(2019)132) arXiv:1810.10017
157. L. Buonocore, U. Haisch, P. Nason, F. Tramontano, G. Zanderighi, Lepton-quark collisions at the large hadron collider. *Phys. Rev. Lett.* **125**(2020). <https://doi.org/10.1103/PhysRevLett.125.231804> arXiv:2005.06475

158. CMS Collaboration, Search for pair production of first generation scalar leptoquarks at $\sqrt{s} = 13$ TeV. CMS-PAS-EXO-17-009 (2018)
159. CMS Collaboration, A.M. Sirunyan et al., Search for high-mass resonances in dilepton final states in proton–proton collisions at $\sqrt{s} = 13$ TeV. *JHEP* **06**, 120 (2018). [https://doi.org/10.1007/JHEP06\(2018\)120](https://doi.org/10.1007/JHEP06(2018)120). [arXiv:1803.06292](https://arxiv.org/abs/1803.06292)
160. CMS Collaboration, V. Khachatryan et al., Search for single production of scalar leptoquarks in proton–proton collisions at $\sqrt{s} = 8$ TeV. *Phys. Rev. D* **93**, 032005 (2016) <https://doi.org/10.1103/PhysRevD.93.032005>. [arXiv:1509.03750](https://arxiv.org/abs/1509.03750) [Erratum: *Phys. Rev. D* **95**, 039906 (2017)]
161. CMS Collaboration, A.M. Sirunyan et al., Search for new physics in final states with an energetic jet or a hadronically decaying W or Z boson and transverse momentum imbalance at $\sqrt{s} = 13$ TeV. *Phys. Rev. D* **97**, 092005 (2018). <https://doi.org/10.1103/PhysRevD.97.092005>. [arXiv:1712.02345](https://arxiv.org/abs/1712.02345)
162. CMS Collaboration, Search for pair production of second generation leptoquarks at $\sqrt{s}=13$ TeV. CMS-PAS-EXO-17-003 (2018)
163. CMS Collaboration, Search for heavy neutrinos and third-generation leptoquarks in final states with two hadronically decaying τ leptons and two jets in proton–proton collisions at $\sqrt{s} = 13$ TeV. CMS-PAS-EXO-17-016 (2018)
164. CMS Collaboration, Search for singly produced third-generation leptoquarks decaying to a τ lepton and a b quark in proton–proton collisions at $\sqrt{s} = 13$ TeV. CMS-PAS-EXO-17-029 (2018)
165. ATLAS Collaboration, M. Aaboud et al., Search for additional heavy neutral Higgs and gauge bosons in the ditau final state produced in 36 fb^{-1} of pp collisions at $\sqrt{s} = 13$ TeV with the ATLAS detector. *JHEP* **01**, 055 (2018). [https://doi.org/10.1007/JHEP01\(2018\)055](https://doi.org/10.1007/JHEP01(2018)055). [arXiv:1709.07242](https://arxiv.org/abs/1709.07242)
166. QWEAK Collaboration, D. Androić et al., Precision measurement of the weak charge of the proton. *Nature* **557**, 207–211 (2018). <https://doi.org/10.1038/s41586-018-0096-0>. [arXiv:1905.08283](https://arxiv.org/abs/1905.08283)